SSFSW T-joints in different configurations:
Influence of rotational and welding speed

Vasco Duarte Raposo

Dissertação de Mestrado

Orientador na FEUP: Professor Paulo Tavares de Castro

Orientador no HZG: Doutorando Alessandro Barbini

U.PORTO
FEUP FACULDADE DE ENGENHARIA
UNIVERSIDADE DO PORTO

Mestrado Integrado em Engenharia Mecânica

Março de 2017

A todos aqueles que me deram força.

Resumo

Serve este trabalho para encontrar uma solução alternativa à utilização de rebites na construção de painéis que compõem a fuselagem dos aviões, através de um novo processo de fabrico. O processo utilizado é uma variante do processo de soldadura por fricção linear e visa estabelecer os melhores parâmetros de soldadura e número de passagens para uma configuração de junta em forma de "T".

O trabalho divide-se em duas partes: estudo dos parâmetros de soldadura e comparação dos resultados obtidos. Foi realizado um conjunto de soldaduras em chapas utilizando três configurações em forma de T, nomeadamente, junta em T com entalhe de passada simples, junta em T com entalhe de passada dupla e junta em T de 3 peças; variando dois parâmetros de soldadura, nomeadamente, velocidade de soldadura e rotação do pino. Os materiais foram caraterizados com a realização de ensaios de microdureza e dois ensaios de tração em diferentes direções. As direções dos ensaios de tração são semelhantes às direções em que um painel da fuselagem é solicitado. A microstrutura de cada provete também foi analisada e foi medido o tamanho de grão das amostras. Estes ensaios foram realizados com o objetivo de se estudar o comportamento do material ao se variar os parâmetros de soldadura acima mencionados.

De seguida, após todos os ensaios terem sido realizados e todos os resultados terem sido analisados, os resultados obtidos foram comparados a fim de se averiguar qual é a melhor configuração de juntas em T e, especificamente, quais os melhores parâmetros de soldadura que possibilitam esses resultados.

A configuração que apresenta as melhores propriedades é a configuração de junta em T de 3 peças, sendo que estas propriedades são maximizadas quando a junta é fabricada com 3 mm/s de velocidade de soldadura e 1200 RPM de rotação do pino. A rotação do pino é o parâmetro de soldadura que mais influenciou os resultados obtidos.

Palavras-chave

Soldadura por fricção linear, SSFSW, parâmetros de soldadura, análise metalográfica, ensaios mecânicos, ligas de alumínio

SSFSW T-joints in different configurations: Influence of rotational and welding speed

Abstract

This report aims to find an alternative solution to the use of rivets in the construction of panels that compose the airplanes' fuselage through a new manufacturing process. The used process is a variant of the friction stir welding process and intends to find the best parameters and optimized number of passes, regarding a typical T-joint configuration.

This work is separated in two parts: parameter study and comparison of results. A group of welds were performed using three T-joint configurations, namely, notch-skin single pass, notch-skin double pass and three-parts welds; by varying two welding parameters, namely, welding speed and rotational speed. The working materials were characterized by performing micro-hardness experiments, as well as hoop-strength and pull-out experiments. The directions involved in the last two experiments are similar to the ones in which a fuselage panel is being loaded. The specimens' microstructures were also analyzed and grain sizes were measured. These tests were accomplished aiming to characterize the material's behaviour by varying the weld parameters mentioned above.

Later, after all experiments have been performed and all results have been analyzed, the obtained results were compared in order to understand which T-joint configuration is the best and, specifically, which are the weld parameters that give those results.

The best T-joint configuration in terms of mechanical properties is the three-parts joint, in which these properties are obtained by welding with 3 mm/s of welding speed and 1200 RPM of rotational speed. Rotational speed was the most significant influent parameter in mechanical properties.

Keywords

Friction Stir Welding, SSFSW, welding parameters, metallographic analysis, mechanical testing, aluminium alloys

Acknowledgements

For the time I spent in Germany, I show deeply gratitude to:

Professor Paulo Tavares de Castro, supervisor at FEUP, for giving me the unique opportunity of performing a master thesis at Helmholtz-Zentrum Geesthacht (HZG), Germany, for orienting my work and my dissertation outside Portugal, for showing great interest about my progress and for providing me the best support that I could get;

Jorge dos Santos, head of WMP department at HZG, for providing the opportunity of performing my master thesis on a world leading institution of scientific research, for giving me the chance to learn and push myself on my work and for the respectful attitude towards me;

Alessandro Barbini, supervisor at HZG, for the teamworking, for teaching me during my stay, for guiding me when I was feeling I was lost, for recognizing all my work performed at HZG and for being my friend;

Dagmar Koschek, administrator at WMP department, for getting all the necessary thing ready for my mobility, for helping me when I needed and for all the kindness;

All the colleagues from WMP department, for keeping up with my work, for giving me all the motivation that I needed to move on and for all the kindness;

My family and my friends, for encouraging me to go abroad and perform my dissertation, for the provided support and for believing in me;

The staff from the Cooperation division at FEUP and from the Service of International Relations at UP for providing a scholarship to work and live in Germany and for showing great support during my stay.

Contents

List of Acronyms

3P – Three parts
AA – Aluminium Alloy
AS – Advancing Side
ASTM – American Society for Testing and Materials
BM – Base Material
CNC – Computer Numerical Control
DoE – Design of Experiments
DP – Notch-skin double pass
FEUP – Faculty of Engineering of the University of Porto
FSW – Friction Stir Welding
HAZ – Heat Affected Zone
HZG – Helmholtz-Zentrum Geesthacht
RS – Retreating Side
RS – Rotational Speed
SP – Notch-ski single pass
SSFSW – Stationary Shoulder Friction Stir Welding
SZ – Stirred Zone
TMAZ – Thermo-Mechanical Affected Zone
TWI – The Welding Institute
UP – University of Porto
UTS – Ultimate Tensile Strength
WMP – Solid State Joining Processes department
WS – Welding Speed
YS – Yield Strength

Index of Figures

Index of Tables

1 Introduction

The present work is part of a four year scientific project entitled “Damage tolerance behaviour of integral aircraft structures obtained by SSFSW”, which is divided in four main working packages:

1) Tool & clamping system development:
    a) Understanding of the reasons for probe failure;
    b) Development of a new tool validated by simulation.
2) Determination of the effect of process parameter on properties:
    a) Application of DoE for maximisation of:
        i) Pull-out strength experiments;
        ii) Hoop-strength experiments;
        iii) Welding Speed (minimum requirement for industrial acceptability).
3) Analysis of the fatigue behaviour of the process variants:
    a) Use of fatigue test in hoop direction to determine the best between:
        i) Fillet weld;
        ii) Notch-skin weld;
        iii) Overlap-skin weld.
4) Final Analysis of the chosen process and mechanical model validation:
    a) Fatigue initiation;
    b) Crack-growth resistance;
    c) Residual strength analysis;
    d) Buckling analysis (Barbini, 2016).

Specifically, this work is included on the third main working package, concerning the parameter study for welding the plates, material characterization through mechanical experiments and further comparison among the different T-joints configurations and weld parameters. The experimental approach is presented on the chapter Experimental Procedure.

The project came from a scientific institution called *Helmholtz-Zentrum-Geesthacht* (HZG), a public institution on materials and coastal research located in Geesthacht, Germany. The institution is divided in five main institutes. This work was realized specifically on the Institution of Materials Research, Materials/Mechanics, and its main working facilities were the *Solid State Joining Processes* department (WMP).

1.1 Societal Relevance

The transportation sector is facing a deep change regarding the way people are moving nowadays. A growing demand of flights is fulfilling the need to manufacture more aircrafts, as it was studied by a publication (Leahy, 2016) evidenced in Figure 1:

Figure 1 – Global Market Forecast for the Aircraft Industry in 2016 (Leahy, 2016).

The growing demand for aircrafts makes the companies to push the boundaries of manufacturing lighter, safer, more economical, environmental friendly, more reliable and with optimized design aircrafts. There are three main topics that today's manufacturers must face to fulfill the market's needs:

- Efficient and cost effective production process for aircraft panels: Reduce the amount of manufacturing processes, use of faster production processes, reduce the part reject rate, use of simple repair technology;
- Environmental Friendly Manufacturing – Clean Manufacturing: Use of energy efficient manufacturing processes, no thermal, particle or gas emissions from the manufacturing process, no chemical preparation of base materials, operator friendly processes;
- Efficient use of materials: Use joint designs leading to optimized material use.

Specifically, the last topic is the point of interest on this study. An alternative solution for the weight issue related with the usage of rivets in joining panels for manufacturing the fuselage will be presented, which aims to reduce its weight and to increase its fatigue life, by design optimization.

1.2 Knowledge gap

To reduce the overall costs, weight reduction is a must for aircrafts. The current panel manufacturing is using riveted structures which is a weight issue that can be enhanced. At this moment, aircrafts use thousands of rivets to join skins to stringers to form the fuselage. Figure 2 presents a typical fuselage joint manufactured using rivets (Barbini, 2016).

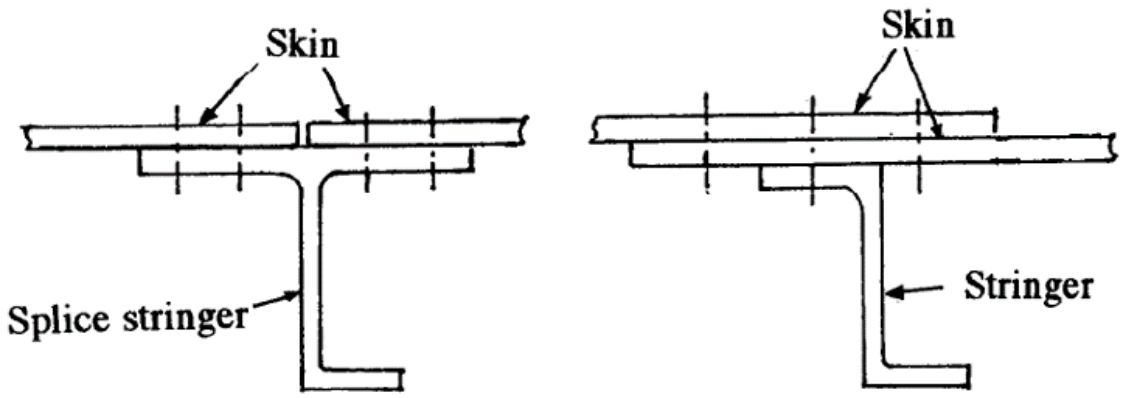

Figure 2 – Joint of skin and stringer using rivets (Barbini, 2016).

The introduction of composite fuselage to reduce the overall weight is a possible alternative for weight reduction. However, there are still some problems persisting on the fuselage design when this technique is applied, as discussed by Dursun & Soutis (2013):

- Riveting for skin-stringer connection;
- Corrosion of fasteners;
- Expensive and time consuming manufacturing process;
- Increase of thickness due to lack of in-flight experience and buckling.

Attempts of using conventional FSW in T-joints have been made as an alternative solution to the problems caused by the composite fuselage solution (Silva et al, 2013) (Fratini, 2012). However, there were some problems regarding the feasibility of the process:

- High distortion;
- Impossibility to use thin walled structures;
- Poor surface finishing;
- Serious problems of skin thickness reduction.

Since SSFSW is a new variant from FSW and little information is known about it, no attempts have been made using a non-rotating shoulder friction stir welds in skin-stringer joints as an alternative solution for the weight issue. So, it would be interesting to find out about the feasibility of the process and if it truly fits the requirements of the aircraft manufacturers. Basically, the aim is to find out about the following topics regarding the new variant of FSW:

- Defect development;
- Stability of the process;
- Robustness of the process.

Moreover, no damage tolerance analysis exists for T-joints welds obtained by SSFSW. Therefore, a specific study on the topic was proposed with the main objectives of finding out about:

- Local properties determination;
- Joint strength;
- Fatigue initiation points and fatigue behaviour;
- Damage tolerance;

- Fatigue crack propagation resistance;
- Critical crack length and residual strength (Barbini, 2016).

These six topics are the main issues regarding this project. This report is a contribution for that project and consists of a parameter study, followed by a comparison between the three different processes in terms of best mechanical performance.

1.3 Objectives

The project's overall objectives are divided in two categories, regarding the field of study, as it follows:

- Scientific Objectives:
    - Correlation between process parameters and local properties;
    - Correlation of the local properties and the global mechanical behaviour;
    - Understanding crack propagation behaviour.
- Technical Objectives:
    - Development of a robust process;
    - Maximization of the welding speed for industrial application;
    - Comparison with existing processes (i.e. riveted joints).

For the present work, the objectives are:

- Correlation between welding parameters and T-joints configurations with the mechanical properties;
- Evaluation of the best skin-stringer configuration.

1.4 Outline of the Dissertation

In Chapter 2 – 'State of the Art', it is presented the thesis's state of the art, where an overview of SSFSW is presented. It starts with an introduction to the process, then the new process is compared to the conventional FSW. After that, alternative SSFSW weld techniques that are impossible to replicate using FSW are presented, and it concludes with a few remarks about T-joints configurations.

In Chapter 3 – 'Experimental Procedure', the experimental approach of this work is presented. It starts with the equipment's description, followed by material characterization. The working plan is also described in Chapter 3, as well as the mechanical testing and metallographic analysis.

In Chapter 4 – 'Results and Discussion', all results are presented, followed by a proper discussion. It is also in Chapter 4 that the comparison between the different skin-stringer configurations is exposed.

In Chapter 5 – 'Final Remarks', conclusions about all the experiments are presented, a possible future work is proposed, following the report's study.

2 State of the Art

A review on the theme Stationary Shoulder Friction Stir Welding is presented in this chapter. Aspects like working principle, comparison with conventional FSW, SSFSW techniques and T-joints will be presented.

An introduction about Friction Stir Welding will not be presented in this report, since there are a lot of literature and information available in academic and engineering databases. Moreover, FSW is one of the engineering topics that is nowadays the object of large research effort, therefore it is wise to focus on the specific theme of the present study. For a general overview about FSW, as well as FSW of aluminium alloys, it is advisable for the reader to search on the following sources:

- *Friction Stir Welding and Processing* (Mishra & Ma, 2005);
- *Recent advances in friction-stir welding – Process, weldment structure and properties* (Nandan et al, 2008);
- *Friction stir welding of aluminium alloys* (Threadgill et al, 2009);
- *Advances in Friction Welding* (Li et al, 2014).

2.1 Introduction to Stationary Shoulder Friction Stir Welding

Stationary Shoulder Friction Stir Welding is a new variant of conventional Friction Stir Welding that was first reported in 2006 to improve the friction stir welding of low thermal conductivity titanium-based alloys. Only the probe has rotational movement, while the shoulder slides on top of the surface during the welding process (Li et al, 2015) (Ahmed et al, 2010). SSFSW creates local heat input around the probe area and eliminates unnecessary material flow under the shoulder, which leads to a better joint symmetry consisted by a narrow heat affected zone (HAZ) and a thermo-mechanical affected zone (TMAZ) (Li et al, 2015). The shoulder relates to the probe through bearing assembly, or separated without physical contact with a small gap between the two components, making it stationary while the probe rotates, unlike the conventional FSW tool, where both are physically connected, and sometimes, both are the same component. Figure 3 shows the two different tools with similar dimensions.

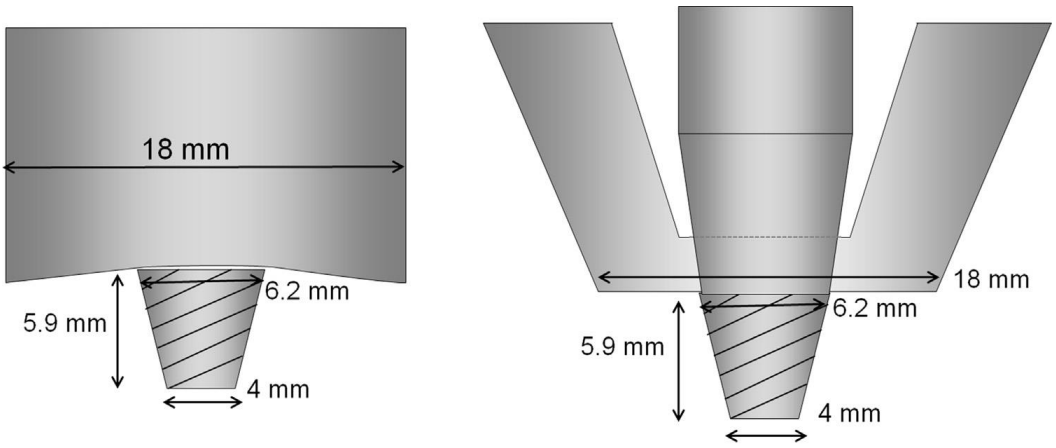

Figure 3 – Schematic diagrams of the FSW tool (on the left) and the SSFSW tool (on the right) (Wu et al, 2015).

Since the shoulder is stationary, most of the heat comes from the probe rotation, keeping the shoulder with little contribution. This is an advantage because the torque applied is reduced, which means that it is possible to obtain a smoother surface, considering that the shoulder is just sliding on the surface and contributes to soften the material close to the stirred zone. The heat input is now localized close to the probe, and it is uniformly distributed through the thickness, which improves the process's stability and reduces the chance of surface overheating (Ahmed et al, 2010). Even if more conductive material would be welded, like aluminium alloys, the SSFSW process can still be advantageous. When the rotational movement comes only from the probe, a narrower parallel through-thickness thermal field is expected, which reduces the heat affected zone width, as well as the material distortion (Li et al, 2015).

High strength 7000 series aluminum alloys are widely used in structural conditions in aircraft and aerospace structures. Along with 2000 series aluminum alloys, which are known to be damage tolerant, it is difficult to weld these materials using fusion welding techniques because of the crack sensitivity and severe mechanical property decrease. Nevertheless, SSFSW has a great potential of welding these two materials without facing the fusion-welding processes' issues (Li et al, 2015). Although SSFSW presents unique capabilities compared to the conventional FSW, limited work has been published, especially studies about SSFSW of 2000 or 7000 aluminium alloys. Due to a technical issue regarding the probe and the shoulder, there are just a few research studies about SSFSW. A small part of the plasticized material tends to flow to the space between the probe and the stationary shoulder, creating additional friction and increasing pressure on the tool. With the high torque coming from the machine's spindle and the accumulation of material on that interface, premature failure of the tool can happen and it is generally an overheating of the entire tool system (Barbini, 2014).

2.2 Comparison between SSFSW and conventional FSW

Studies were made about a comparison between the two processes, and have proposed a proper approach for directly comparing both processes based on their power-rotation rate curves, and later, selecting the best welding conditions (Wu et al, 2015). High strength AA7050-T7651 aluminium alloy was the chosen material for performing the welds.

The study had come up with the following conclusions:

- A non-rotating shoulder reduced significantly the power dissipated by the tool;
- Stationary shoulder welding requires 30% lower heat input than conventional FSW;

- Welding with a stationary shoulder produced welds with a narrower, more parallel, HAZ and smoother gradients of mechanical properties;
- Stationary shoulder welds performed better than FSWs in cross-weld tensile tests;
- The ironing effect generated by shoulder deeply reduced the weld's surface roughness.

Despite the present conclusions are good, a negative effect was also found out. Welding with a non-rotating shoulder can lead to 'speed cracking' like that found in extrusion under hot welding conditions, which is a longitudinal crack on the surface formed by either very high rotational or welding speeds.

2.3 Welding Techniques

To understand the SSFSW process, a study was performed at the TWI Technology Centre about the different techniques of SSFSW (Martin, 2013). It was reported that the new welding tool had the potential to weld plates mounted in different configurations, such as T-joints, by using a non-rotating shoulder, as well as adding material to fill the gaps between the parts to be welded, using approaches that were not possible to use with conventional FSW. The new techniques performed by SSFSW are presented below.

2.3.1 Corner SSFSW Joints

This technique is also known as fillet welding. The welding mechanism consists of a probe rotating on a stationary shoulder that approaches the internal corner of the T-shaped plates. Figure 4 shows a scheme of fillet welding applied to a T-joint configuration.

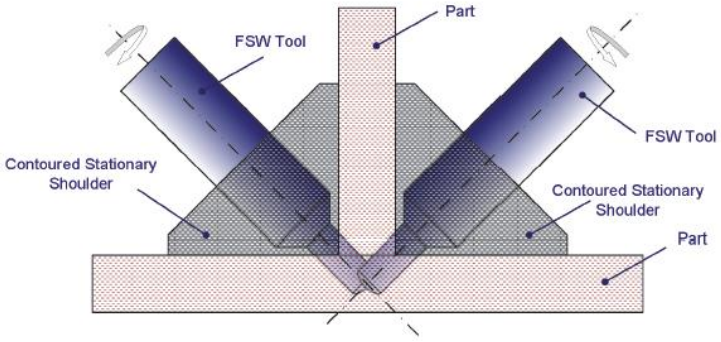

Figure 4 – Schematic of T-joint using corner SSFSW (Martin, 2013).

Experiments shown that, using the fillet weld technique, typical benefits obtained by SSFSW were achieved. However, the internal corners presented a sharp edge, creating a potential fatigue crack initiation problem.

2.3.2 Corner AdStir Fillet SSFSW Joints

To overcome the sharp edges issue, a wire-shaped filler material was added. The new solution aims to minimize the stress concentration located on the sharp edges, by creating a radius between the plates, thus extending the fatigue life of the joint. Figure 5 shows a scheme of AdStir fillet welding applied to a T-weld specimen and evidencing the radius created to minimize the fatigue crack growth.

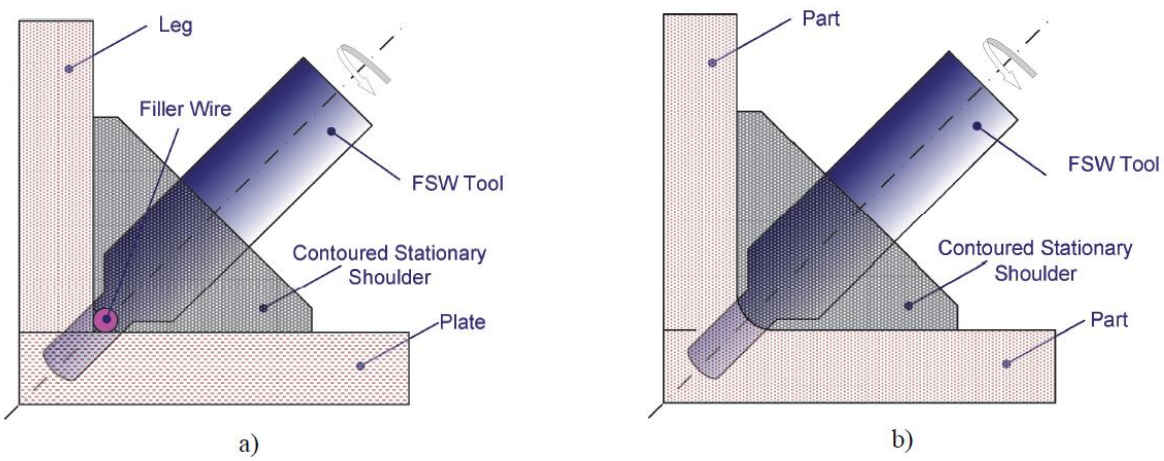

Figure 5 – Schematic of Corner AdStir Fillet SSFSW: a) Before welding and b) After welding (Martin, 2013).

2.3.3 AdStir Butt-Joints with gaps

The solution of adding a filler material to overcome the potential fatigue issues had been also introduced on butt-joints configurations. The configuration is very similar to the well-known butt-joint but, in this case, it was stated that the AdStir technique can weld together plates which contain a gap up to 16 % of plate's thickness without undercutting it. Figure 6 exhibits a scheme of AdStir butt-joint welding applied to a butt-joint configuration.

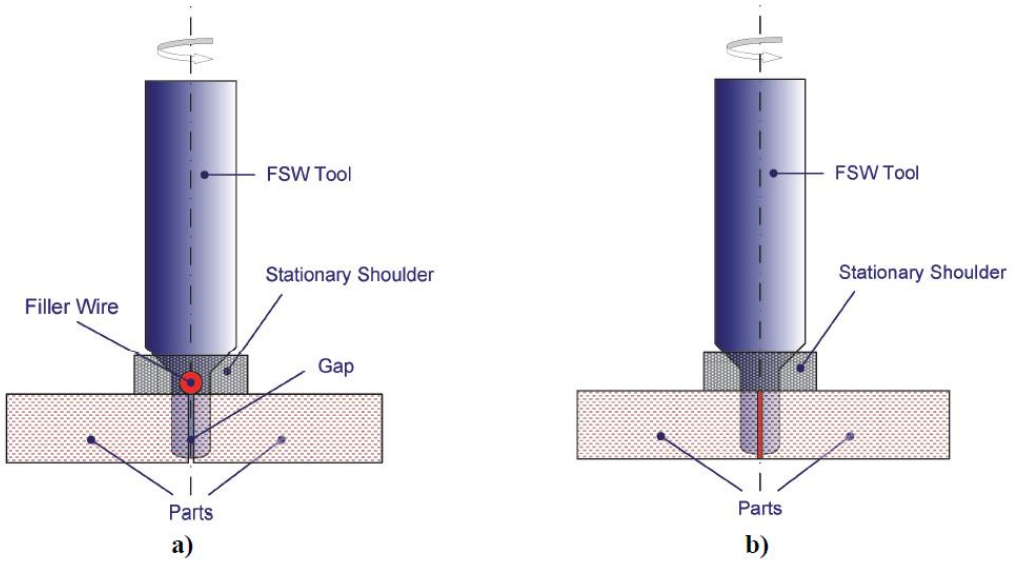

Figure 6 – The AdStir principle applied to butt-joints: a) Front of the tool and shoulder and b) Rear of the tool and shoulder (Martin, 2013).

The butt-joints welds with AdStir principle also presented the typical characteristics of a non-rotating shoulder welds:

- Excellent component surface finish;
- Low distortion;
- No 'undercutting' of the component top surface;
- Lower heat input.

2.3.4 AdStir Deposition

Similar to the AdStir butt-joints with gap, as material could be added to the weld, it raises up the opportunity for depositing material on top of the surface. The non-rotating shoulder was designed to have a chamber inside that can hold a filler wire at the front. As the material is stirred with the plates, it is then forged and extruded trough the shoulder's exit creating a shaped bead. A deposit on the joint may have applications of creating crack arrestors or strengthening ribs on panels. Figure 7 shows a scheme of AdStir deposit welding, evidencing the shaped bead.

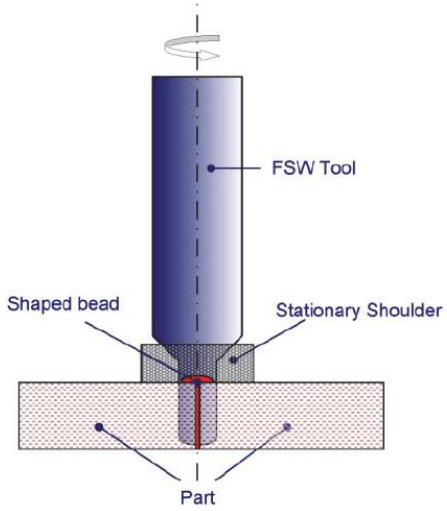

Figure 7 – Schematic diagrams of the AdStir deposition technique (Martin, 2013).

2.4 Introduction to T-joints

T-joints have been used as a reinforcement of aircraft fuselages and railway cars, among other applications that require high stiffness and low weight. It is an important material configuration when improved strength, lightweight structures and optimized inertia are needed. Welding aluminium alloys with a T-joints configuration using fusion welding techniques would bring problem of high residual stress and distortion due to high temperatures. FSW is an alternative candidate for replacing the fusion welding techniques to fabricate better T-joints, as it was evidenced on a study about T-joints optimization (Silva et al, 2013). They performed a study about the optimization of friction stir welded T-joints using the Tagushi method, and the optimization method was performed for AA6082-T6 aluminium alloys, and the following topics sum up the study's remarks:

- For the optimized T-joints, the rotational speed was the most significant influent parameter in tensile properties;
- The welding speed does not present a significant influence on the mechanical properties of the joint, when optimal results were achieved;
- High rotational speeds lead to high temperatures, which enables metallographic modifications, therefore mechanical properties decreased;
- Low rotational speed lead to insufficient heat required for plastic deformation, as well as high welding speed.

Although these remarks were drawn on a specific study, some of them were spotted on this work's experiments, meaning that some conclusions are inherent to the T-joints weld configuration.

3 Experimental Procedure

As it was mentioned previously, the aim of this dissertation is to determine the best T-joint configuration, manufactured by stationary shoulder friction stir welding. Several panels were welded using a CNC-controlled gantry machine with a spindle entirely designed for FSW. Later, microstructural analysis, static tests and fatigue tests were performed to understand the influence of process parameters on the microstructure and the mechanical performances of the joints.

In this chapter, the manufacturing of panels, as well as testing procedure, will be presented, including a short description of the machines involved in the process and which tests were performed.

3.1 Equipment's description

T-joint welds were performed at the HZG facilities, specifically at the Solid State Joining Process department (WMP), using the FSW Robotic Gantry T9000, a 5 degrees of freedom welding machine.

Since there are a lot of different welds carried by this machine, proper specimen identification is a must. All the specimens performed within this dissertation have been identified according to this designation rule: the first group of letters are related with the type of welding process, the second group identifies which machine was used to perform the welds, a third group indicates the welds' author, and finally, the last group of digits are numbers corresponding to the amount of welds performed on the specified machine. As an example, one of the welds performed at WMP facilities (SSFSW-T9G-AB-154) is identified as:

- SSFSW – Stationary Shoulder Friction Stir Welding;
- T9G – Robotic Gantry T9000;
- AB – Alessandro Barbini;
- 154 – notch-skin weld, with 5 mm/s and 800 RPM as parameters.

This designation, used at the WMP department, is very important; since it is critical to keep the specimens' nomenclature well organized. Therefore, throughout this document, this designation will be always present. The specimen identification table can be found in this document on the annex A.

3.1.1 Specifications

The T9000 robot is used for friction stir welding. The processes can be performed under position or force control. Process parameters like torque, axial force and in-plane forces can be recorded while the weld is performed. The T9000 consists on a moveable gantry, a moveable tricept-module (three linear actuators, one sliding tube, and wrist), a spindle, a table and the control desk. In general, the T9000 robot is used for machining large parts for the

railway industry (Carstensen et al, 2015). For the welds, the linear movement has been provided by the gantry, to increase the system's stiffness.

The gantry machine is presented in Figure 8, including a list of the main components.

Figure 8 – T9000 robot (Carstensen et al, 2015).

T 9000 main components:

- 1. Gantry;
- 2. Linear actuator;
- 3. Sliding tube;
- 4. Wrist;
- 5. Spindle;
- 6. Table;
- 7. Control desk.

The machine's technical data is presented next:

- Actuator stroke: 1 m;
- Actuator acceleration: 4 m/s²;
- Actuator velocity: 24 m/min;
- Actuator force continuous: 20 kN;
- Actuator force peak: 40 kN;
- Axis 4 rotational angle: 640 °;
- Axis 4 rotational acceleration: 715 °/s²;
- Axis 4 rotational velocity: 145 °/s;
- Axis 4 torque continuous: 1961 N·m;
- Axis 4 torque peak: 4900 N·m;

- Axis 5 rotational angle: vertical=0 ° – 55 °;
- Axis 5 rotational acceleration: 400 °/s²;
- Axis 5 rotational velocity: 90 °/s;
- Axis 5 torque continuous: 980 N·m;
- Axis 5 torque peak: 2450 N·m;
- Wrist axial thrust: 60 kN;
- Wrist radial thrust: 15 kN;
- Weight: 220 kg;
- Number of revolutions: 6000 1/min;
- Torque: 90 N·m;
- Tool diameter: 2 mm – 25 mm;
- Axial stroke for force control: 20 mm;
- Table's dimensions: 6×2,4 m²;
- Gantry's travel: 6×2 m² (Carstensen et al, 2015).

3.1.2 Clamping System

The clamping system plays a critical role on the welds performance since there are significant loads involved in the process. A strong mechanical clamping system was set to ensure the correct plate's placement. Since there is a considerable force applied on the welding direction, there is the need to fix the parts horizontally by forcing the plates against the working table, to prevent sheet displacement during the process. Also, for the 3-parts weld configuration, there is the need to fix the plates transversally, so that it would avoid a gap opening.

A clamping system like the one presented in Figure 9 was applied on each weld to avoid sheet metal bending, lack of penetration, porosity, among other types of weld defects.

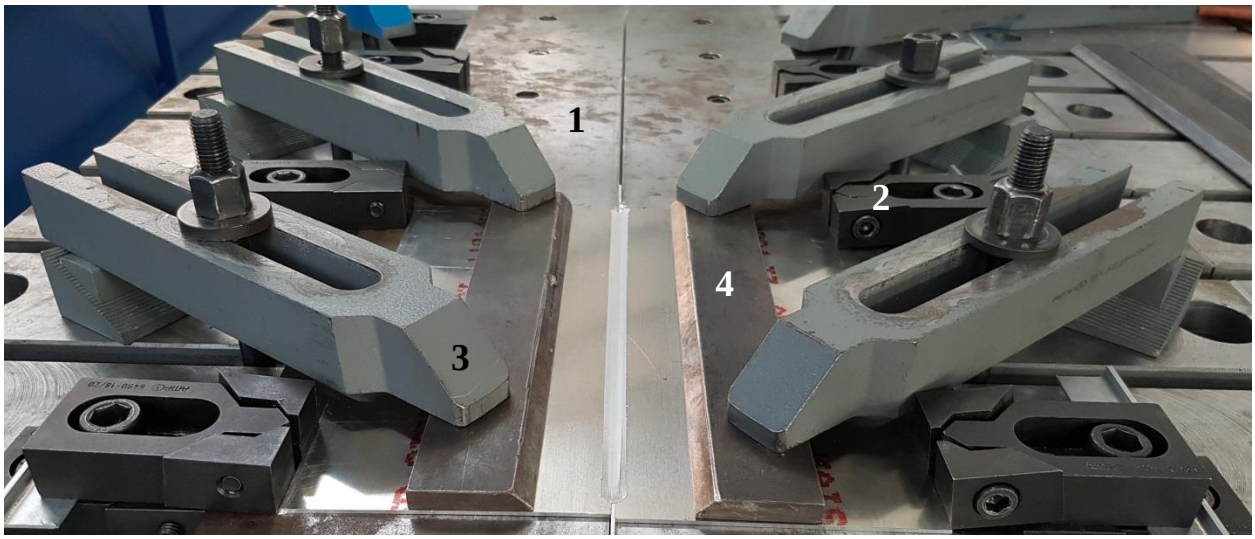

Figure 9 – Clamping system.

This system is composed of the following items (see Figure 9):

- 1. Backing bar, made of steel – the basis component where the skins and stringer are positioned and act as an anvil for the forming process;

- 2. Horizontal adjustable steel blocks – in the notch-skin welds, they fix the position of the backing bars, and in the 3-parts welds, another group of blocks are installed to hold the skin horizontally;
- 3. Vertical mounting adjustable steel blocks, fork shape – to hold the specimen against the backing bars;
- 4. Steel bars – To ensure that the vertical clamping force is spread uniformly across the skins, since this is the major load applied on the specimen.

3.1.3 SSFSW Tool

The tool and its geometry play a critical role in the process. Their main objectives are to generate the heat necessary for the process, produce the material stirring with consequent plasticized flow and keep the stirred material in the correct position to realize the joint (Barbini, 2014). Unfortunately, the technical drawings of probe and shoulder are not presented here, due to trade secret. The probe is directly connected with the spindle, and bypasses completely the shoulder, since this doesn't rotate and it is bolted with a static flange. The configuration of stationary shoulder and probe is presented in Figure 10.

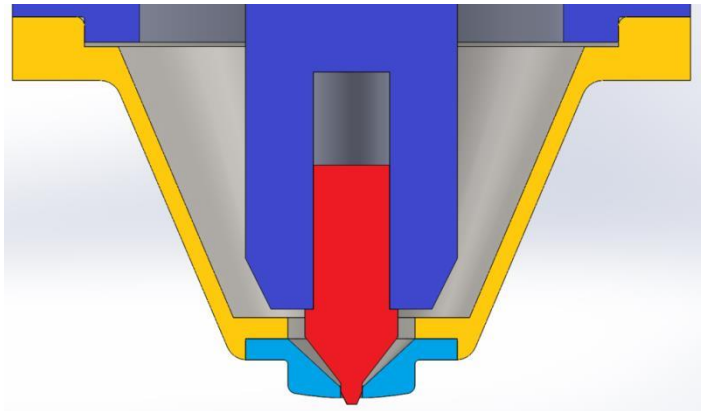

Figure 10 – Stationary shoulder and probe configuration (Barbini, 2014).

The probe is made of MP159™, a nickel-cobalt based alloy that was heat-treated to increase strength and durability. This alloy is used on components that require high tensile strength, such as prosthetic devices, jet engine components, fasteners, marine applications and petroleum industry applications (D, 2016). It presents a taper angle of 22,60 °, and a maximum diameter of 5 mm. It also presents three flat areas to increase the material stirring, as it acts as a velocity gradient. Table 1 shows its chemical composition and Table 2 shows its mechanical properties after the heat-treatment.

Table 1 – Chemical Composition of MP159™ (Unit D, 2016).

Element	Ni	Co	Cr	Fe	Mo	Ti	Cb	Al
Weight %	25,5	35,7	19,0	9,0	7,0	3,0	0,6	0,2

Table 2 – Mechanical properties of MP159™ (Unit D, 2016).

Tensile strength [MPa]	Yield strength [MPa]	Elongation [%]	Reduction of area [%]
1586	1413	12	46

The shoulder is made of chromium-molybdenum-vanadium alloyed tool steel, commercially known as Unimax™. This material was designed for cold work tooling operations such as cold forging, blanking or thread rolling, where chipping resistance is required (AB, 2015). Table 3 shows its chemical composition and Table 4 shows its mechanical properties at room temperature. The shoulder contributes to the process by keeping the material in position. For this reason, it has a flat area of 8 mm of diameter, along with a concave part of radius 60 mm to reduce the friction.

Table 3 – Chemical Composition of Unimax™ (UDDEHOLM, 2015).

Element	C	Si	Mn	Cr	Mo	V
Weight (%)	0,5	0,2	0,5	5,0	2,3	0,5

Table 4 – Mechanical properties of Unimax™ (UDDEHOLM, 2015).

Tensile strength [MPa]	Yield strength [MPa]	Elongation [%]	Reduction of area [%]	Hardness [HV]
2050	1720	9	40	576

3.2 Material characterization

This work aims to produce dissimilar welds on a T-joint configuration, using SSFSW as manufacturing process. All T-joint configurations are composed by a skin made of AA2024-T3 and a stringer made of AA7050-T651, as a common combination of materials typically found on civil aircrafts (Dursun & Soutis, 2013). It should be stated that this work is a continuation of the previous work reported on Barbini's MSc thesis (Barbini, 2014), meaning that the materials and manufacturing technology are the same.

Currently, the 7000 series aluminium alloys are used where the main limiting design parameter is strength and the 2000 series aluminium alloys are used for fatigue applications, since these alloys are more damage tolerant (Dursun & Soutis, 2013).

3.2.1 AA 2024-T3

The 2000 series aluminium alloys have been widely used in fuselage construction, normally where the main criteria is damage tolerance. The 2000 series alloys, containing magnesium and copper, have superior damage tolerance and good resistance to fatigue crack growth when compared to other series of aluminium alloys. AA2024 is a common example for Al–Cu–Mg 2000 series alloys (Dursun & Soutis, 2013).

The 2024 aluminium alloy has been used as an aircraft structural material because it has very high damage tolerance and because it is very resistant to fatigue crack growth, when tempered at T3-aged condition (Dursun & Soutis, 2013). However, the presence of copper in high amounts is detrimental for the corrosion resistance (Barbini, 2014). Table 5 and Table 6 present the chemical composition and mechanical properties of AA2024-T3, respectively.

Table 5 – Chemical composition of AA 2024 (%) (Dursun & Soutis, 2013).

Cu	Mg	Mn	Fe	Si	Cr	Ti	Al
4,4	1,5	0,6	≤0,5	≤0,5	0,1	0,15	Remainder

Table 6 – Mechanical properties of AA2024-T3.

Density [g/cm^3]*	Hardness [HV]**	Yield Strength [MPa]**		UTS [MPa]**		Elongation at break [%] **	Modulus of Elasticity [GPa]**	Fracture Toughness, K_{IC} [MPa·m$^{1/2}$]*
2,78	134	L	T	L	T	20,15	72,5	37
		379	319	487	474			

*Literature (Barbini, 2014)

** Tested by Anne Groth (WMF, HZG)

The term T3 following the aluminium alloy identification number indicates the type of heat treatment applied to the aluminium alloy, which in this case, T3 represents "Solution heat treated, cold worked, and naturally aged to a substantially stable condition" (Barbini, 2014).

3.2.2 AA 7050-T651

The 7000 series alloys present higher strength when compared to other aluminium alloys series. These alloys are used for producing parts when compressive strength and the fatigue resistance are the main design parameters, such as upper wing skins, stringers and stabilizers (Dursun & Soutis, 2013).

Just like the 2000 series aluminium alloys, the 7000 series alloys are also heat treatable. Although these alloys are susceptible to corrosion due to their compositions (Barbini, 2014), some 7000 series alloys contain copper that, in combination with magnesium and zinc, provide the highest strengths of all aluminium alloys (Dursun & Soutis, 2013).

Table 7 and Table 8 present the chemical composition and mechanical properties of 7050-T651, respectively.

Table 7 – Chemical composition of AA 7050 (%) (Dursun & Soutis, 2013).

Cu	Zn	Mg	Fe	Si	Zr	Al
2,3	6,2	2,25	≤0,15	≤0,12	0,1	Remainder

Table 8 – Mechanical properties of AA7050-T651 (Barbini, 2014).

Density [g/cm^3]*	Hardness [HV]**	Yield Strength [MPa]*	UTS [MPa]*	Elongation at break [%]*	Modulus of Elasticity [GPa]*	Fracture Toughness, K_{IC} [MPa·m$^{1/2}$]*	
2,83	158	490	552	11	71,7	L	T
						30,8	26,4

*Literature (Barbini, 2014)

**Measured at WMP, HZG

The T7651 following the aluminium alloy identification number indicates the type of heat treatment, and in this case, it means "Solution heat-treated, stress relieved by stretching a controlled amount and then artificially over aged in order to achieve a good exfoliation corrosion resistance. The aluminium receives no further straightening after stretching" (Barbini, 2014).

3.3 Weld configurations

In the current study two different welding configurations have been analyzed: notch-skin welds, see Figure 11, and 3-parts welds (3P), see Figure 12. The notch-skin configuration is characterized by a notch located in the skin with a depth of 0,5 mm and a width of 1,6 mm (equal to the stringer's thickness) that was realized by milling, so that the stringer can be inserted. The 3-parts configuration consists on joining two separated skins of AA2024-T3 with the stringer in the middle, placing the stringer top surface at the same height as the skins.

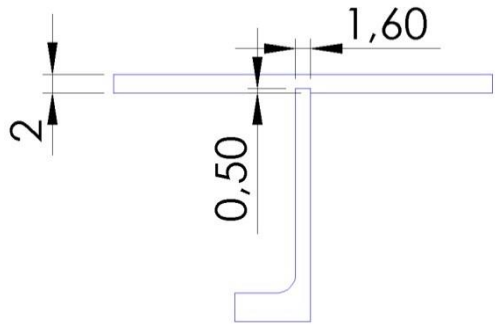

Figure 11 – Notch-skin configuration [mm].

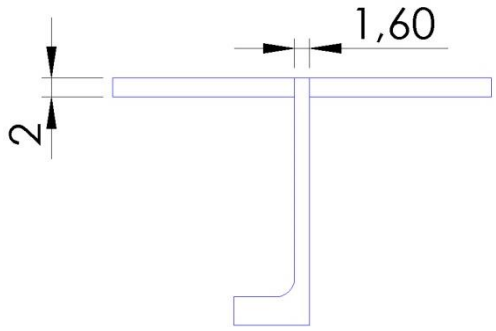

Figure 12 – 3-Parts configuration [mm].

In the case of the notch-skin weld configuration, the study has been performed by welding the two parts in a single time (single pass) or in two consequent steps (double pass). For the single pass (SP) welds, the probe was centered in the middle of the stringer, while for the double pass (DP) welds each weld was located on the direction of the vertical interface between the stringer and the notched-skin, as shown in Figure 11. The justification for having these two weld passes is to avoid having an un-welded line at the corner between the skin and stringer, as it is evidenced in Figure 13. In the 3-parts welds, only SP welds were performed due to the impossibility to develop such a type of defect for this kind of configuration.

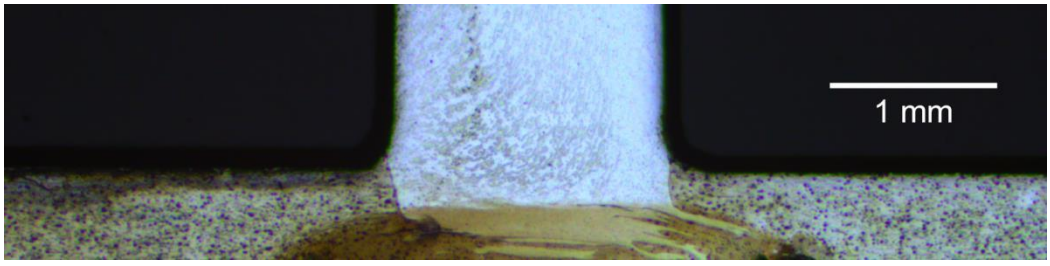

Figure 13 – Detail showing an un-welded line.

3.4 Experimental approach

Previous work was focused on defining a parameter window in terms of feasibility of the process. The first step of this work is the parameter study, which consists in finding out the correlation between process parameters and joint performance in terms of microstructure and strength for the three different T-joint configurations. Four main characterizations were performed to obtain the T-joints' microstructural configuration and mechanical properties. The second step is a comparison between the three different processes in terms of best mechanical performance, according to the best parameters' set found for of each weld. Later, when the parameters are known, fatigue tests will be performed in order to determine the fatigue life of the welded panels and final comparison with the current solution.

The tasks incorporated on the working plan are valid for all welding configurations: Notch-skin welding and 3-parts welding. The experimental method is schematically presented in Figure 14.

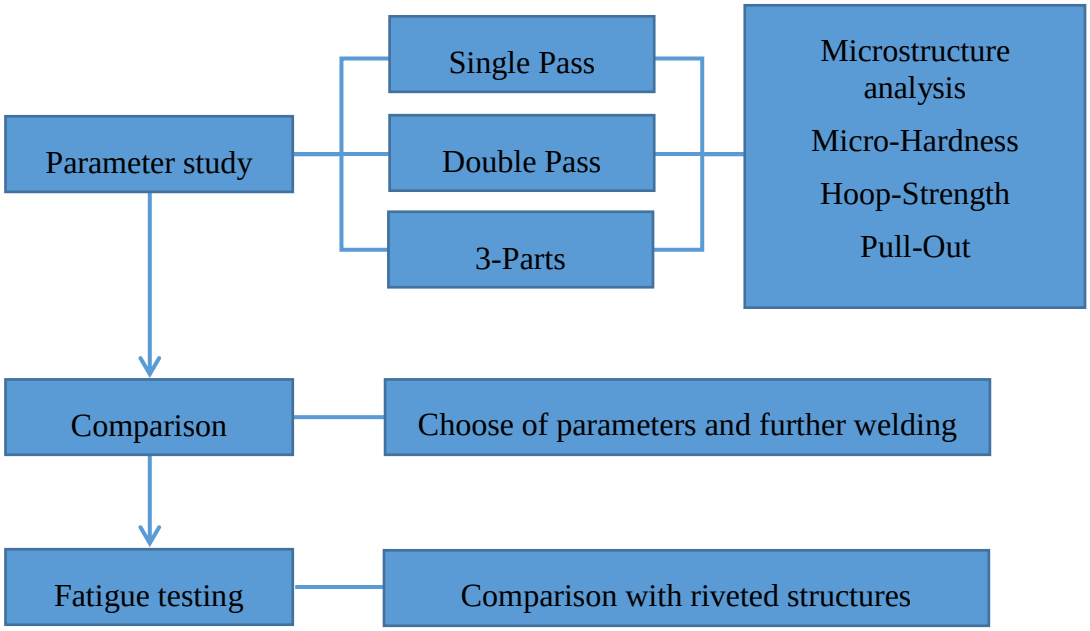

Figure 14 – Working Plan.

Unfortunately, the working plan had suffered a few changes throughout the study. Due to experiments' delays, lack of machine availability, and specimen processing and machinery, fatigue testing were not performed and further comparison with riveted structures could not be done. So, on this report, it is presented the manufacturing process, material characterization, parameter study, and comparison among the different T-joint configurations. A brief note on fatigue testing is presented on the subchapter Future work perspective.

3.5 Experimentation

In order to understand the mechanical behaviour of the T-joints created by stationary shoulder friction stir welding, microstructure analysis and three mechanical tests were performed: hoop-strength, pull-out and micro-hardness. The obtained results were later correlated with the specimens' microstructure, and each test is presented in detail below.

For each welded panel, a specific cutting plan was created that fits every specimen. The cutting plan is presented in this report on the annex B.

3.5.1 Welding parameters

All the welds were performed in position control. The main weld parameters are: tilt angle; probe length; plunge depth; welding speed and rotational speed. For the manufactured specimens for the first group of tests, Table 9 presents the specimens' identification according to the weld parameters that were varied for these tests: welding speed (WS) and rotational speed (RS). This parameters variation came out of the previous parameters' window defined at the facilities of WMP. For the mechanical testing experiments, a total of 18 welds were performed. The rest of the parameters were already fixed and they are presented below:

- Tilt angle – 2 °;
- Probe length – 1,9 mm;
- Plunge depth – 2,05/2,1/2,15 mm.

Table 9 – Parameter window for mechanical testing.

Parameters	Rotational Speed [RPM]	800		1000		1200		
	Welding Speed [mm/s]	5	7	5	7	5	7	3*
Notch-skin	SP	154	155	156	157	158	159	160
	DP	161	162	163	164	165	166	167
3-parts SP		172			171	173		170

*The set of parameters (3 mm/s of welding speed and 1200 RPM of rotational speed), with the best results obtained on Barbini's MSc thesis (Barbini, 2014), have been used as a reference for all the process variants.

3.5.2 Samples preparation

Before presenting the procedure of the mechanical tests, it is appropriate to state that, for the case of micro-hardness tests and the metallographic analysis, the samples had to be prepared to perform micro-indentations and to be analyzed on the microscope, respectively. Small samples (cross section of 15 mm × 40 mm) from the welded panels were cut and embedded (cured in a pressurized vessel of 2 bars at room temperature) in a 50 mm diameter mold using Demotec 20™, Demotec 30™ or EpoxyCure™ 2. Later, the samples were grinded and polished with the help of automatic polishing machines, following a specific grinding/polishing set of discs and cloths tailored to aluminium alloys. The automatic machines are exposed in Figure 15 and Figure 16, respectively, and the grinding/polishing preparing steps are presented in Table 10.

Figure 15 – Struers TegraPol-31 polishing machine.

Figure 16 – Struers Tegramin-30 polishing machine.

Table 10 – Sample preparation steps.

Step		Disc or cloth	Lubricant	Time [min]
1	Grinding	SiC-Paper #320 µm	Water	1
2	Polishing	Largo	Diamond Pro 9 µm	5
3		Dac	Diamond Pro 3 µm	5
4		Chem	OP-S 1 µm	3

3.5.3 Microstructure analysis

Metallographic analysis was performed to observe the metal interlocking between skin and stringer, to evidence the grain size of each specimen, to understand the different welded zones and to check if there were any defects or cracks in the welds. Microstructure's observations were performed by a Leica Microsystems™ microscope, using a 100X zoom lens. The Heyn Linear Intercept Procedure was adopted to measure the average grain size. These experiments were performed according to the standard ASTM E112 – 12 (ASTM, 2013) .

3.5.4 Micro-Hardness tests

Micro-Hardness tests were performed to evidence the differences in hardness from base material to the different welded zones. These measurements were performed using a Zwick/Roell Indentec™ micro-hardness machine, using a plunge time of 10 seconds, and a 2 N load (HV 0,2). The samples were fixed with the help of a sample holder to avoid any movement during the indentation. The machine is shown in Figure 17. These experiments were performed according to the standard ASTM E384 (ASTM, 2010).

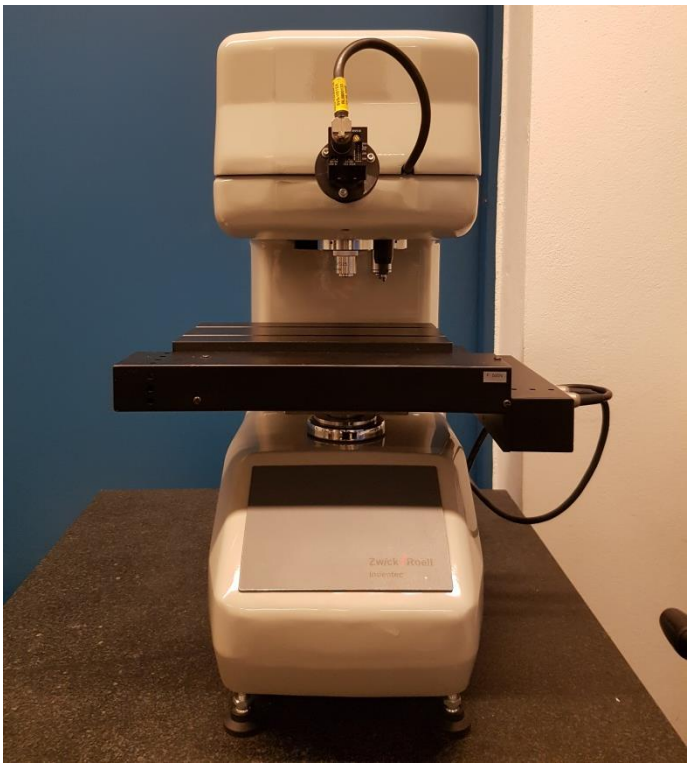

Figure 17 – Micro-Hardness machine.

Two perpendicular indentation lines for each specimen were performed, one horizontal and another vertical, to account for the hardness variations in the skin and in the stringer direction respectively. Table 11 shows the number of indentations and positioning. Figure 18 presents a scheme of the indentation lines and specimen drawing, as well as the path direction.

Table 11 – Number of indentations and positioning.

Orientation	Horizontal	Vertical
Space between indentations [mm]	0,4	0,4
Number of indentations	76	15
Starting point [mm]	-15	-0,6
Ending point [mm]	15	5
Total length [mm]	30	5,6

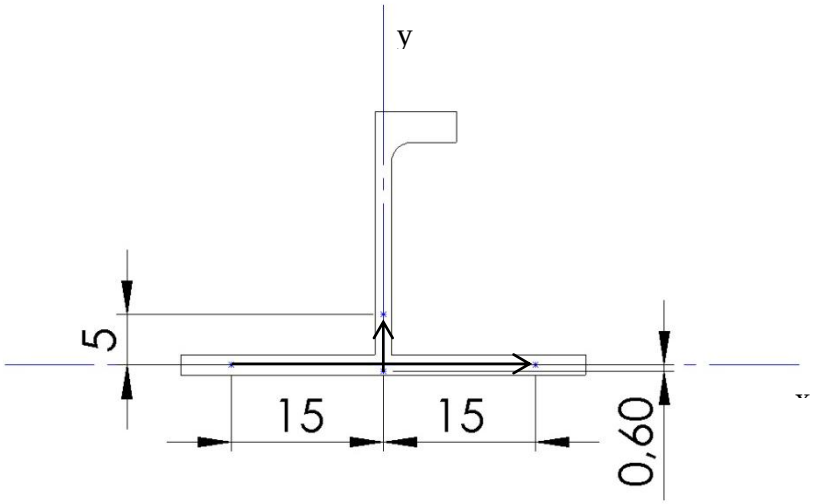

Figure 18 – Positioning scheme [mm].

3.5.5 Hoop Strength tests

Hoop-Strength tests were performed to understand the ultimate strength of the welded T-joint on the circular direction of an aircraft fuselage. These experiments were performed on a Zwick/Roell testing machine with a load capacity of 100 kN, and an extensometer with a gage length of 50 mm was applied to measure the elongation. Tests were performed at room temperature, 21 °C to be precise, with a constant travel speed of 1 mm/min. Figure 19 shows the machine used for these tests.

Figure 19 – Zwick/Roell universal tensile machine.

In total, four tests per each analyzed parameter were performed. Even if no standards were available for the hoop-strength experiments, the flat part of the specimens were realized according to the standard ASTM E8, for tensile testing. A pair of universal clamping system (with clamping blocks made of steel) was used and the tests consisted of pulling both extremities of the skin. Figure 20 shows a scheme of the experiment, evidencing the pulling direction and the clamping blocks. The vertical mounting indicates that the experiment would bring up the ultimate rupture force correctly, since no bending would occur in the specimen. So the results obtained are trustful.

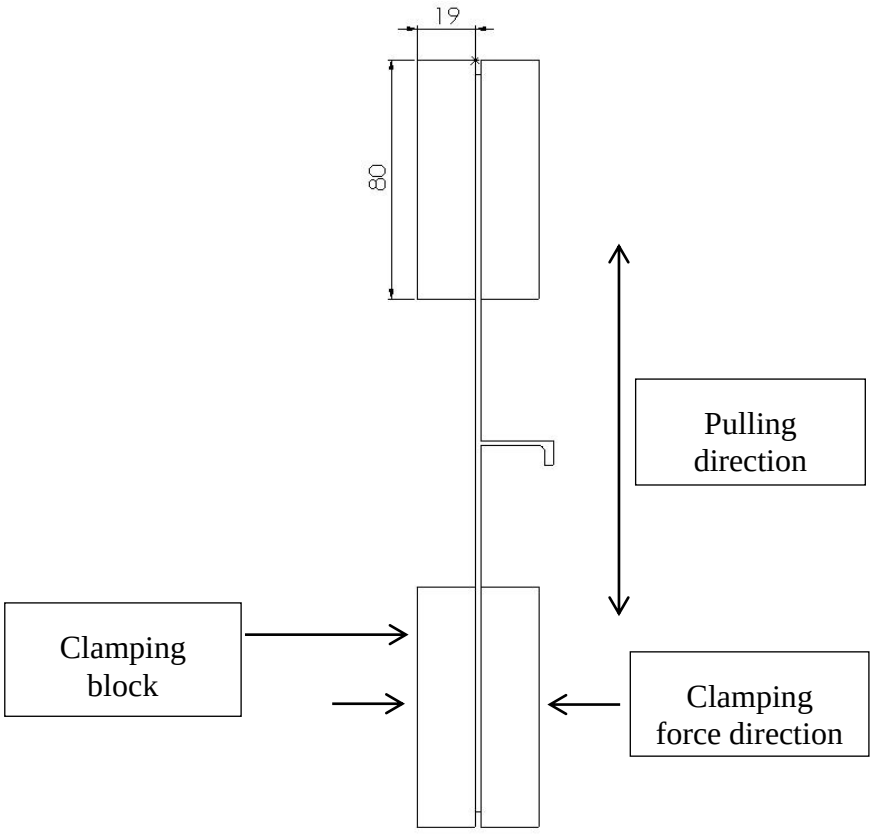

Figure 20 – Hoop-strength test scheme [mm].

3.5.6 Pull-Out tests

Pull-Out tests were performed to evaluate the ultimate strength of the welded T-joint on the stringer direction. Four specimens per each set of parameters investigated have been used as in the case of hoop-strength. Even if this is not a standard load case for aeronautical structures, it provides an insight on the bounty of the weldments since the force is applied directly in the welded zone. These experiments were performed using the same machine used for hoop-strength experiments (see Figure 19). Again, tests were performed at a temperature of 21 °C with a constant travel speed of 1 mm/min.

Just like the hoop-strength tests, there are no standards for this specific test, so there was a certain freedom in performing the experiments, and the way the specimens were clamped to the machine. The setup scheme is shown in Figure 21.

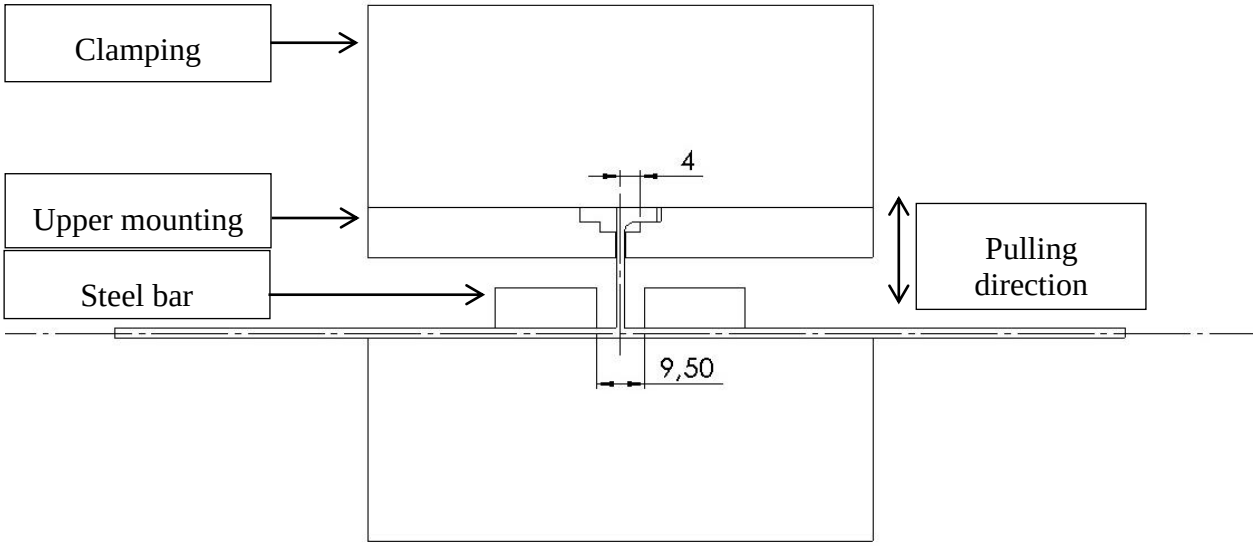

Figure 21 – Pull-Out scheme [mm].

To fix the specimen, an upper mounting plate made of steel was machined, with a notch to slide trough the stringer's flange. This upper mounting was bolted to the machine's testing basis. On the other side, the skin was fixed to the lower part of the machine, by bolting down two steel bars. The distance between the bars has been set at 9,5 mm to minimize the bending of the skin.

Although this was the best solution found to perform the tests, it is clear, by observing the testing scheme (Figure 21), that there are two parameters that inconveniently influence the test procedure. The "4 mm" distance between the mounting plate and the stringer web causes a bending load on the stringer flange, as the stringer is pulled out from the skin.

The second issue is the "9,5 mm" distance between the bars, which leads to skin bending as the stringer is pulled out. There is a local momentum that was unintentionally created, thus influencing the results obtained. Figure 22 evidences this bending issue obtained from a pull-out experiment (one specimen from the weld SSFSW-T9G-AB-170). It must be noticed that a similar test on a riveted structure would cause a higher amount of bending load on the joint due to the impossibility to clamp the specimens so close to the stringer itself.

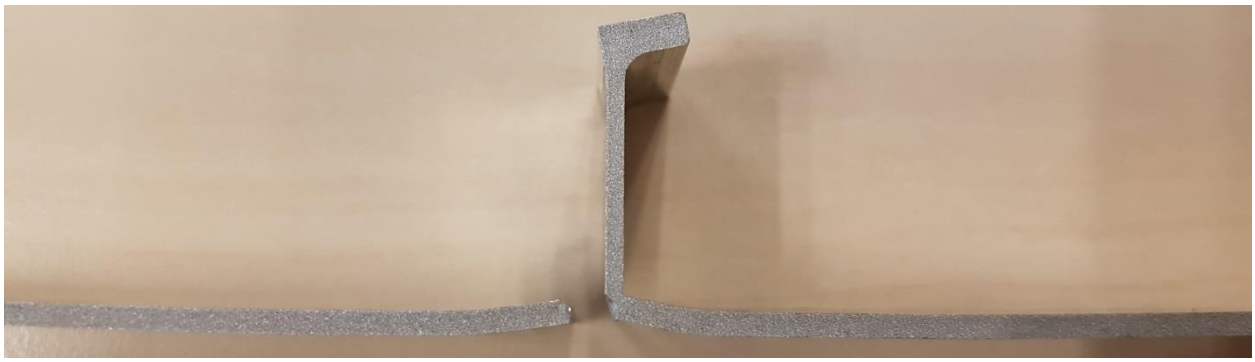

Figure 22 – Bending issue obtained by local momentum unintentionally created.

4 Results and Discussion

Results from all the experiments will be presented and discussed in this chapter. First, the results from the parameter study are presented and discussed to understand how the parameters are affecting the specimens' mechanical properties; then, a comparison between the three weld configurations is presented to evidence which welding parameters are giving the best mechanical performance.

All the results were processed using the computer software Origin 2016 (Corporation, 2016), in terms of calculations, tables and plotted graphs. Again, since a lot of testing was put through, the specimen' identification table is attached after the chapter References to be consulted.

To characterize the specimens, three experiments have been performed: micro-hardness tests, hoop-strength tests and pull-out tests. The specimens' microstructure was also analyzed to evidence the way the grains were stirred and grain size measures were performed. The results are shown per type of T-joint to present a single overview of each configuration. For hoop-strength, micro-hardness and pull-out experiments, as well as grain size measurements, test results are presented in graphs, followed by a brief explanation on the influence of changing parameters on mechanical properties. For the obtained microstructures, figures of specimens are presented per each welding parameters.

For the hoop-strength and pull-out tests, additional studies were performed. The hoop-strength results were later compared with the interface angle between the different materials. The interface angle is the angle between the skin direction and the interface between both materials. The pull-out results were later compared with the interface length between the different materials. The interface length was established has a visible and measurable length presented on the side view of the specimen, between the AA2024-T3 and the AA7050-T651.

4.1 Notch-skin single pass welds – SP

4.1.1 Microstructure analysis

4.1.1.1 General overview

The following tables stand for the single pass specimen's microstructure according to its welding parameters, grouped by the same rotational speed. Below, a brief explanation about the microstructure with the parameters is presented.

Table 12 – Microstructures obtained at 800 RPM of rotational speed.

5 mm/s	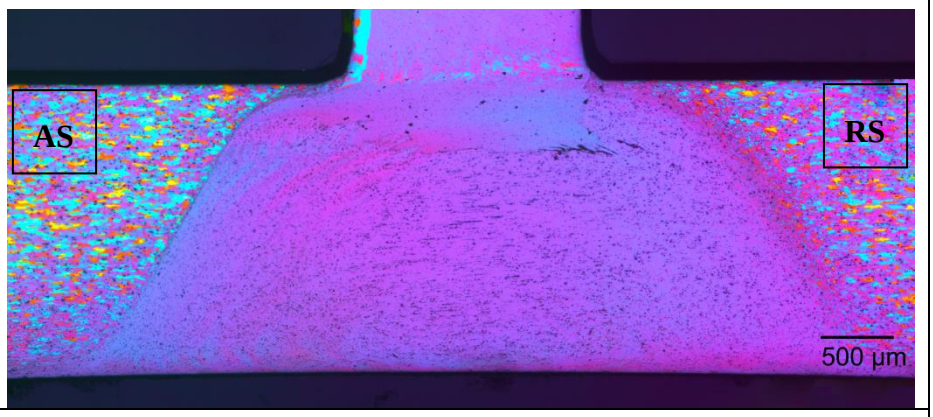
7 mm/s	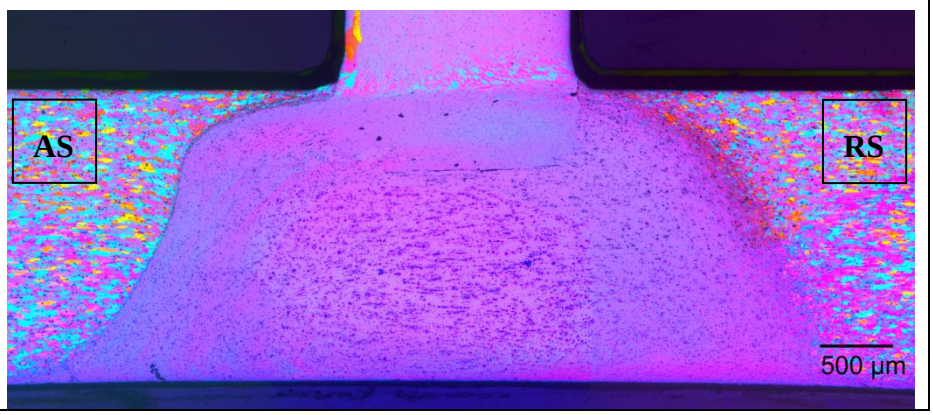

Table 12 presents the microstructure of the two SP specimens that were welded with 800 RPM of rotational speed. In first place, because this was expected in all microstructures, it is easy to identify the advancing side and the retreating side. When the welding speed is increased, the SZ appears to shorten up. This happens because, as the welding speed is increased, the probe has less time to stir the material to provide a good metal interlocking.

With a higher welding speed, it is clearer the presence of a non-welded area, which has derived from the notch horizontal surface. This means that the connection between the skin and the stringer is weaker. Also, the TMAZ looks thinner, as the grain size change between the BM and the SZ is sharper when the welding speed increases.

Table 13 – Microstructures obtained at 1000 RPM of rotational speed.

5 mm/s	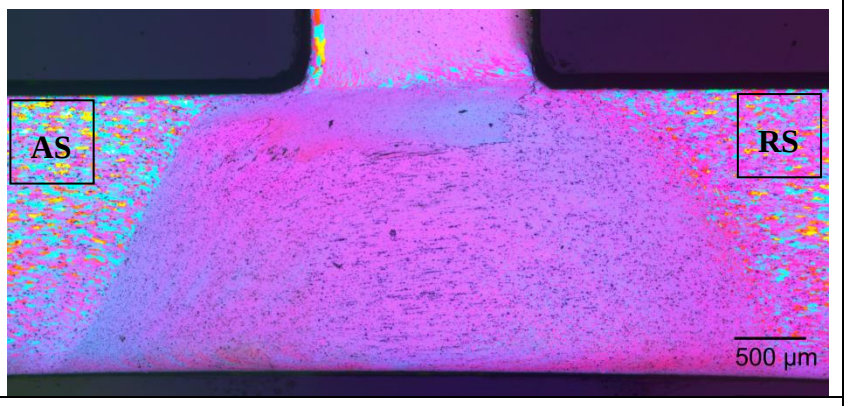
7 mm/s	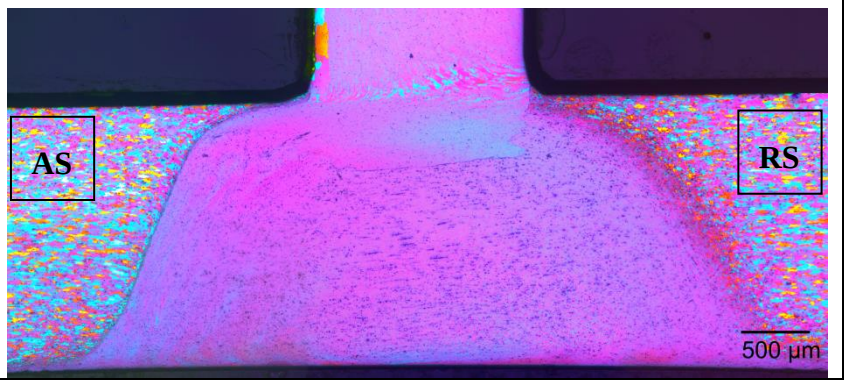

Table 13 presents the microstructure of the two SP specimens that were welded with 1000 RPM of rotational speed. Like the previous comparison, as the welding speed increases, the stirred zone slightly decreases. Also, the TMAZ is thinner, and it is easier to identify both advancing and retreating sides.

For the same welding speed, by increasing the rotational speed, the SZ appears to have a smoother shape. Also, the notch interface seems to be less sharp, thus leading to a stiffer metal interlocking between the skin and the stringer.

Table 14 – Microstructures obtained at 1200 RPM of rotational speed.

3 mm/s	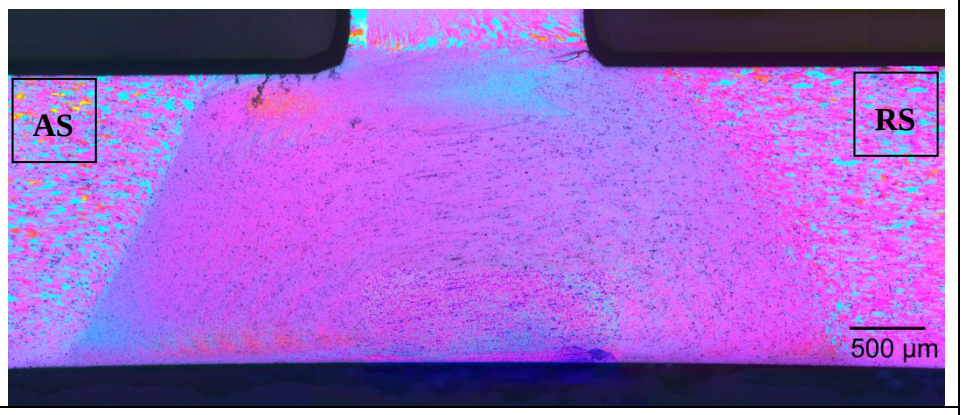
5 mm/s	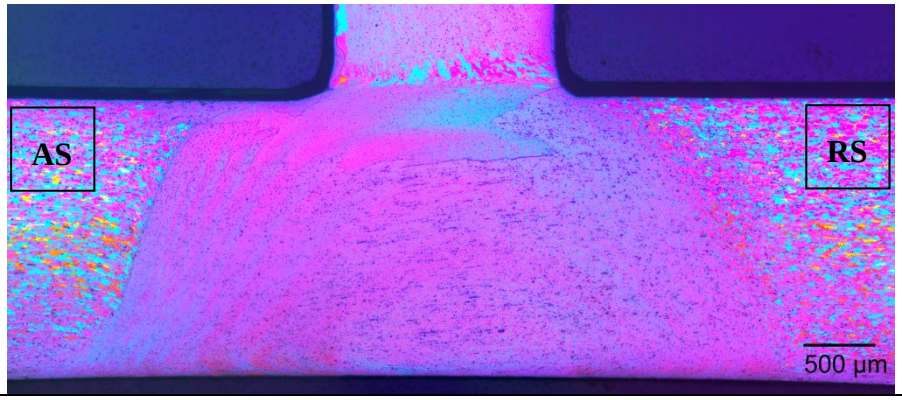
7 mm/s	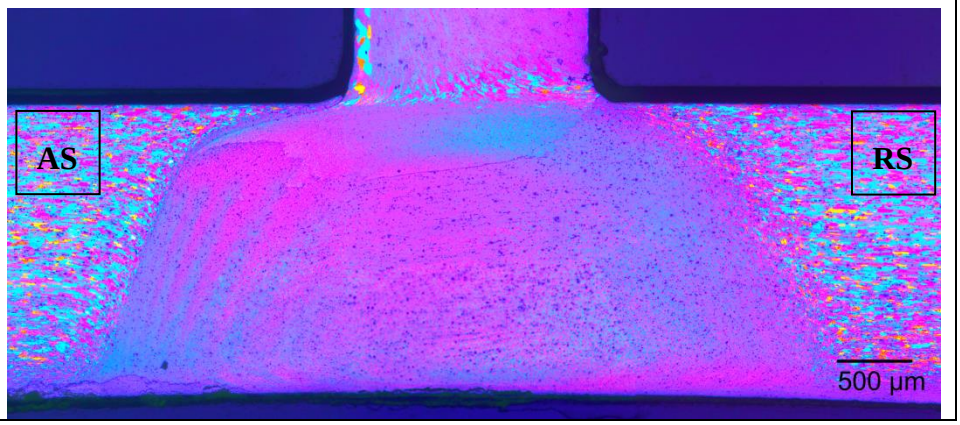

Table 14 presents the microstructure of the three SP specimens that were welded with 1200 RPM of rotational speed. As it was evidenced in Table 12 and Table 13, the smoothest intersection between the SZ and the BM occurs for the lowest welding speed. Here, with the lowest welding speed and the biggest rotational speed, the TMAZ is the thickest. Also, as the welding speed diminishes and the rotational speed increases, the notch interface seems to be faded, meaning that, with a higher heat input the connection between the skin and the stringer is stronger.

When the welding speed decreases and the rotational speed increases, the SZ becomes more homogeneous. This means that the grains had more time to recrystallize. Therefore, as the heat input increases, it is expected that the SZ is becoming softer. This will be evidenced on the micro-hardness experiments.

4.1.1.2 Grain-size measurements

The following figures stand for the single pass specimen's grain size measurements according to its welding parameters, grouped by the same rotational speed. Below, a brief explanation about the obtained results is presented.

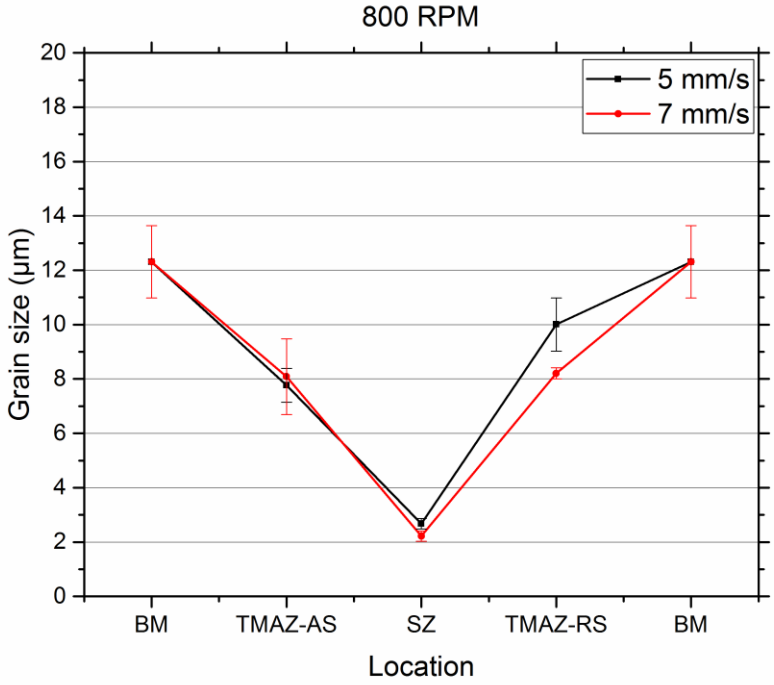

Figure 23 – Grain size evolution for 800 RPM.

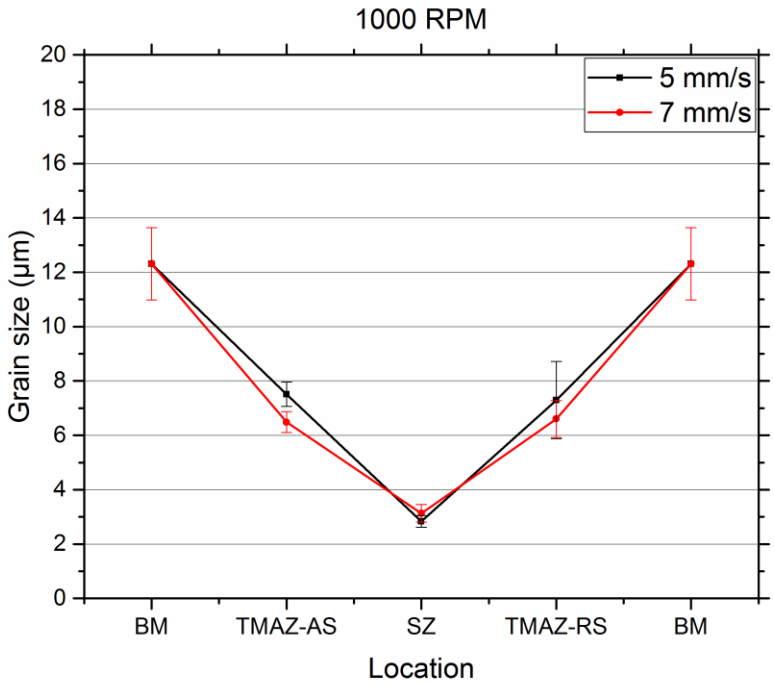

Figure 24 – Grain size evolution for 1000 RPM.

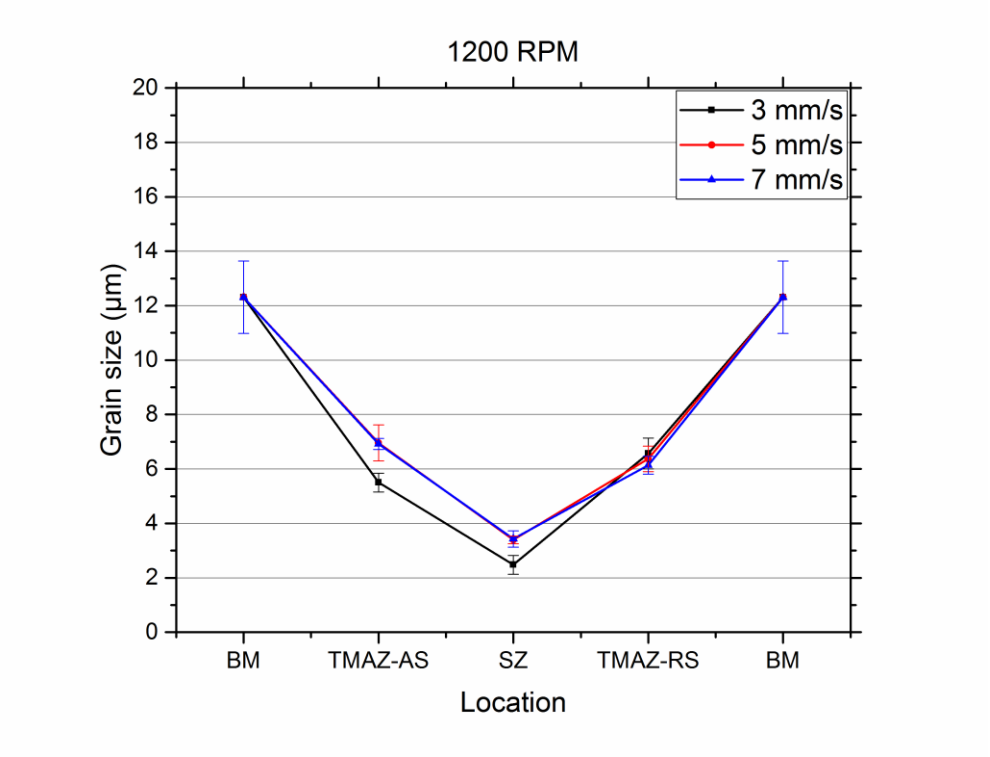

Figure 25 – Grain size evolution for 1200 RPM.

It is observed that, for the entire parameter window, the smallest grain size is in the stirred zone because this is the weld region where the material is plasticized the most. Moving up from the SZ to the samples' edges, the grains are becoming coarser until the base material is reached (where the grain size is approximately constant), as the probe's influence on stirring the material and promoting the metal interlocking is getting weaker.

For the welds performed with the lowest rotational speed – 800 RPM – it seems that the major difference in grain size is located on the retreating side of the TMAZ. Specifically, the grains are smaller when the welding speed is lower. With a low rotational speed, a weaker metal interlocking is obtained, particularly on the retreating side. No major differences were detected on the advancing side and the stirred zone.

Considering the rotational speed of 1000 RPM, there are significant differences in grain size on the TMAZ, which smaller grains seem to exist when a weld of higher welding speed is performed. A lower weld allows the grains to be stirred for longer time.

For the welds performed with the biggest rotational speed – 1200 RPM – there are no significant differences in the TMAZ located on the retreating side. However, grains in SZ and TMAZ located on the advancing side are smaller. As the welding speed is low and the rotational speed is high, this means that the action of material stirring happens more on welds using these parameters, as the material presents a stronger metal interlocking.

No relevant pattern of different grain size was evidenced when the welding speed is fixed and the rotational speed changes. The only recorded observation is that the grain size reaches its peak welding at 1000 RPM.

4.1.2 Micro-Hardness tests

4.1.2.1 Horizontal direction

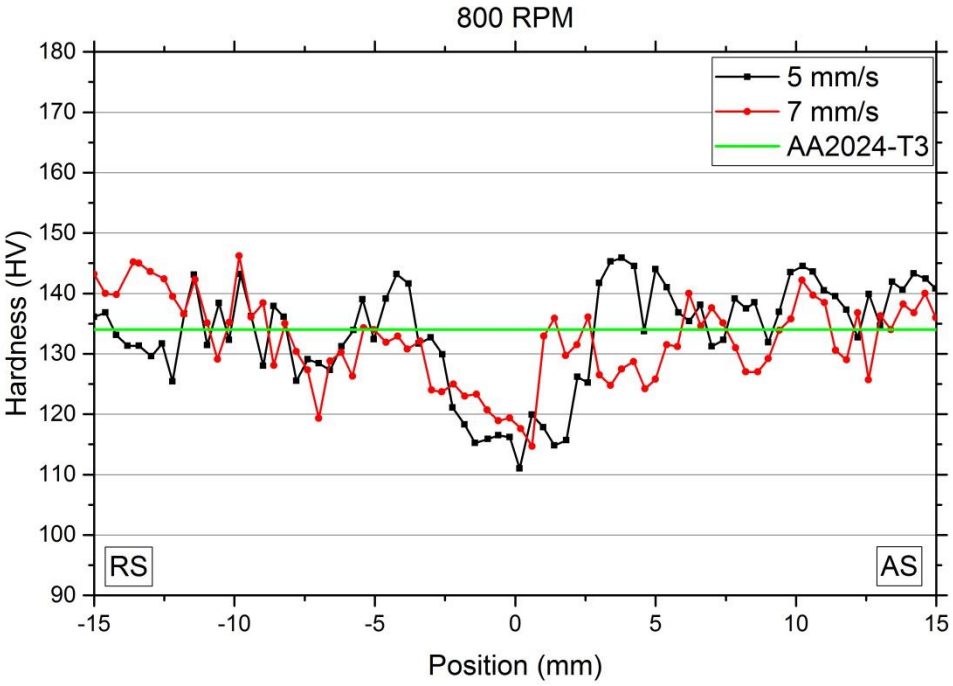

Figure 26 – Hardness values of 800 RPM welds.

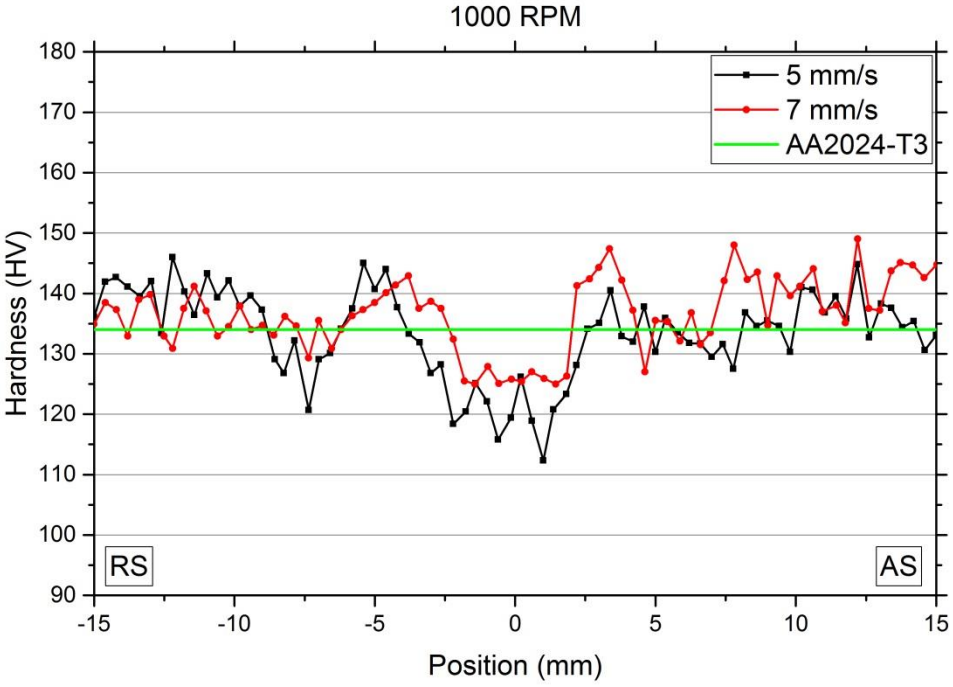

Figure 27 – Hardness values of 1000 RPM welds.

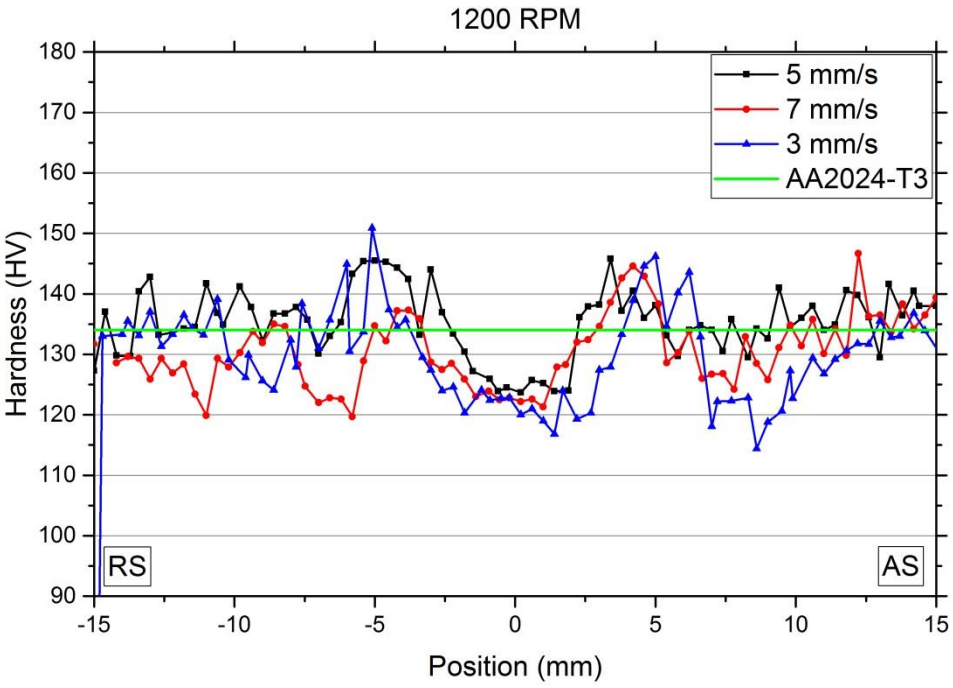

Figure 28 – Hardness values of 1200 RPM welds.

In general, the softest zone for the SP tests of the indentation region is the SZ (located in the middle of the weld). This is the area where the heat input is the biggest, which generated by the action of the rotating probe, leading to a higher grain dissolution. Thus, ductility increases and hardness decreases. Also, the probe is contacting the plate (made of AA2024-T3), which is the softest alloy. From the middle to the extremities, the hardness increases. This hardness-increasing zone is the thermo-mechanically affected zone (TMAZ), where a thermo-mechanical treatment generated by both the friction between the probe and the material, and the stirred material usually happens. Normally, this seems to be the hardest region. Then, the hardness tends to decrease, now entering in the heat affected zone (HAZ), and finally reaching the base material, which, in this case, is the AA2024-T3.

Normally, as the rotational speed increases, the hardness for the same position slightly decreases. This is related with the heat input that is bigger for these cases, thus leading to a smoother surface. For this parameter window, the rotational speed has little effect in altering the hardness values. As an example, the parameter for welding speed of 5 mm/s, and comparing the rotational speed of 800 RPM and 1000 RPM, Figure 26 and Figure 27, respectively, do not seem to present a significant difference in hardness. Considering the SZ (the most critical zone from the weld), there is an average of 5 HV of difference in hardness, which is not relevant.

The different welding speed has a bigger effect on the hardness than the rotational speed. For the same rotation, with an increased welding speed, in general, the hardness tends to increase on the SZ. This is somehow related to the low heat input that is created by friction from the probe/shoulder set. If the welding speed is bigger, it means there is less time to create friction between surfaces, meaning less heat input, therefore less precipitates dissolution.

For high rotational speed (see Figure 28), there is not a big difference on the hardness on the SZ. This means that the high hardness obtained by a theoretical lower heat input (bigger welding speed), is being overcome by a lower ability of the probe in creating a strong interlocking connection in AA2024-T3 with AA7050-T651, due to increased welding speed.

4.1.2.2 Vertical direction

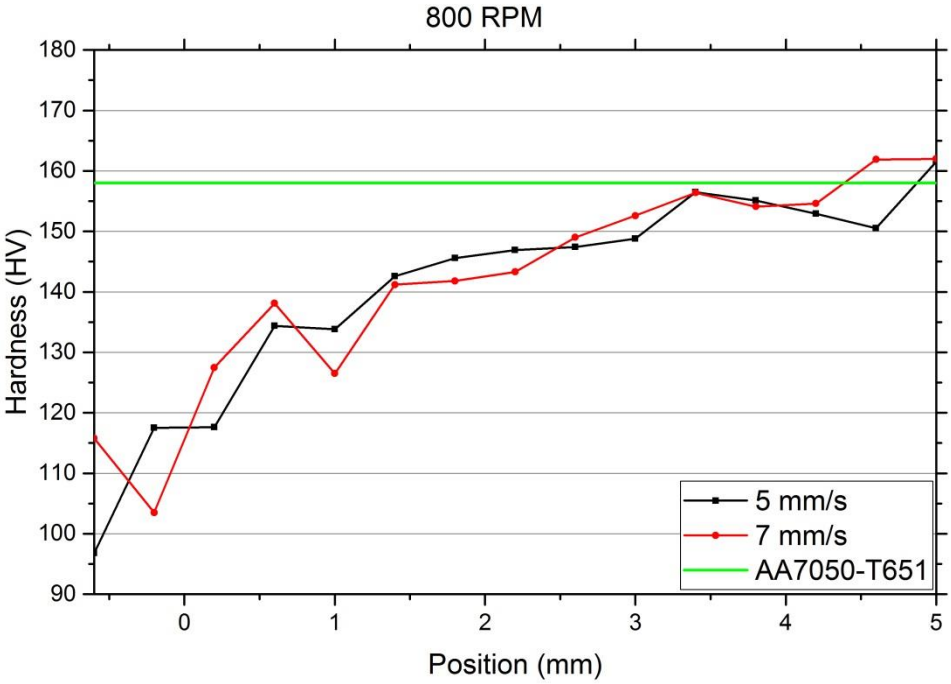

Figure 29 – Hardness values of 800 RPM welds.

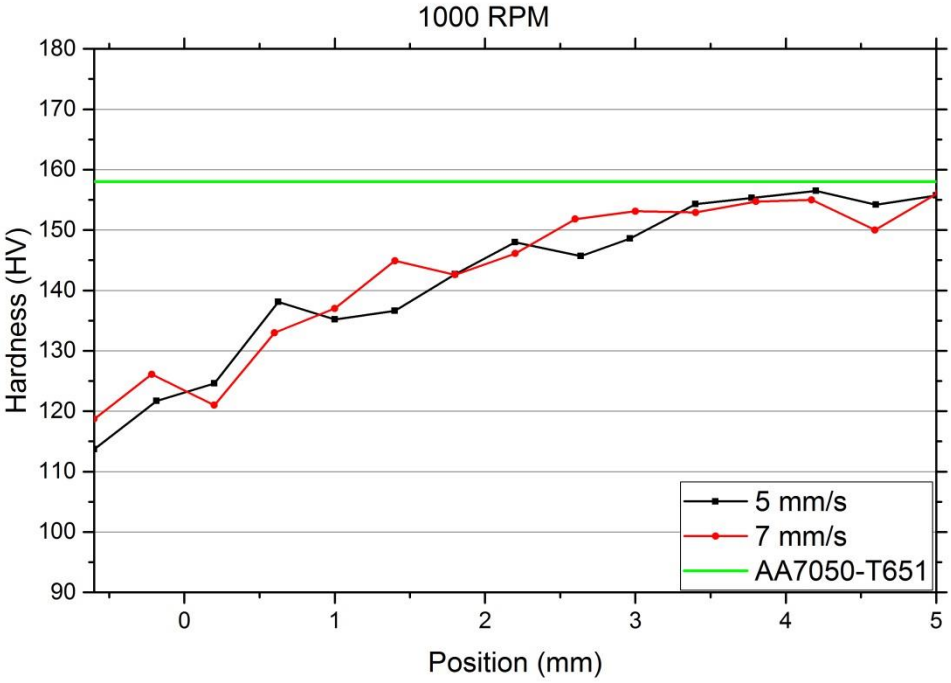

Figure 30 – Hardness values of 1000 RPM welds.

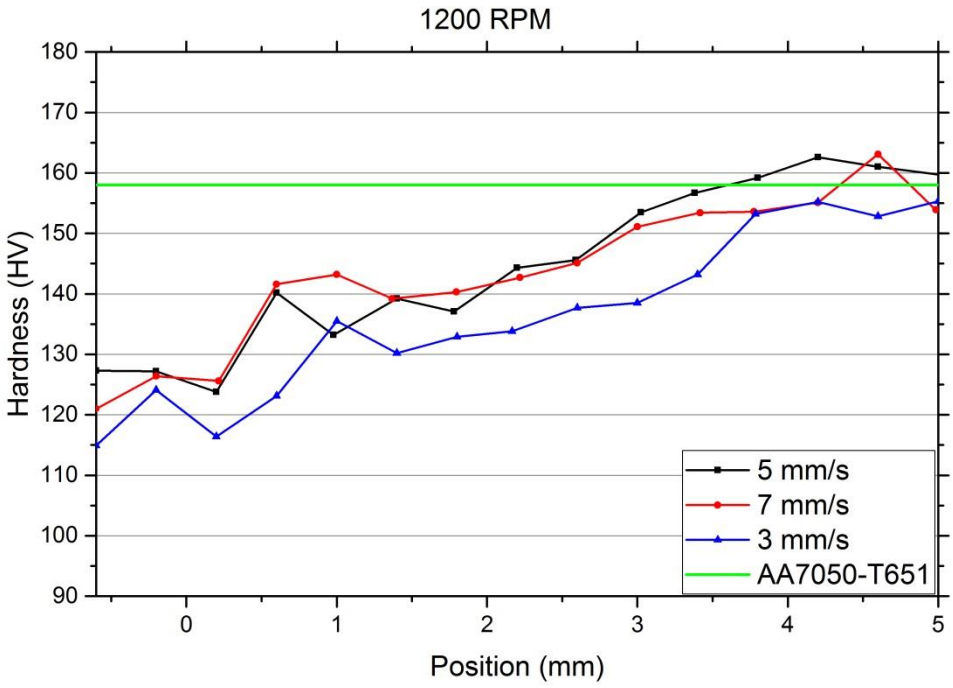

Figure 31 – Hardness values of 1200 RPM welds.

In a first analysis, the scatter presented on these curves is much more consistent than the horizontal tests. Considering that the AA7050-T651 has a hardness of 158 HV, BM was reached.

In some cases of the SP tests, it was found out that, in the section that links the stringer to the skin (between “1 mm” and “1,5 mm”), there is a slight decrease in hardness. The heat input generated by the probe movement spreads from the probe contact to the far extremities of the specimen, namely the skin’s edges and stringer edge. As it passes from the skin to the stringer, considering the heat flow direction which is parallel to the probe’s axis, there is a reduction of section on the T-joint, which means that the same heat flow will pass throw a smaller material section, which means in this case that the obtained temperature is locally higher, thus leading to a bigger heat input. A local grain recrystallization occurs which makes the local hardness decrease. This phenomenon is possible to see on every figure regarding the microstructure.

In general, there is no big difference in hardness by changing the weld parameters. This means that, in general, the changing weld parameters did not significantly alter the stringer’s microstructure. The only case where the hardness is significantly different (smaller) is the weld parameter of 3 mm/s and 1200 RPM (see Figure 31). In this case, the heat input might be sufficient to reduce the hardness, as it was explained before.

4.1.3 Hoop-Strength tests

4.1.3.1 Ultimate tensile strength

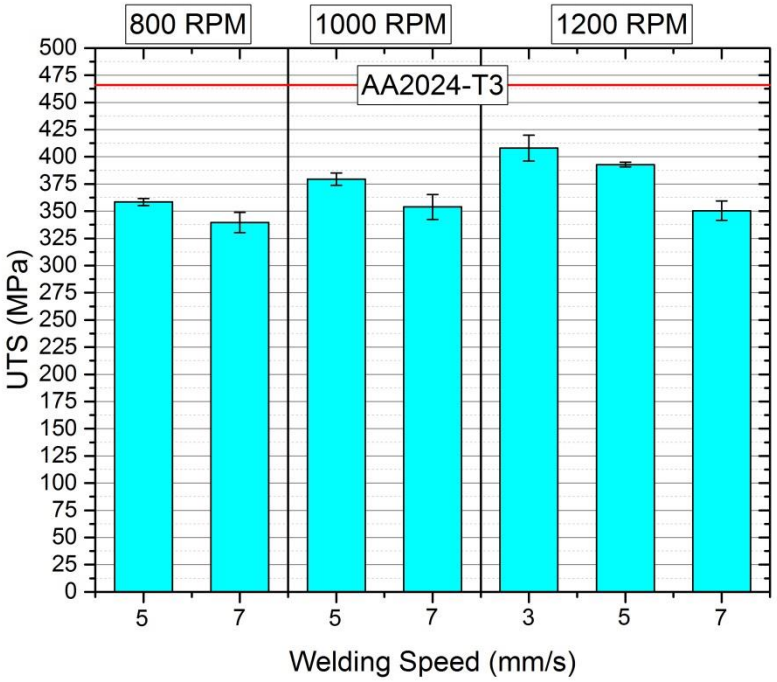

Figure 32 – Ultimate tensile strength.

Figure 32 shows the obtained UTS on the hoop-strength tests for each SP specimen. A tendency in ultimate tensile strength is evidenced on the graph. In general, for the same welding speed and with increasing rotational speed, there is a small increase in strength. Fixing the rotational speed and increasing the welding speed, the strength diminishes significantly, in particular, when rotational speed is high (see 1200 RPM). The difference in strength between consecutive welding speeds is higher as the rotational speed is increasing. Both changing parameters promote differences in UTS.

4.1.3.2 Yield strength

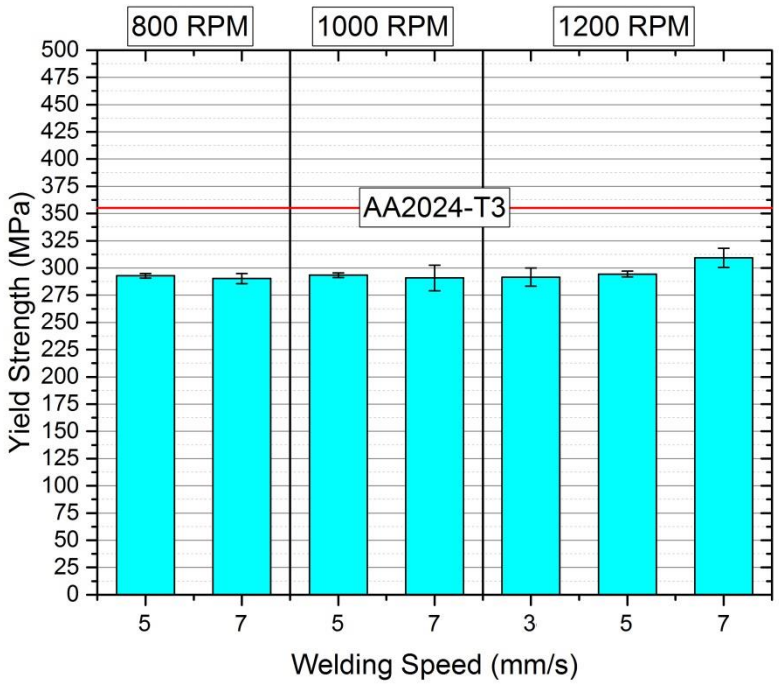

Figure 33 – Yield strength.

Figure 33 presents the obtained YS in the hoop-strength tests for each SP specimen. Unlikely the UTS graph (presented in Figure 32), it seems that there is no identifiable tendency concerning the relationship between the specimen's yield strength and the changing parameters. Just the test with the highest rotational speed and welding speed (1200 RPM, 7 mm/s) presents a higher result for yield strength, although the difference from the rest is not that significant. Thus, for this weld configuration and considering the parameter window, there is not a significant change on yield strength with the changing parameters. So, this means that the changing parameters don't affect the material's elastic behaviour.

4.1.3.3 Interface angle vs Ultimate Tensile Strength

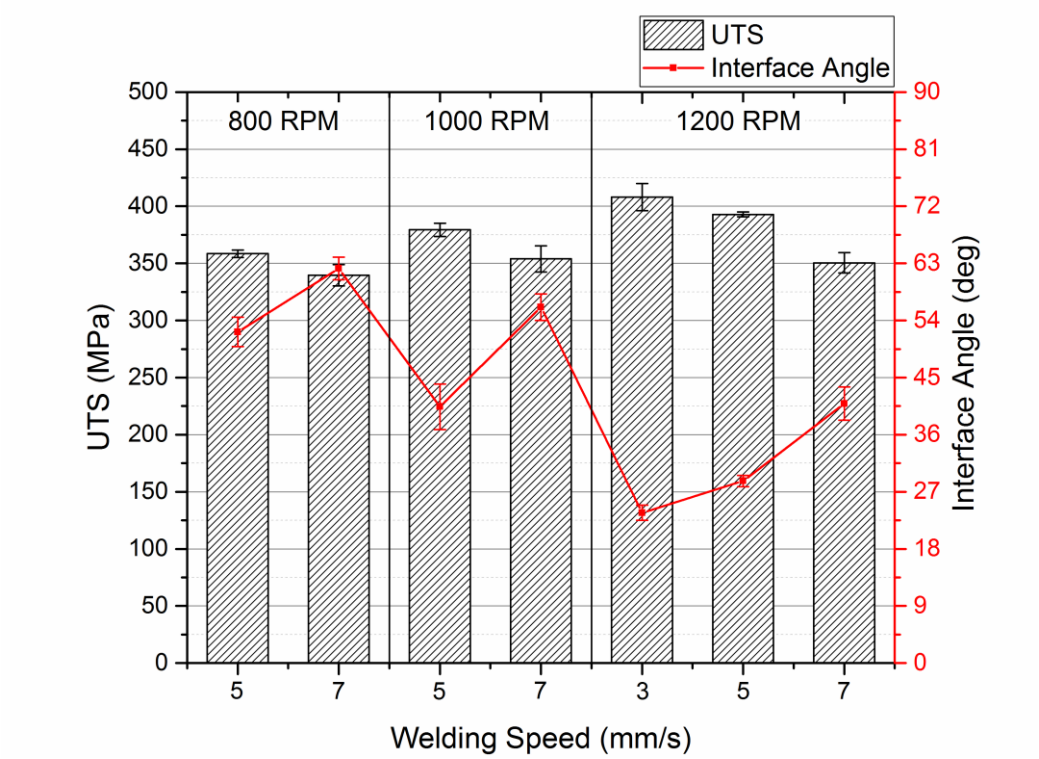

Figure 34 – Interface angle vs UTS.

Figure 34 presents a comparison between the interface angle and the obtained UTS from the hoop-strength tests and for the SP weld configuration. A tendency is presented on the curve of interface angle with the obtained results for ultimate tensile strength (as also the changing parameters). In general, in a presence of a bigger interface angle, a lower UTS is obtained on the results. Also, for the same rotational speed, the angle increases with the increased welding speed.

For the same welding speed, the opposite occurs. When rotational speed is increased, the interface angle decreases. Considering the pulling direction, a smaller angle makes that it is harder to break the interface, thus, a higher UTS is obtained when in presence of a more stirred material.

4.1.3.4 Fracture Surface of hoop-strength tests

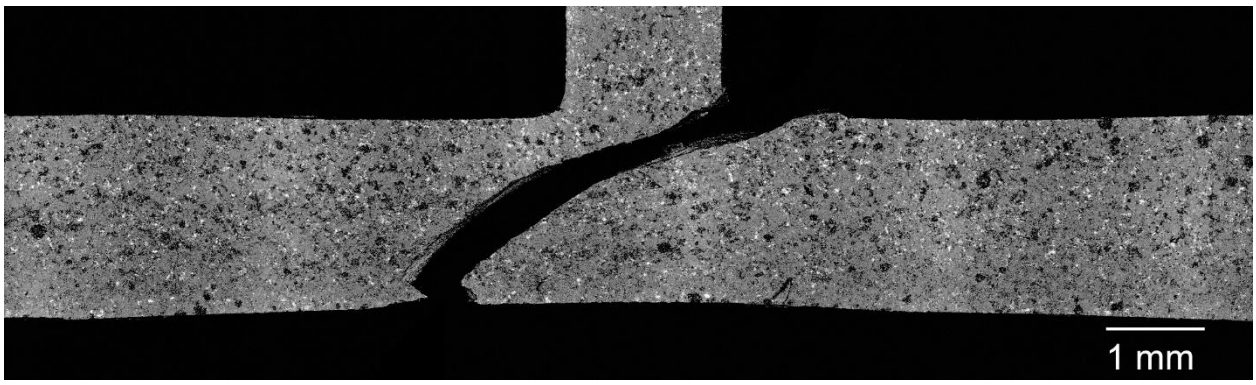

Figure 35 – Example of a fractured surface after hoop-strength test.

Figure 35 presents the fractured surface from a sample that belongs to the specimen SSFSW-T9G-AB-160 after the hoop-strength test was performed. Most cracks started on the retreating side (top right side of the fracture) and propagated in a 45 ° plane across the stirred zone and reaching the advancing side. It was somehow expected to be fracture on the retreating side of the weld because this side is the one that presents a weaker metal interlocking. The samples that failed on the advancing side had performed an early rupture.

A few specimens presented a secondary crack parallel to the skin surface in the retreating side, because part of the skin surface was not welded in the notch. Others presented an early rupture, mainly due to the presence of defects in the welds.

4.1.4 Pull-Out tests

4.1.4.1 Maximum Load

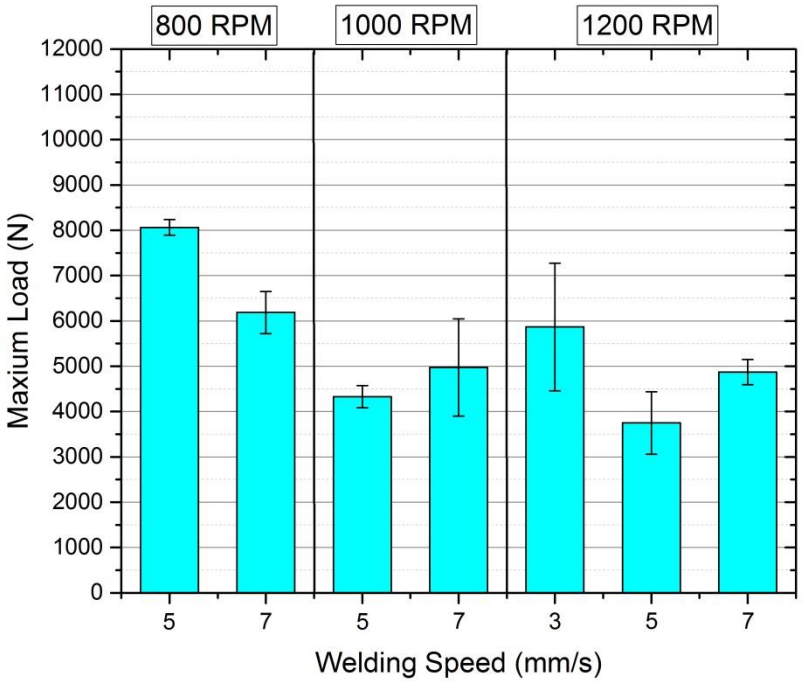

Figure 36 – Maximum load.

Figure 36 presents the maximum load obtained from pull-out tests for each SP specimen. As it is clear by observing the graph, is it difficult to find any tendency of maximum load with the changing parameters. Also, in some cases, there is a lot of value variability, meaning that the experiment was not accurate. In these cases, there were some specimens that perform a premature failure, meaning that the maximum load achieved was significantly lower than the other specimens from the same plate.

4.1.4.2 Interface Crack Length vs Maximum Load

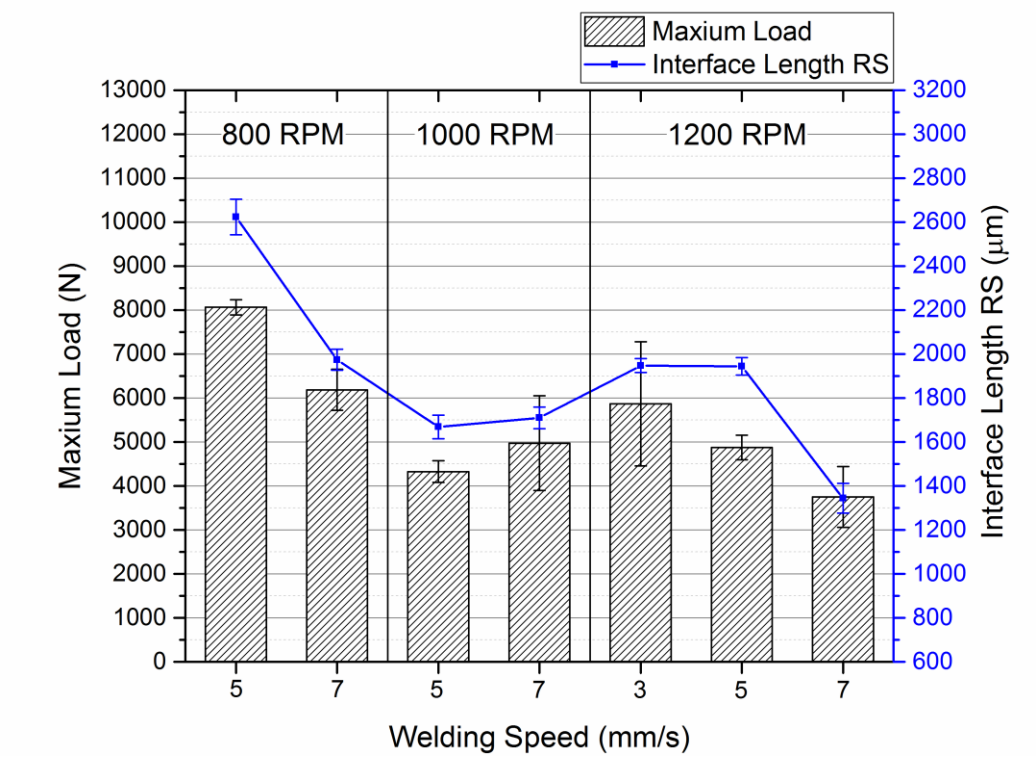

Figure 37 – Interface Length vs Maximum Load.

Figure 37 presents a comparison between the interface length and the obtained maximum load from the pull-out tests for each SP specimen. A tendency is clearly evidenced in the graph; the interface length keeps up with the variable maximum load. When the interface presents a bigger length, the outputted result for maximum load is also bigger. As the interface between the materials becomes longer, means that there is more material stirring, which means a better metal interlocking is generated, thus a bigger resistance to pull-out loads is achieved.

4.1.4.3 Fracture Surface of pull-out tests

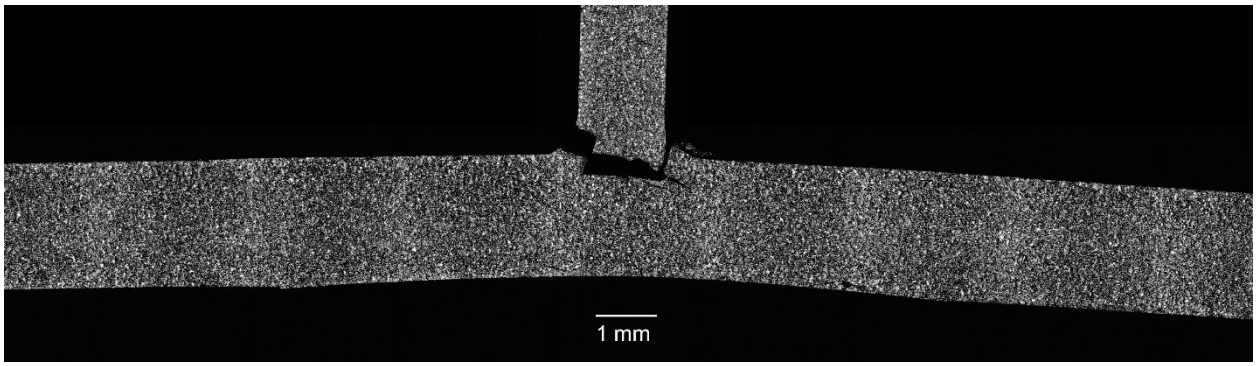

Figure 38 – Example of a fractured specimen after pull-out test.

Figure 38 presents the fractured surface from a sample that belongs to the specimen SSFSW-T9G-AB-160 after the pull-out test was performed. The mechanical behaviour was similar on almost all the samples. Basically, in all of them, the stringer was pulled out of the skin, starting to fracture on one side and propagating to the other side throw the notch-skin surface. After the test, all samples presented a flat area where the stringer was located, meaning that there is an un-welded area, thus obtaining a failure located on the notch, by pulling out the stringer.

4.2 Notch-skin double pass welds – DP

4.2.1 Microstructure analysis

4.2.1.1 General overview

As it was presented for the SP specimens, the following tables grouped by the same rotational speed stand for the double pass specimen's microstructure. Below, a brief explanation about the microstructure with the parameters is presented.

Table 15 – Microstructures obtained at 800 RPM of rotational speed.

5 mm/s	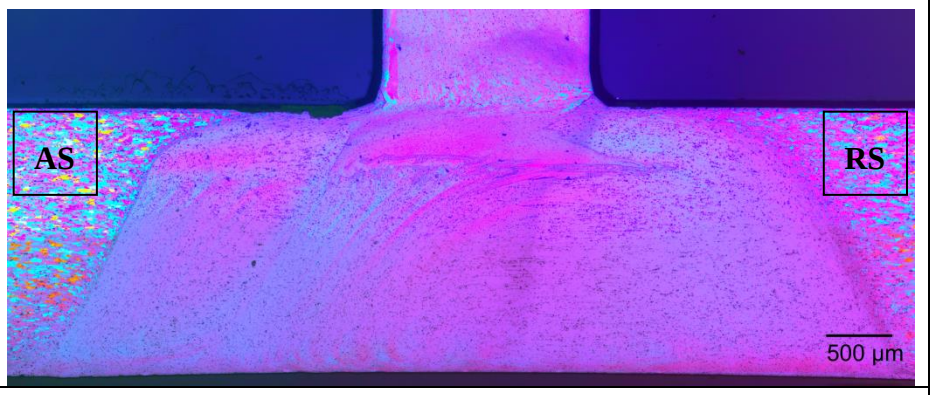
7 mm/s	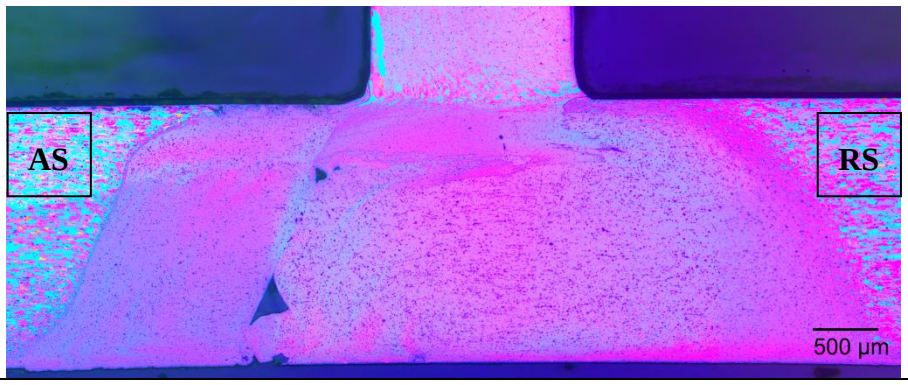

Table 15 presents the microstructure of the two DP specimens that were welded with 800 RPM of rotational speed. As a first analysis, compared to the previous microstructures, the stirred zone is wider, which is an evidenced characteristic on every microstructure from DP specimens. Just like happened with the SP specimens, as the welding speed increases, the TMAZ gets thinner, meaning that it is clearer to evidence the difference between the BM and the SZ.

With a higher welding speed, it is clearer the presence of a non-welded area that was derived from the second weld passing, located on the interface between the advancing side of the new pass and the previous stirred zone (the second pass was performed on the right side of the specimen). This defect was created by the second pass of the probe in which there was not enough capacity to completely stir the material from the previous passing. Also, one must point out that part of the stirred material on the second passing was already been stirred, which means it was already hardened. The probe failed to stir it again because the passing occurred too rapid and also because the material was too hard to plasticize.

When the weld was performed with low rotational speed and increased welding speed, there is a presence of defects located on the interface, due to lack of material stirring. This is an indicator of local crack initiation, thus leading to a possible early rupture when performing

tests. In both cases, a non-welded area is evidenced, derived from the interface of skin-stringer.

Table 16 – Microstructures obtained at 1000 RPM of rotational speed.

5 mm/s	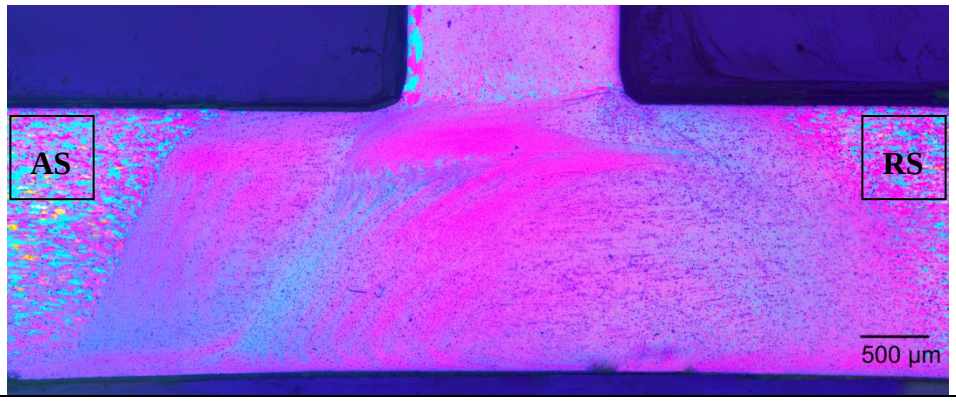
7 mm/s	

Table 16 presents the microstructure of the two DP specimens that were welded with 1000 RPM of rotational speed. As the rotation increases, the interface between the skin and the stringer is less visible and becoming less clear as the welding speed increases. This means the metal interlocking located in the stirred zone is stiffer. The spot presented on the lower microstructure was obtained by a poor surface preparing.

Like the previous comparison, as the welding speed increases, the stirred zone slightly decreases. Also, the TMAZ is thinner, and it is easier to identify both advancing side and retreating side. For the same welding speed, by increasing the rotational speed, the stirred zone appears to have a smoother shape.

Despite presenting a better metal interlocking, there are still defects in the weld when the welding speed is increased. In this case, these are located on the advancing side of the first pass. This defect may had been created by higher welding and rotational speeds, in which the probe had failed to completely stir the material.

Table 17 – Microstructures obtained at 1200 RPM of rotational speed.

3 mm/s	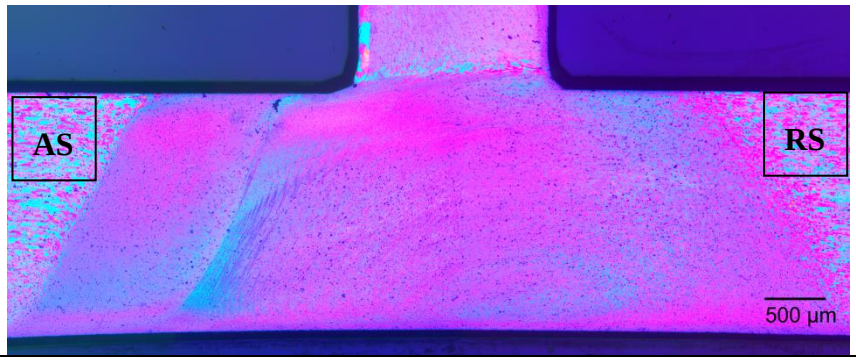
5 mm/s	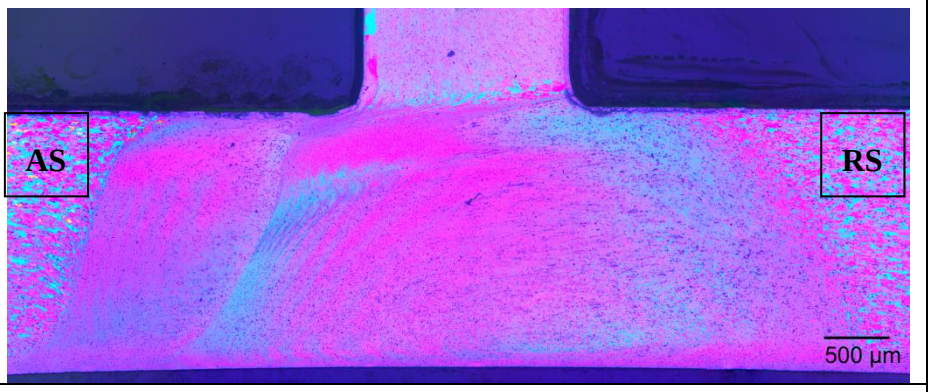
7 mm/s	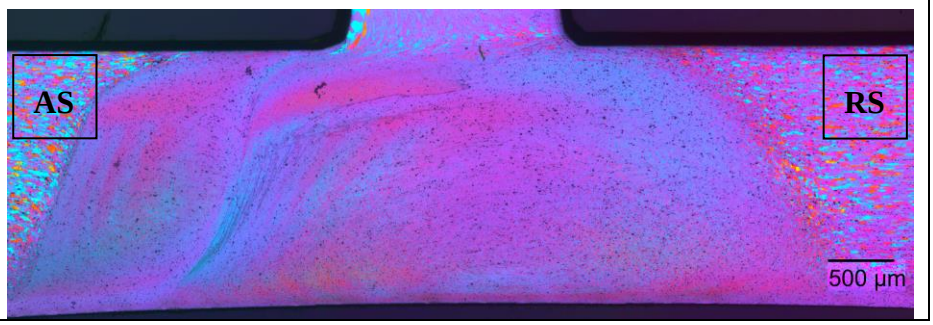

Table 17 presents the microstructure of the three DP specimens that were welded with 1200 RPM of rotational speed. As it was evidenced for the SP specimens, the smoothest intersection between the SZ and the BM occurs for the lowest welding speed. Here, the TMAZ is the thickest. Also, as the welding speed decreases and the rotational speed increases, the stirred zone becomes more homogeneous, meaning that there is a good metal interlocking but, just like it had happened to the SP specimens, also means that the grains had more time to recrystallize. Therefore, as the heat input increases, it is expected that the SZ is becoming softer. This will be evidenced on the micro-hardness experiments below.

4.2.1.2 Grain-size measurements

The following figures stand for the double pass specimen's grain size measurements according to its welding parameters, grouped by the same rotational speed. Below, a brief explanation about the obtained results is presented.

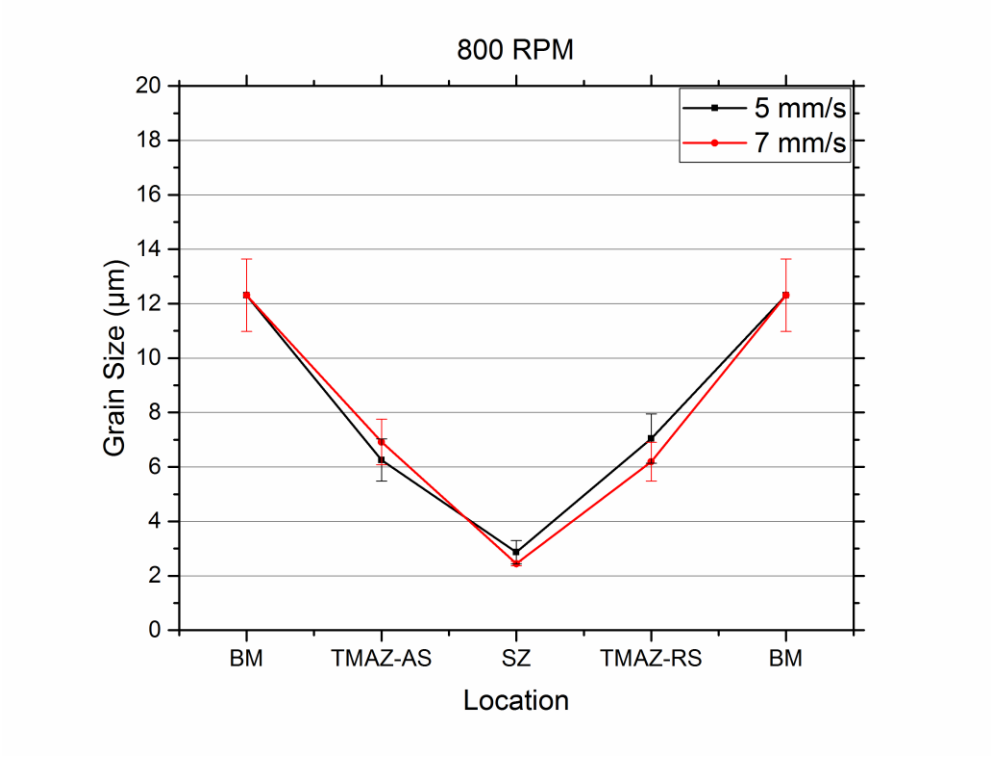

Figure 39 – Grain size evolution for 800 RPM.

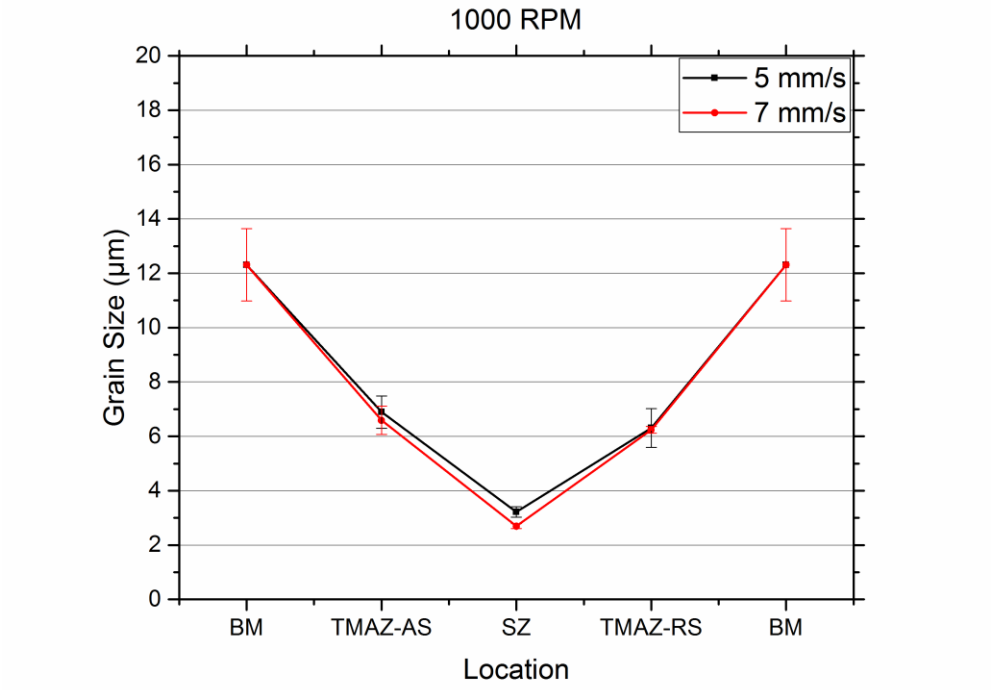

Figure 40 – Grain size evolution for 1000 RPM.

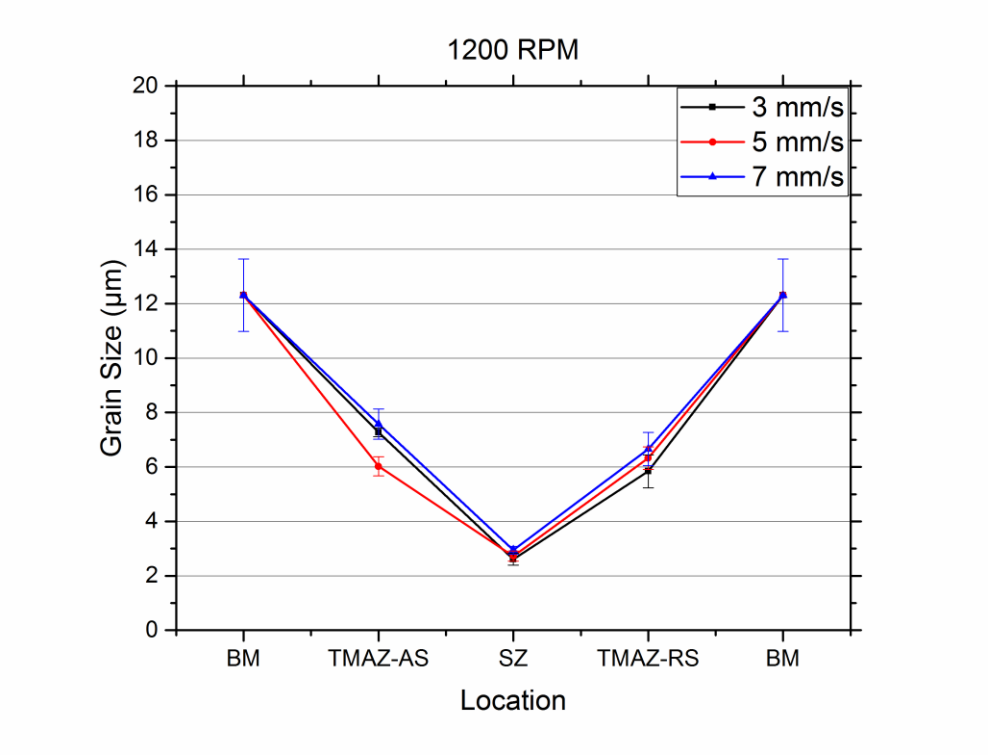

Figure 41 – Grain size evolution for 1200 RPM.

As it happened with the SP weld's results, it was also expected that the smallest grains were located on the SZ, and the grains are getting bigger until the base material is reached.

Considering the curves for 800 RPM, the advancing side presents bigger grains when the welding speed is increased. The welding speed is sufficient high that doesn't promote material stirring. On the other hand, as the welding speed increases, the grains located in the TMAZ on the retreating side are smaller. Perhaps there may be wrong grain size measurements.

The obtained results for performed welds with a rotational speed of 1000 RPM show that there is not a significant difference in grain size, meaning that grain size shows little dependence of different welding speeds.

For the welds performed with the biggest rotational speed – 1200 RPM – the most significant difference occurs on the grain size from the advancing side, obtained with a welding speed of 5 mm/s. As for the remaining results, no major differences were evidenced on the grain size curves.

4.2.2 Micro-Hardness tests

4.2.2.1 Horizontal direction

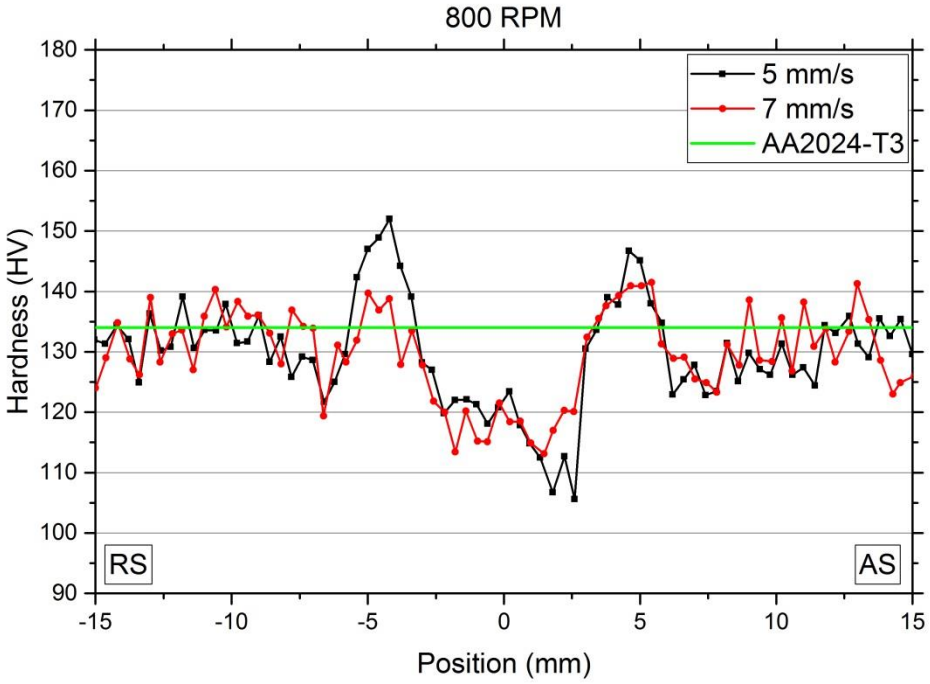

Figure 42 – Hardness values of 800 RPM welds.

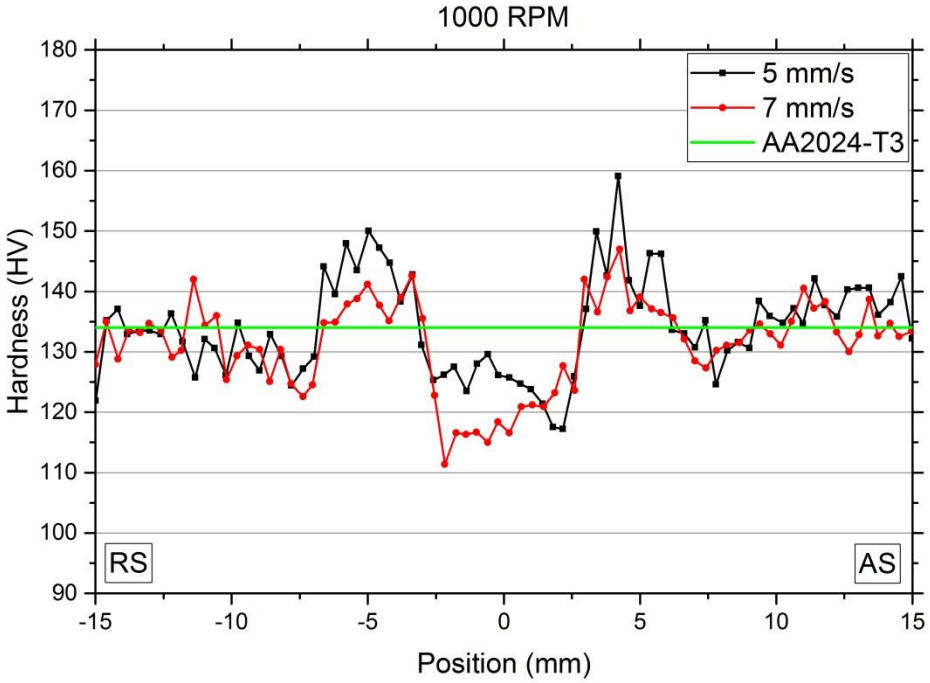

Figure 43 – Hardness values of 1000 RPM welds.

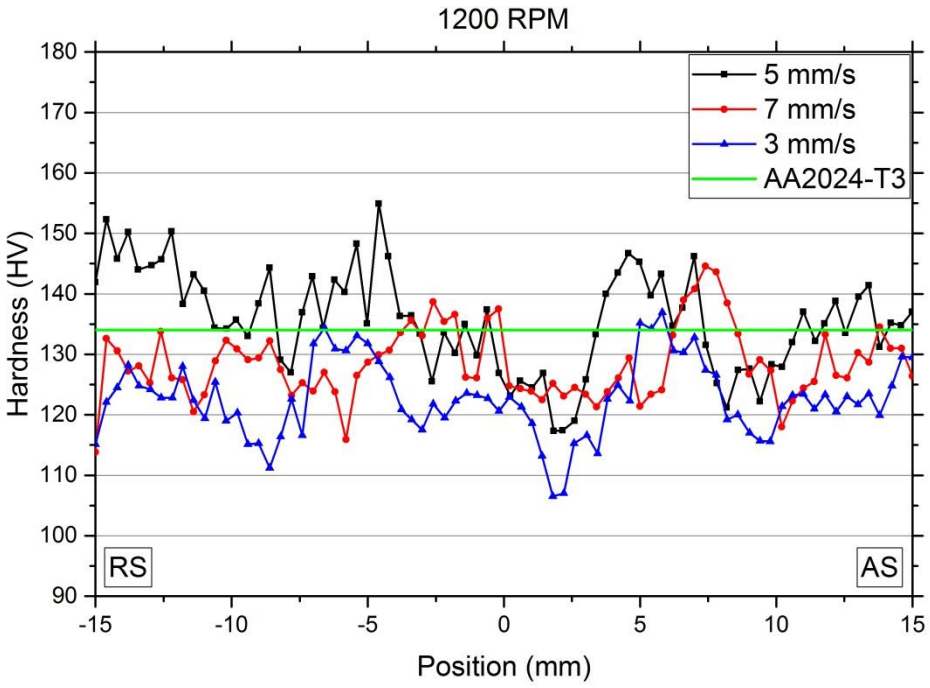

Figure 44 – Hardness values of 1200 RPM welds.

In general, and considering the curve's shape for each set of parameters, both SP and DP curves are similar. The SZ of the DP tests looks slightly larger because the probe passes 2 times on the T-joint, so it makes sense that the SZ is wider. Again, as there is a double passing, the heat input is significant bigger, which means that the contrast between the different zones is bigger too. Clearly, the SZ from DP welds shows a decrease in hardness compared to SP welds. At the same time, TMAZ present an increase in hardness, as it was explained before. Then, hardness decreases, where it is reaching the HAZ.

In contrast with SP welds and comparing the same weld parameters, Figure 42 and Figure 43 present smoother curves, where it is easier to observe the BS. Unfortunately, results from RS of 1200 RPM presented on Figure 44 have too much scatter, which turns it very inaccurate.

Just like the experiments for SP welds, the changing rotational speed for the same welding speed makes a small difference in hardness. As an example, the welding speed of 7 mm/s is analyzed (considering approximate hardness values for the SZ): 116 HV with a rotational speed of 800 RPM (see Figure 42); 118 HV with a RS of 1000 RPM (see Figure 43); and 124 HV with a rotational speed of 1200 RPM (see Figure 44). Considering the parameter window, it is about 8 HV of difference, which is not relevant.

Considering the same rotational speed, there is not a significant difference between different DP welds for different welding speed, unlike the previous cases.

4.2.2.2 Vertical direction

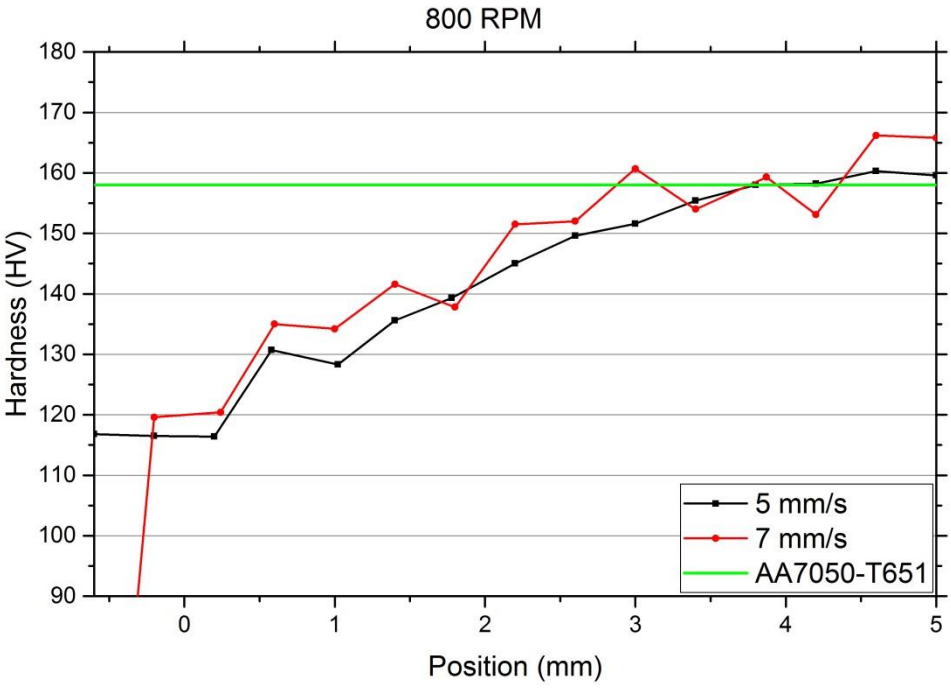

Figure 45 – Hardness values of 800 RPM welds.

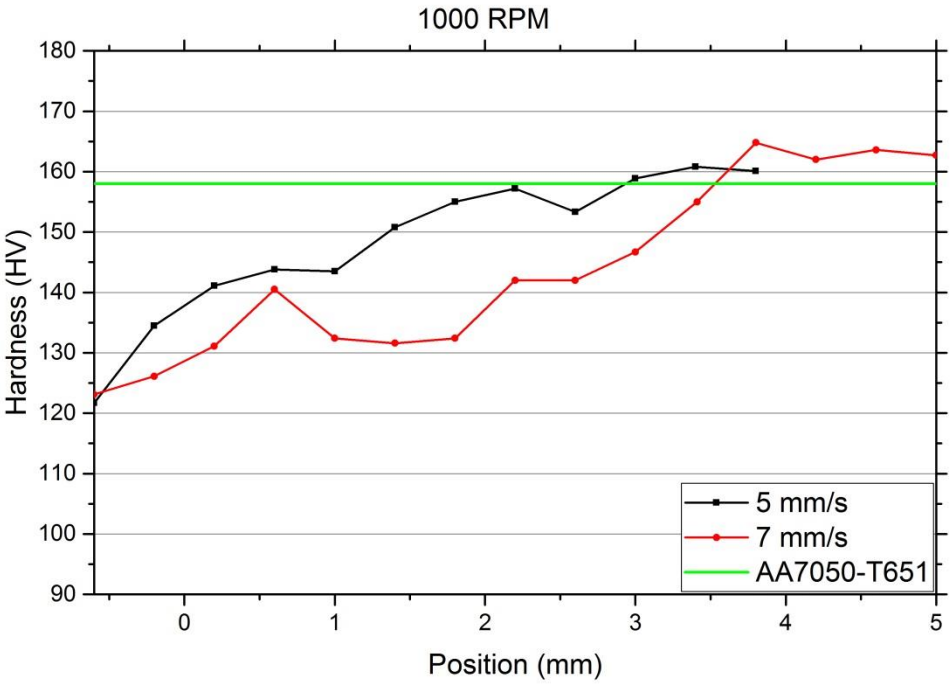

Figure 46 – Hardness values of 1000 RPM welds.

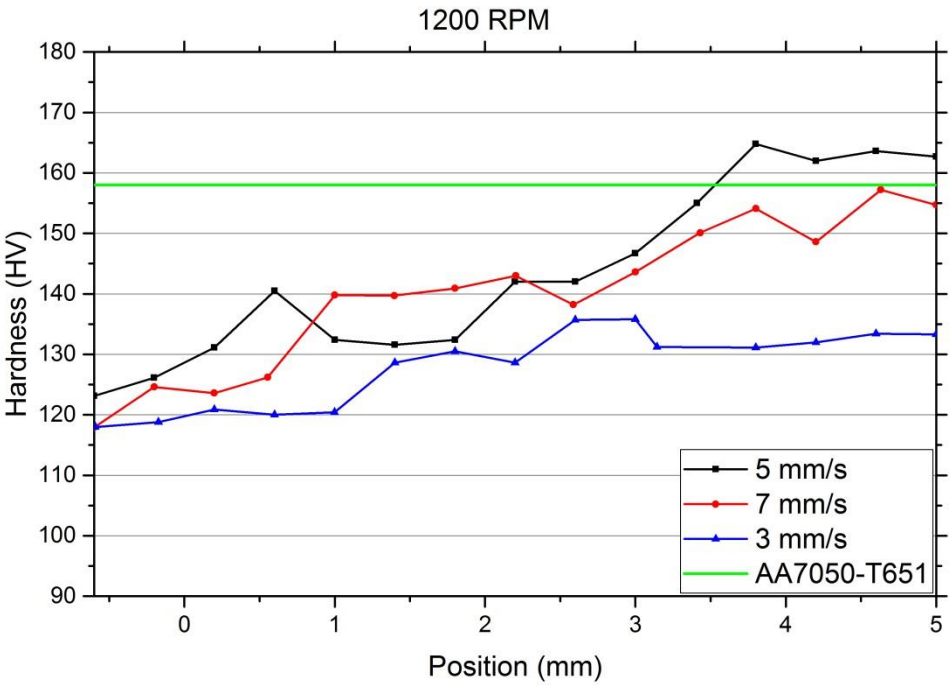

Figure 47- Hardness values of 1200 RPM welds.

For the case of the DP tests, the indentations also reached the BM, except the reference weld parameter (3 mm/s, 1200 RPM). Perhaps the heat input was so dense, that an upper limit of 5 mm was not enough. The grain recrystallization zone, evidenced in SP micro-hardness tests, not presented here, maybe due to some indentations that were not performed specifically on the interface skin-stringer.

Like SP welds and in general, there is no big difference in hardness by changing the weld parameters. Again, this means that the changing weld parameters are not altering much the stringer's microstructure.

4.2.3 Hoop-Strength tests

4.2.3.1 Ultimate Tensile Strength

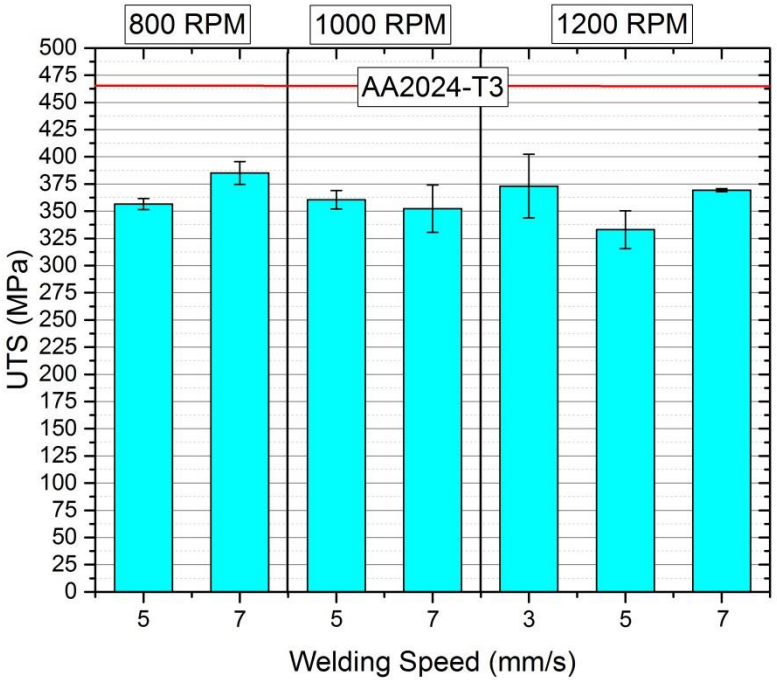

Figure 48 – Ultimate tensile strength.

Figure 48 shows the obtained UTS of the hoop-strength tests for each DP specimen. On this case of DP configuration specimens, a tendency is not so clear, since there is some variability. For example: for a welding speed of 5 mm/s, there is not a significant difference of UTS with the changing rotational speed. The variability on the results for Ultimate tensile strength may have been obtained by local defects in the welds.

4.2.3.2 Yield Strength

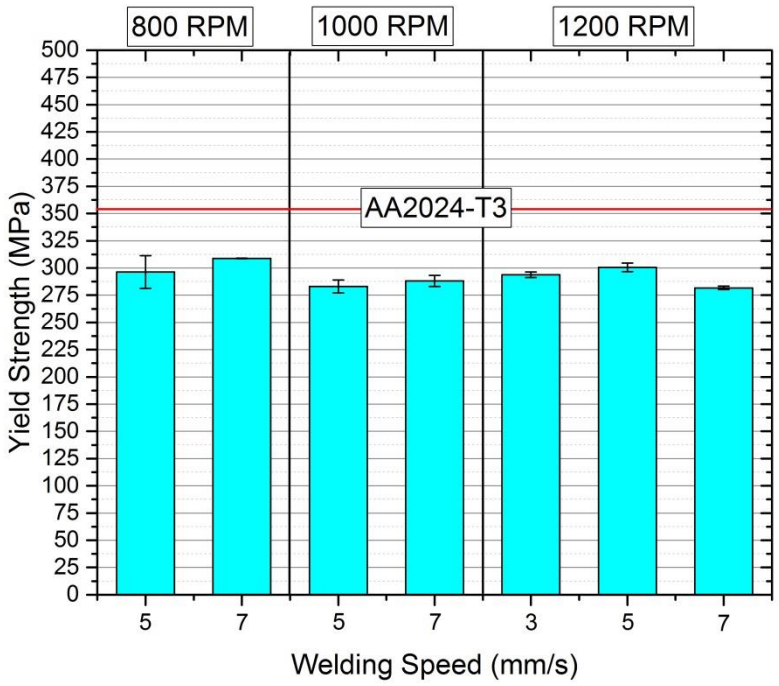

Figure 49 – Yield strength.

Figure 49 presents the obtained yield strength of the hoop-strength tests for each DP specimen. For almost samples, a slight increase of yield strength with the increasing welding speed is evidenced. Despite the evidence of an increasing strength, the differences in yield strength results seem not to be sufficient to admit that there is a tendency. Also, it is not clear the obtained results for yield strength with the changing rotational speed. Therefore, just like it was found out for the single pass configuration, the changing parameters don't affect the material's elastic behaviour.

4.2.3.3 Interface angle vs Ultimate Tensile Strength

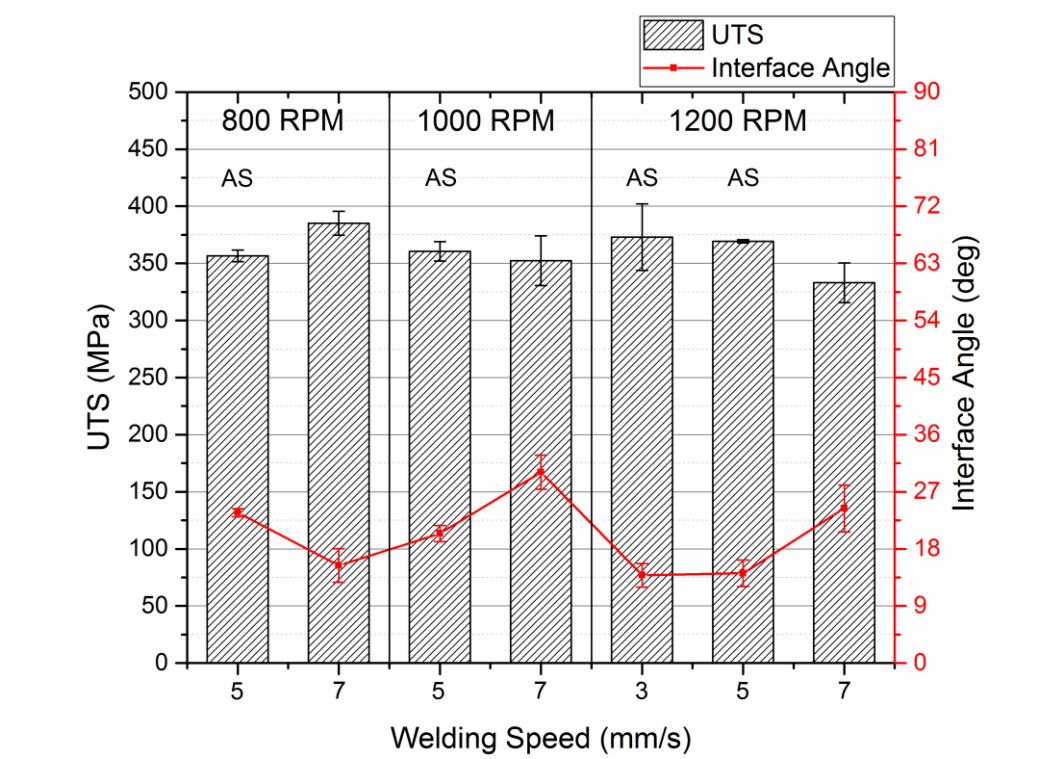

Figure 50 – Interface angle vs UTS.

Figure 50 presents a comparison between the interface angle and the obtained UTS from the hoop-strength tests, for each DP specimen. Although it is not clear a tendency of a variable UTS with the changing parameters, a tendency is presented on the curve of interface angle with the obtained results for ultimate tensile strength, like the SP specimens' results. In general, a bigger interface angle makes a specimen to underperform in ultimate tensile strength. As it was explained before, a lower interface angle makes the specimen to perform better, since there is a smaller resistance to the pulling direction as the angle is smaller.

4.2.3.4 Fracture Surface of hoop-strength tests

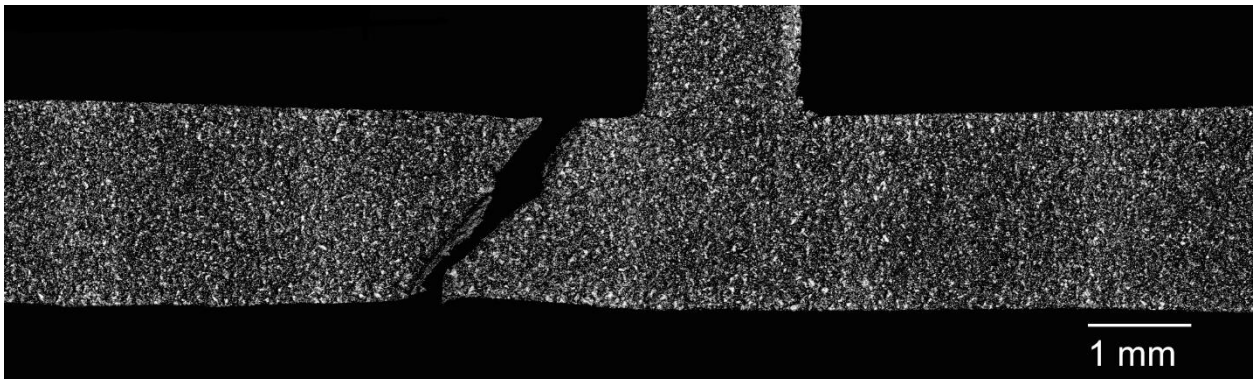

Figure 51 – Example of a fractured surface after hoop-strength test.

Figure 51 presents the fractured surface from a sample that belongs to the specimen SSFSW-T9G-AB-162 after the hoop-strength test was performed. Most cracks started on the advancing side (top right side of the fracture) and propagated on the advancing side plane until reaching the other extremity. Some samples had a crack initiated on the advancing side that was propagated throw the stirred zone and ending up on the retreating side.

A few specimens presented a secondary crack parallel to the skin surface in the retreating side because part of the skin surface was not welded in the notch, while others presented an early rupture, mainly due to concentrated forces.

4.2.4 Pull-Out tests

4.2.4.1 Maximum Load

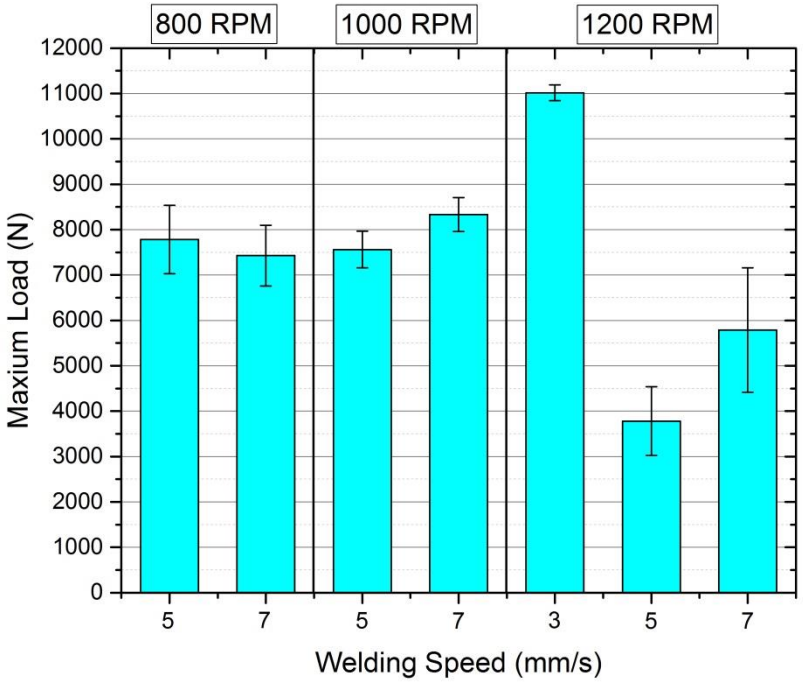

Figure 52 – Maximum load.

Figure 52 presents the maximum load of the pull-out tests for each DP specimen. Considering the obtained results with a rotational speed of 800 and 1000 RPM, a significant difference in maximum load is not perceptible. Perhaps, for the low and middle range of rotational speed, little dependence has the maximum load with the changing parameters. Moreover, for 1200 RPM of rotational speed, a result pattern is hard to observe.

The best obtained result for maximum load of the pull-out tests was obtained with 1200 RPM of rotational speed and 3 mm/s of welding speed as parameters. This result was expected to be the best one because, since the DP configuration was performed to avoid having an un-welded line at the corner between the skin and stringer, the entire stringer base was inter-locked with the skin. Also, the weld parameters (3 mm/s, 1200 RPM) are the ones that provide the best material stirring of the stringer into the skin. The highest probe rotation combined with the slowest welding speed allows enough time for the probe to completely stir the material, thus leading to a better interlocking.

4.2.4.2 Interface Length vs Maximum Load.

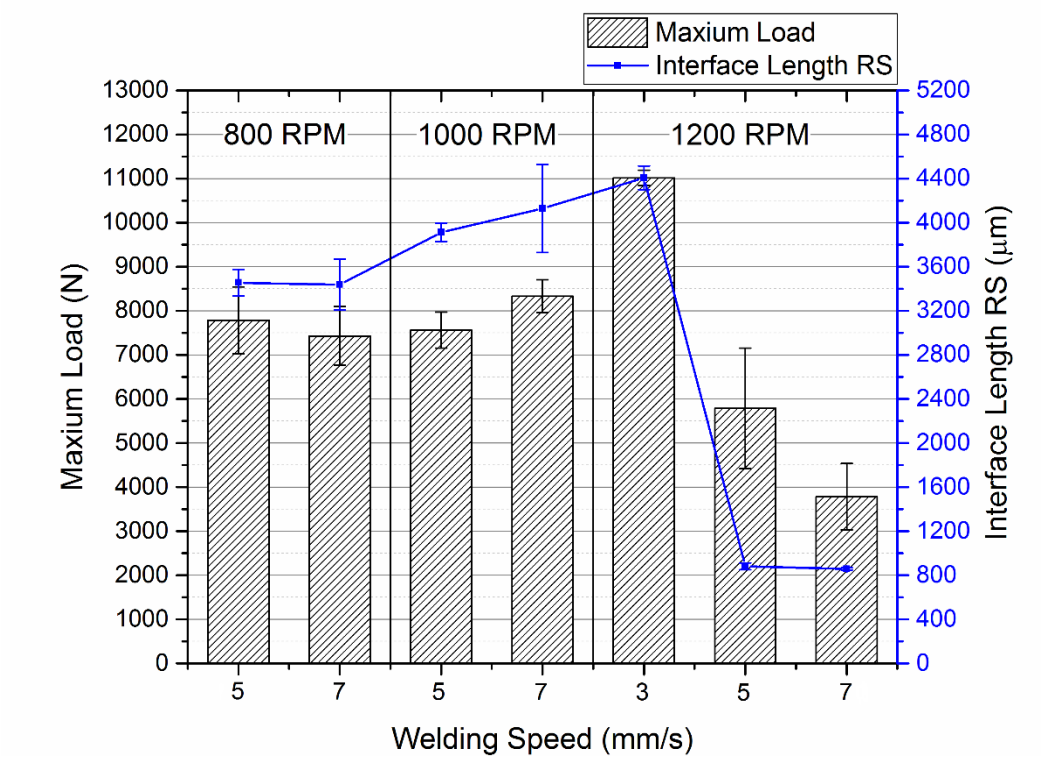

Figure 53 – Interface Length vs Maximum Load.

Figure 53 presents a comparison between the interface length and the obtained maximum load from the pull-out tests, for the DP specimens. Just as with the SP specimens' tests, a tendency on the interface length with the maximum load is clearly evidenced in the graph. When the interface presents a bigger length, the outputted result for maximum load is also bigger. The same reason that justifies this tendency on the SP tests is also valid for these DP specimens' results.

4.2.4.3 Fracture Surface of pull-out tests

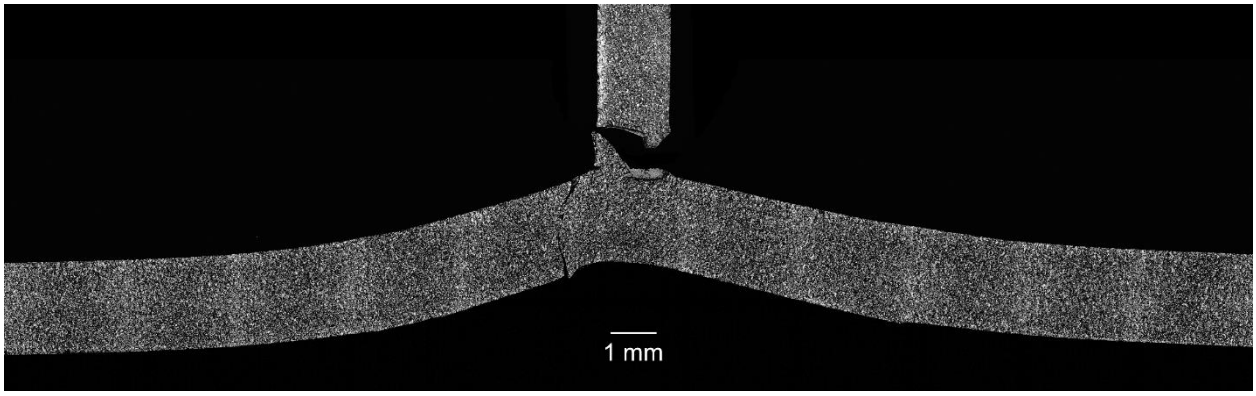

Figure 54 – Example of a fractured surface after pull-out test.

Figure 54 presents the fractured surface from a sample that belongs to the specimen SSFSW-T9G-AB-167 after the pull-out test was performed. Almost all the samples presented a flat area after the stringer was pulled out, meaning that the fracture surface was in the notch, similar to the majority of fractured surfaces after pull-out tests for the SP specimens. This means that double passing weld didn't stir enough material to perform a strong T-joint.

4.3 Notch-skin 3-parts welds – 3P

4.3.1 Microstructure analysis

4.3.1.1 General overview

As it was presented for the SP and DP specimens, Table 18 stands for the 3-parts specimen's microstructure. Since only four specimens were available, they are presented all in the same table. Below, a brief explanation about the microstructure, and the respective parameters, is presented.

Table 18 – Microstructures obtained for the 3P specimens.

3 mm/s; 1200 RPM	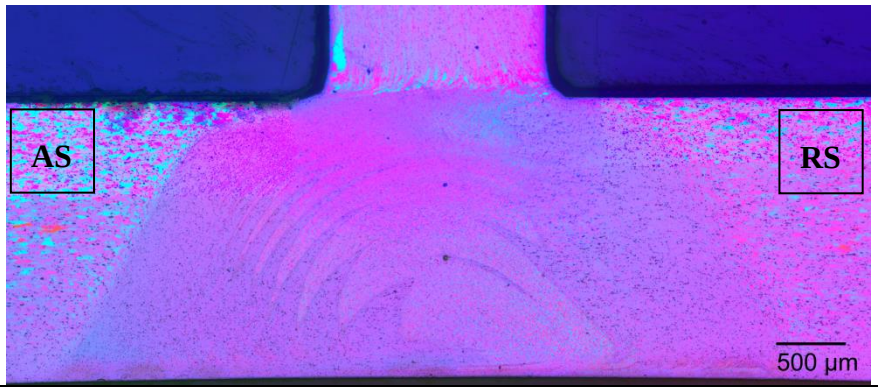
7 mm/s; 1000 RPM	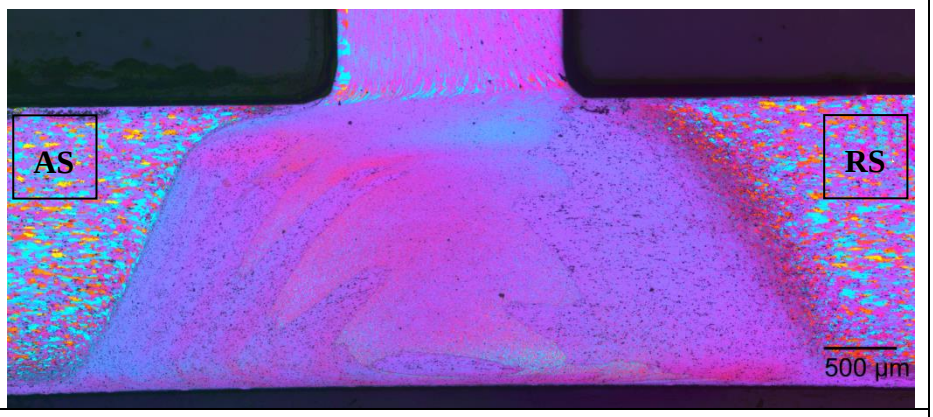
5 mm/s; 800 RPM	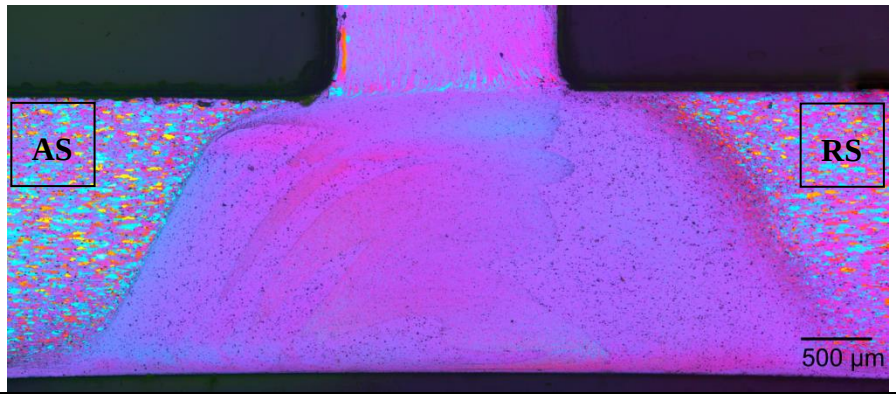
7 mm/s; 1200 RPM	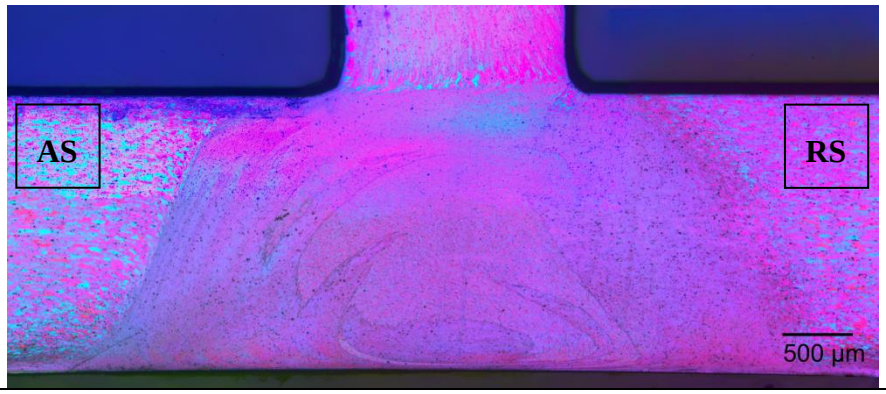

Table 18 presents the microstructure of the four 3P specimens. In a first analysis, since the stringer is placed in the middle and separates the plates, it is clear in all the microstructures that the stirred zone presents a strong metal interlocking, mostly on the advancing side.

As the welding speed increases, it is clearer the difference in microstructure between the stirred zone and the base material, as the TMAZ gets thinner. When the rotational speed decreases, the interface between the skin and the stringer located on the retreating side is becoming less wavy, which means that the metal interlocking is weaker. This may lead to early rupture.

4.3.1.2 Grain-size measurements

Figure 55 stands for the 3-parts specimen's grain size measurements per its welding parameters. As they were just four specimens, all the curves were plotted on the same graph. Below, a brief explanation about the obtained results is presented.

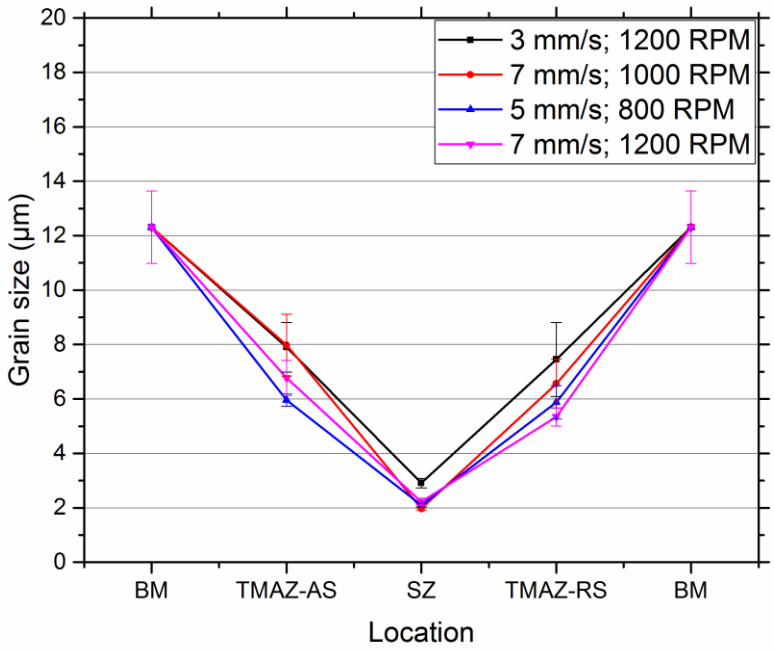

Figure 55 – Grain size evolution.

In general, there is a significant difference in grain size of the specimens welded with 3 and 7 mm/s, both obtained with a rotational speed of 1200 RPM, which means that, there is a major contribution from a different welding speed. A different rotational speed (and the same welding speed) also presents a significant difference in grain size, which also means that a changing welding speed also influences the grain size, but only for the TMAZ, since the SZ did not present relevant differences in size.

When both welding speed and rotational speed are reduced, grains are becoming smaller. This happens because there is more time available to stir the material, and that means grains are getting smaller.

4.3.2 Micro-Hardness tests

4.3.2.1 Horizontal direction

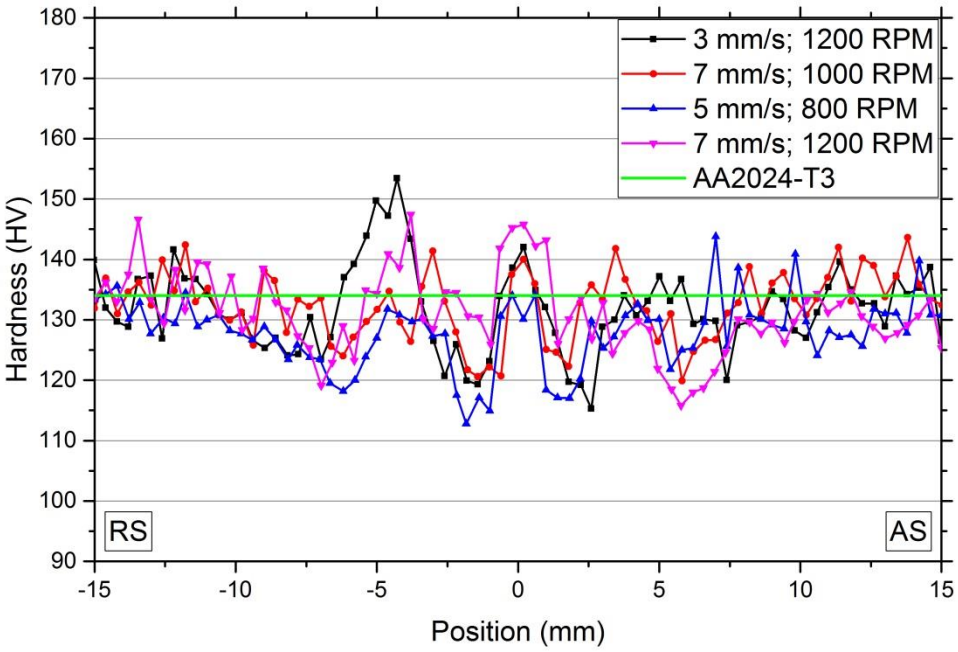

Figure 56 – Hardness values.

Although there is still some scatter, the 3P tests present a more accurate pattern, as it can be seen in Figure 56. Clearly, the biggest difference from the previous weld configurations is that the SZ presents an increased level of hardness. This makes sense because, in the 3P configuration, the stringer is in the middle and has physical contact with the probe, thus meaning that the stirred material on top is mainly AA7050-T651, which is the hardest aluminium alloy.

Although there are not enough parameters to draw a consistent comment about different rotational speed and welding speed, there are a couple of observations that can be made. In terms of different welding speed (3 and 7 mm/s, for 1200 RPM), there is a significant difference only on the HAZ. In terms of altering rotational speed (1000 and 1200 RPM, for 7 mm/s), there is not any relevant difference.

In this case, the critical zone is the TMAZ, and the parameter set that presents the best result is the weld with a rotational speed of 1200 RPM and a welding speed of 7 mm/s, which is the set of parameters that presents the lowest heat input.

4.3.2.2 Vertical direction

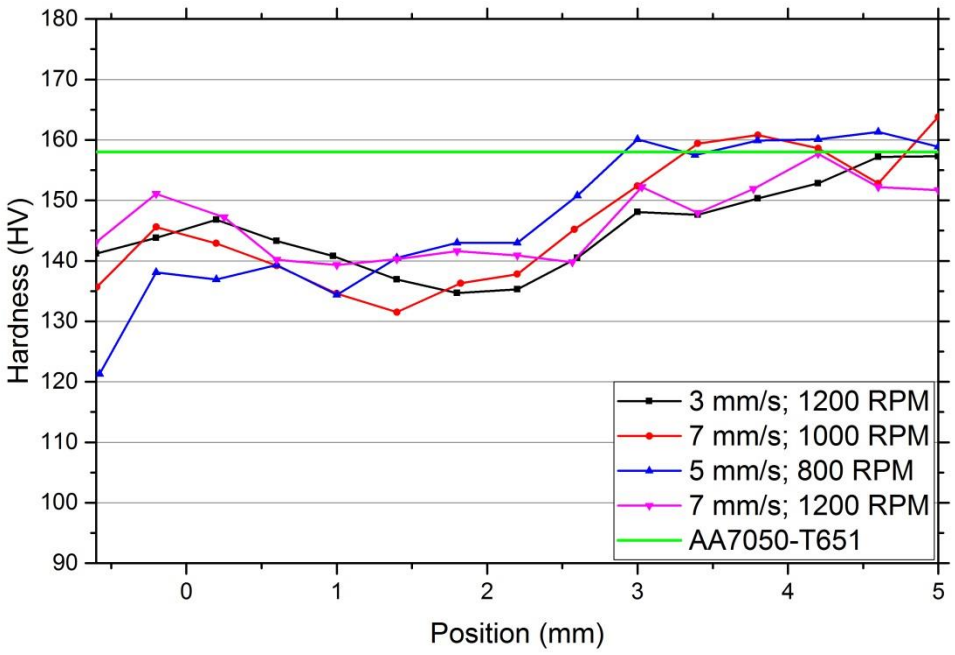

Figure 57 – Hardness values for 3P tests.

Considering all the 3P configuration welds, there is not a relevant difference on hardness values for the changing weld parameters. Also, the mechanical behaviour seems to be similar in all the different cases. This means that, for the case of vertical direction of micro-hardness, this weld configuration present the most stable behaviour and the changing parameters do not significantly change the local hardness.

Just like the SP welds, there is an interval whereas the hardness is lower than the SZ (between “0 mm” and “2,5 mm”), possibly caused by a local grain crystallization generated by the heat input.

4.3.3 Hoop-Strength tests

4.3.3.1 Ultimate Tensile Strength

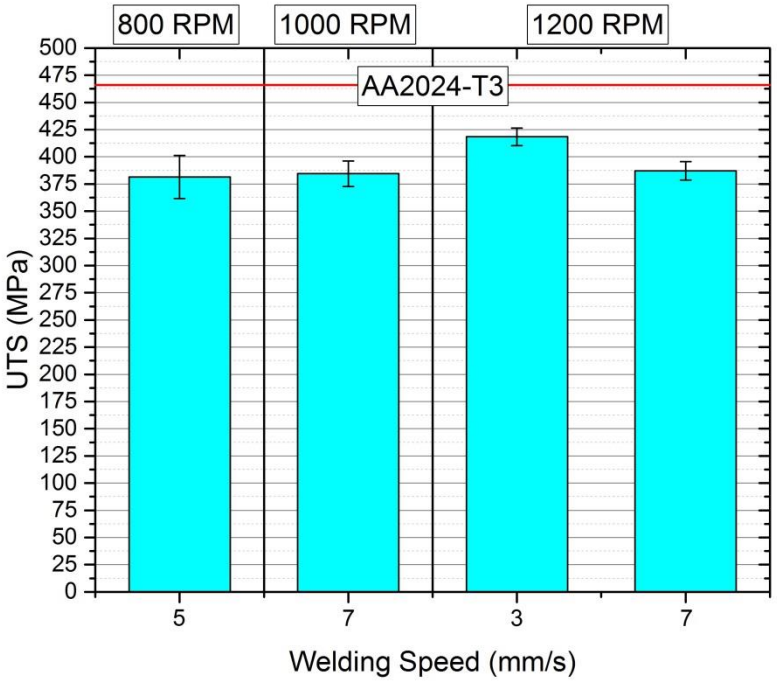

Figure 58 – Ultimate tensile strength.

Figure 58 shows the obtained UTS on the hoop-strength tests for each 3P specimen. As a first look, the obtained results are generally higher on these specimens than the notch-skin configuration specimens, which means that this 3P configuration presents the most resistant metal linkage between skin and stringer. Among these specimens, the ones that present bigger UTS are the ones obtained with a rotational speed of 1200 RPM, the one with the lowest welding speed (3 mm/s), which means that, using this T-joint configuration, the smaller the welding speed and the bigger the rotational speed, the bigger is the interlocking between the stringer and the skin.

4.3.3.2 Yield Strength

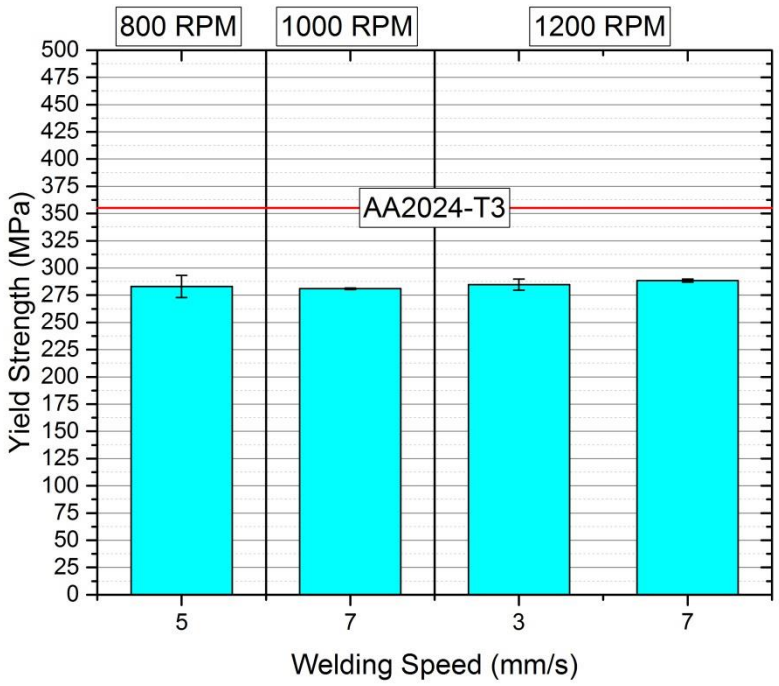

Figure 59 – Yield strength.

Figure 59 shows the obtained YS on the hoop-strength tests for each 3P specimen. As it was evidenced in the previous T-joint configurations, seems that there isn't a relevant difference of yield strength with the changing parameters. Thus, considering the studied parameter window, the changing parameters don't affect the material's elastic behaviour.

4.3.3.3 Interface angle vs Ultimate Tensile Strength

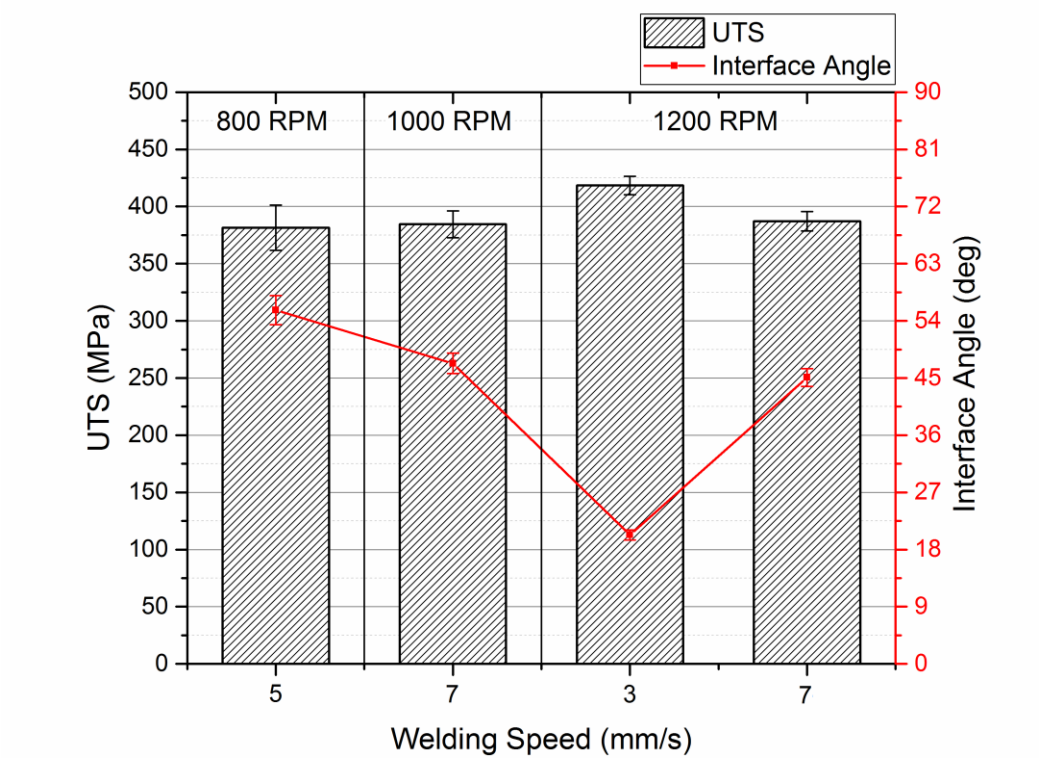

Figure 60 – Interface angle vs UTS.

Figure 60 presents a comparison between the interface angle and the obtained UTS from the hoop-strength tests. As it happened with the previous weld configuration, a tendency on the changing UTS with the variable interface angle is evidenced. However, a big change in the angle promotes a reduced change in the UTS. This means that an increased interface angle doesn't alter significantly the UTS. The lowest angle was obtained with a weld preformed with the parameters that present the biggest heat input (the biggest rotational speed and the lowest welding speed), as it was evidenced for the case of DP specimens' hoop-strength testing.

4.3.3.4 Fracture Surface of hoop-strength tests

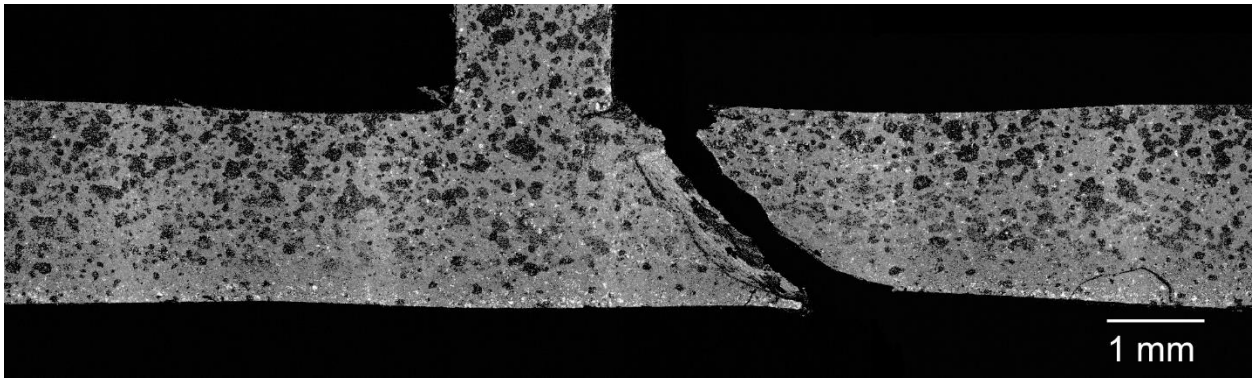

Figure 61 – Example of a fractured surface after hoop-strength test.

Figure 61 presents the fractured surface from a sample that belongs to the specimen SSFSW-T9G-AB-170 after the hoop-strength test was performed. All the specimens presented a failure in the retreating side (top right side of the stringer) with a 45 ° crack plane, initiated on the right side of the stringer and propagating across the skin. The fracture direction was expected to be the one presented because this region is the TMAZ, meaning that the crack had

less resistance to propagate throw the material. As it was seen on the micro-hardness graphs (see Figure 56), the TMAZ is the specimen's softest region.

In overall, the 3P configuration samples performed well on the hoop-strength tests, without evidence of early ruptures or defects in the welds.

4.3.4 Pull-Out tests

4.3.4.1 Maximum Load

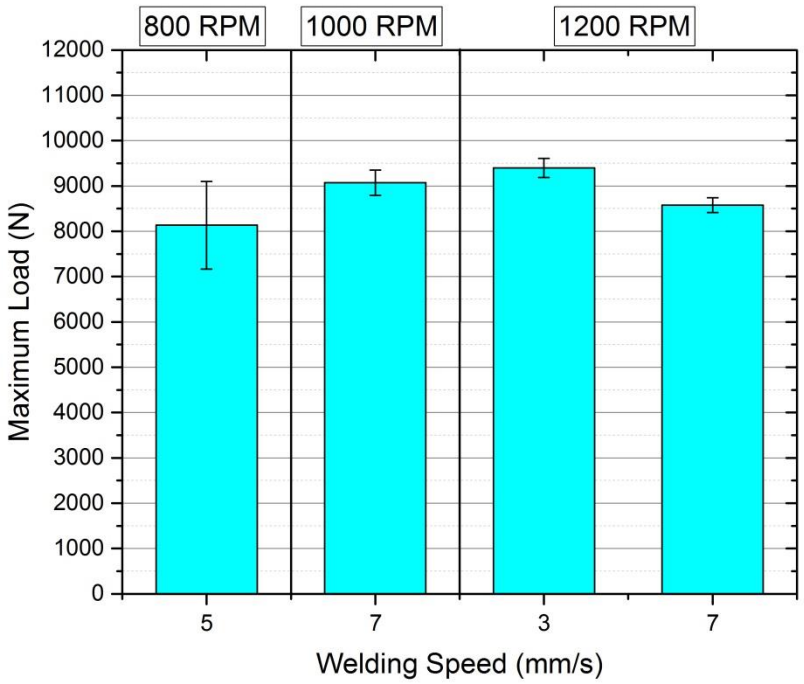

Figure 62 – Maximum load.

Figure 62 presents the maximum load of the pull-out tests for each 3P specimen. As it was evidenced for the DP weld configuration, the highest obtained maximum load for the pull-out tests occurred with 3 mm/s and 1200 RPM as weld parameters. The obtained weld performed with this pair of parameters present the highest material stirring, which means that the material has a better interlocking.

Although there is a difference in maximum load with the changing parameters, one must point out that the other obtained results for maximum load are not significant lower. For this weld configuration, the obtained results are good and, at the same time, they do not vary much with the changing parameters. This means that, considering the pull-out tests results, the process is somehow flexible in terms of parameters, because good results are achieved for all cases.

4.3.4.2 Interface Length vs Maximum Load

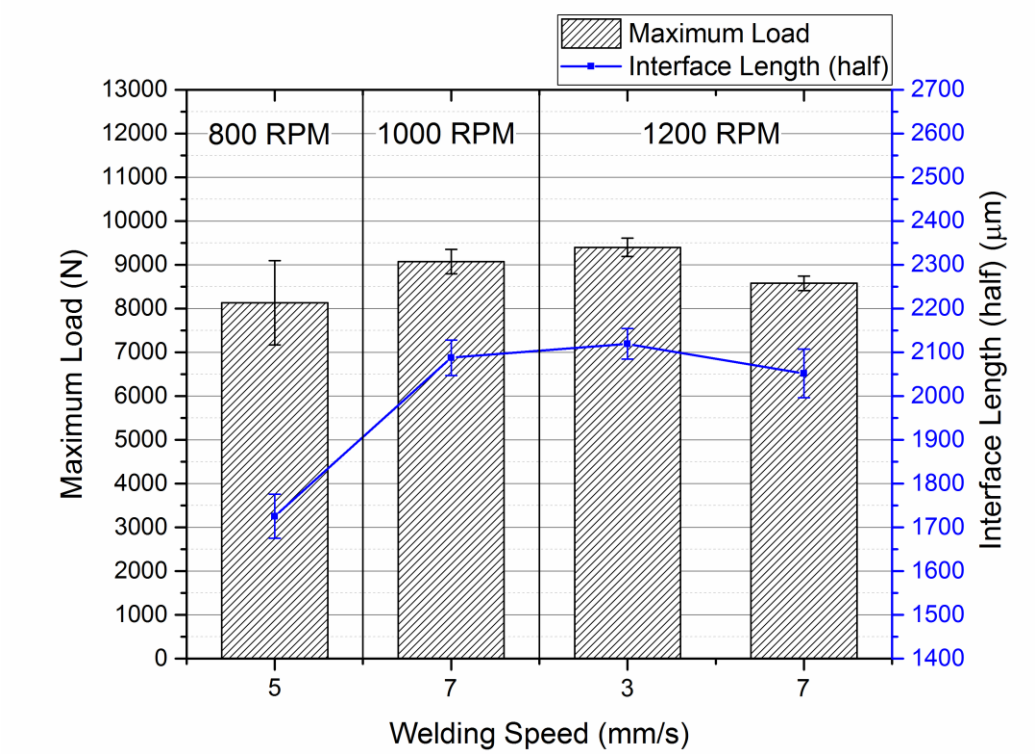

Figure 63 – Interface Length vs Maximum Load.

Figure 63 presents a comparison between the interface length and the obtained maximum load from the pull-out tests. Just like it happened with the previous weld configuration's tests, a tendency on the interface length with the maximum load is clearly evidenced in the graph. When the interface presents a bigger length, the outputted result for maximum load is also bigger. The same reason that justifies this tendency on the notch-skin configuration tests is also valid for these 3P specimens' results.

4.3.4.3 Fracture Surface of pull-out tests

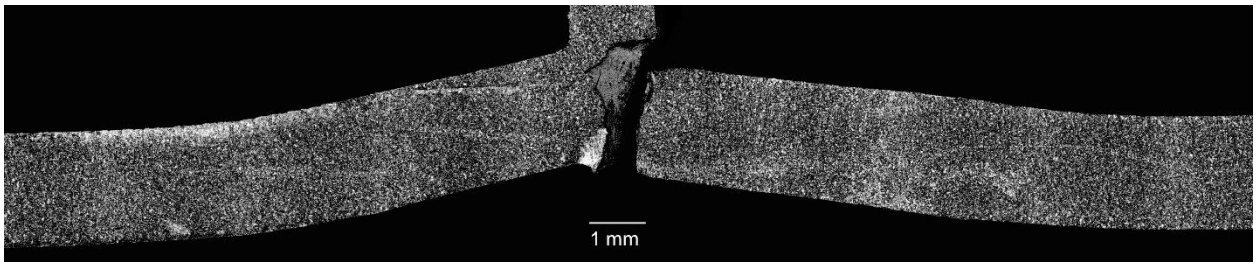

Figure 64 – Example of a fractured surface after pull-out test.

Figure 64 presents the fractured surface from a sample that belongs to the specimen SSFSW-T9G-AB-170 after the pull-out test was performed. Almost all the samples presented a crack in the skin, keeping the stringer attached to the skin on the advancing side. This means that the metal bonding resistance was superior to the shear force from AA2024-T3 as well as the pulling force and clamping of the testing machine. Thus, the configuration's metal interlocking is very strong, compared to the other T-joint configurations.

4.4 Comparison

After all the tests were performed and all results have been discussed, a comparison among all the specimens has been put through. The specimens will be analyzed per each type of test.

4.4.1 Microstructure analysis

Considering in first place the notch-skin T-joint configuration, the DP welds present a much wider SZ, as the weld was generated by a double pass of the probe. In theory, this configuration should present a more homogeneous SZ, but in fact, defects and porosity was evidenced on some microstructures from DP specimens. Some of these defects were located on the edge of the new advancing side with the old SZ (located on the left), while others seem to appear on the TMAZ from the retreating side. These defects were not spotted on the SP weld configuration neither on the 3P weld configuration specimens.

In terms of grain size, all specimens present approximately the same size on the grains located in the SZ. No differences were detected. The only difference was evidenced on the TMAZ, in which the grains were varying their size depending on the weld parameters but, by comparing the different T-joints configurations for the same location and weld parameters, no major differences were found, meaning that a different weld configuration doesn't alter significantly the grain size.

In terms of material stirring of the microstructure, specifically the SZ of each specimen, the configuration that presents the biggest visible metal interlocking is the 3P weld configuration. This means that there is a significant difference in metal bonding when the stringer made of AA7050-T651 is placed in the middle and using two separated sheets made of AA2024-T3. As this was the best visible metal interlocking, it was somehow expected that it would perform well with the remaining experiments, and it did as it was evidenced.

4.4.2 Micro-Hardness tests

For the notch-skin weld configurations, the softest area is the SZ, as it was expected, while for the 3P weld configuration, the softest area is the TMAZ. For the 3P configuration, the stringer is placed in the middle, and the AA7050-T651 is a tougher material, so a harder SZ was obtained. Considering all specimens, the lower values of micro-hardness are in the same range, around 115 HV, so no major differences were evidenced among the three T-joint configurations.

In overall, the obtained results from the micro-hardness tests are not accurate, as it is difficult to find a path between the different obtained results for micro-hardness and the changing welding parameters. Also, only one test per each sample was put through which means that there is no average or standard deviation to understand the veracity of the tests. Therefore, results should not be strictly considered as criteria for understanding which are the best welding parameters, or even the best T-joints configuration.

4.4.3 Hoop-Strength tests

As it was evidenced, considering the SP weld specimens, there is a clear tendency. The ultimate tensile strength tends to increase when the rotational speed increases and the welding speed decreases. The best obtained result was 408 MPa and it was achieved by welding with a rotational speed of 1200 RPM and a welding speed of 3 mm/s.

For the DP weld specimens, the output variability is not clear. It is nearly impossible to identify a tendency of obtained properties with the changing parameters. For the hoop-strength experiment, the DP T-joint configuration is not stable.

The configuration the presented the best obtained result is the 3P weld configuration, reaching an ultimate tensile strength of 418 MPa from a panel welded with 3 mm/s and 1200 RPM as parameters. What is also interesting is that the other specimens that were welded with different parameters didn't underperform at all. For the other welds, the remaining specimens reached an UTS above 375 MPa, which is a superior result compared to the notch-skin specimens. This means that the 3P configuration delivers high outputs in loads with hoop-strength direction without a major interference of its weld parameters.

4.4.4 Pull-Out tests

SP weld graph present a big variability in terms of pull-out loads. As it was mentioned before, it is difficult to find a tendency of loads with the changing parameters. The best result was around 8000 N, obtained from a weld with 800 RPM of rotational speed and 5 mm/s of welding speed. The remaining results were unsatisfactory.

Despite having a great result of 10947 N of maximum load, obtained with a weld of 3 mm/s of welding speed and 1200 RPM of rotational speed, it is just a peak value of DP weld configuration. In general, the results seem not to present a tendency, making it difficult to evaluate its behaviour when the parameters are changed. The results variability with changing parameters is quite big, which means that, considering the parameter window, this configuration is not stable for this experiment.

3P configuration specimens presents a maximum load of 9387 N obtained from a specimen welded with 3 mm/s of welding speed and 1200 RPM of rotational speed. Although this is not the best peak maximum load (the maximum peak load was obtained on a DP specimen mentioned before), this weld configuration presents interesting maximum loads considering the overall experiment. As it was observed in hoop-strength experiments, this weld configuration not only presents a significant variability in terms of obtained results with the changing parameters, but also all results were considered satisfactory. Considering the utilized parameter window, no matter the applied parameters set up for welding, the achieved results will be valid, meaning that there is no relevant dependence in weld parameters.

5 Final Remarks

In this chapter, conclusions related to the current work are evidenced, and the best T-joints configuration is briefly commented, as well as the best welding parameters. A small observation regarding a possible future work is also suggested, as it would be the final item to conclude the present study but, as it was explained before, it was impossible to perform.

5.1 Conclusions

Regarding the current manufacturing process, the global demand for air travel and the challenges placed to the manufacturers concerning a clean manufacturing, effective cost processes and efficiency in materials design, new alternative processes are required for the future's aircrafts.

SSFSW presents interesting characteristics that fulfil the travel companies' needs, concerning the weight issue and the fatigue life of aircrafts, which means a cleaner, more reliable, economical and quicker manufacturing process.

Compared to FSW, SSFSW presents better welding outputs such as better surface finishing or lower dissipated power by the tool. These advantages make the SSFSW technology very suitable for welding AA 2000 and 7000 series, which are very common materials in the aircraft and aerospace industry. SSFSW is suitable for welding stringers to skins to reinforce the fuselage panels hopefully without compromising the structure's fatigue life.

Considering the notch-skin configurations, overall the single pass specimens performed better than the double pass. Results for SP weld tests seem to follow a pattern with the changing parameters, which was hard to find for the DP welds. This means that the initial need of joining the skins to the stringers in a double passing welds is disproved.

Although the SP welds presented more stable results with the changing parameters, compared to the DP welds, it is the 3P design that presents the best T-joint configuration. In the first place, not only the obtained results also follow a pattern with the welding parameters, they are generally higher, which in this case means that a welded structure that follows the 3P design is tougher. Moreover, as it was seen before, besides the best result for each experiment, the remaining results obtained with other parameters presented high outputs, which means little dependence was verified between the obtained results and its weld parameters.

Considering the previous remark, it means that no matter the welding parameters, the obtained results will be valid, therefore there is no relevant dependence in weld parameters for this panel design.

Regarding the process's applicability in the industry, welding panels with the 3P configuration is very interesting, as it is flexible in terms of welding parameters without compromising the joints' mechanical properties.

Considering the welding parameters themselves, overall, the best parameter set for welding are a rotational speed of 3 mm/s and a welding speed of 1200 RPM. This pair of parameters presented welded specimens with a stable microstructure and, for each configuration, good results were obtained when panels were welded with these parameters. Although there is the risk of reaching metallographic crystallization due to heat input, no evidence was found.

5.2 Future work perspective

Even though the objectives that were drawn for this work have been achieved, the complete study is vaster than what was presented on this report. As it was explained in the Experimental approach section, fatigue experiments were not performed and further comparison with riveted structures could not be done due to experiments' delays, lack of machine availability, and specimen processing and machinery.

The work that had to follow for further analysis is the fatigue testing, as well as the comparison with the current fuselage solution, which uses riveting. The fatigue experiments to perform are similar to the ones that were realized for characterizing the materials: hoop-strength and pull-out directions. Although it was not performed for static testing, a longitudinal fatigue experiment is also advisable so that the welded structure can be characterized in the three load directions. An example of hoop-strength test for fatigue is shown in Figure 65.

Figure 65 – Sample performing a hoop-strength fatigue test.

Finally, to finish the study, the results for fatigue should be compared with the values from the riveted solution and conclusion made.

In a different field of study, as all this work was performed for the aircraft industry, it is advisable to evaluate the feasibility of manufacturing hybrid structures of composites with AA panels made by SSFSW, since more and more materials are joined together and this combination is becoming more common to find on nowadays aircrafts.

References

ASTM. (2013). *Standard Test Methods for Determining Average Grain Size*. Designation: E112 – 12. West Conshohocken, Pennsylvania, USA: ASTM International.

ASTM. (2010). *Standard Test Method for Knoop and Vickers Hardness of Materials*. Designation: E384 – 10e. West Conshohocken, Pennsylvania, USA: ASTM International.

Ahmed, M., Wynne, B., Rainforth, W., & Threadgill, P. (2010). *Through-thickness crystallographic texture of stationary*. Scripta Materialia, vol. 64 (pp. 45–48).

Barbini, A. (2014). *Evaluation of the "Stationary Shoulder" Friction Stir Welding Process for Aircraft Applications*. Master Thesis, Università degli Studi di Pisa.

Barbini, A. (2016). *Damage tolerance behaviour of integral aircraft structures obtained by SSFSW*. Presentation of Doctoral Seminar (24th November 2016). HZG, Germany.

Carstensen, Jan, Leon L. Hütsch, Jorge dos Santos. (2015). *FSW Robotic Gantry*. Poster of WMP. HZG, Germany.

Corporation, Origin. (2016). Origin 2016G 64 Bit. Northampton, Massachusetts, USA.

Dursun, T., & Soutis, C. (2013). *Recent developments in advanced aircraft aluminium alloys*. Journal of Materials and Design, vol. 56 (pp. 862–871).

Fratini, L. (2012). *FSW of Lap and T-Joints*. In P. M. Moreira, L. F. Silva, & P. M. Castro, *Structural Connections for Lightweight Metallic Structures* (pp. 125–149).

Leahy, J. (2016). *Global Market Forecast*. Presentation of Global Market Forecast for the Aircraft Industry 2016 Seminar.

Li, D., Yang, X., Cui, L., He, F., & Zhang, X. (2015). *Investigation of stationary shoulder friction stir welding of aluminum alloy 7075-T651*. Journal of Materials Processing Technology, vol. 222 (pp. 391–398).

Li, W., Vairis, A., & Ward, R. M. (2014). *Advances in Friction Welding*. Advances in Materials Science and Engineering. Hindawi Publishing Corporation.

Martin, J. P. (2013). *Stationary Shoulder Friction Stir Welding*. Em Proceedings of the 1st International Joint Symposium on Joining and Welding, (pp. 477–482).

Mishra, R. S., & Ma, Z. Y. (2005). *Friction stir welding and processing*. Materials Science and Engineering. Materials Science and Engineering, vol. 50 (pp. 1–78)

Nandan, R., DebRoy, T., & Bhadeshia, H. (2008). *Recent advances in friction-stir welding – Process, weldment structure and properties*. Progress in Materials Science, vol. 53 (pp. 980–1023).

Silva, A. C., Braga, D. F., Figueiredo, M., & Moreira, P. (2013). *Friction stir welded T-joints optimization*. Materials and Design, vol. 55 (pp. 120–127).

Threadgill, P. L., Leonard, A. J., Shercliff, H. R., & Withers, P. J. (2009). *Friction stir welding of aluminium alloys*. International Materials Reviews, vol. 54 (pp. 49–93).

UDDEHOLM, UNIMAX, (2015). AB, U. Catalog. EU.

Unit D, AirCraftMaterialsUK.com Ltd (2016). *Alloy MP159* (AMS 5841). Obtained from Aircraft Materials: https://www.aircraftmaterials.com/data/nickel/mp159.html

Wu, Hao, Ying-Chun Chen, David Strong, Phil Prangnell. (2015). *Stationary shoulder FSW for joining high strength aluminum alloys*. Journal of Materials Processing Technology, vol. 221 (pp. 187–196).

ANNEX A: Specimen identification table

Specimen Name	Welding configuration (T-Joints)	PL (mm)	PD (mm)	WS (mm/min)	RPM	TA	Comments
WELDS TO ESTABLISH THE PARAMETER WINDOW FOR NOTCH-SKIN CONFIGURATION							• **Tool cleaning necessary each 3.5 m** • **Work-Offset 56**
SSFSW-T9G-AB-122-1	NOTCH-SKIN/SINGLE-PASS	1.9	2.00	300	1200	2	• Macrograph
SSFSW-T9G-AB-122-2	NOTCH-SKIN/SINGLE-PASS	1.9	2.05	300	1200	2	• Macrograph
SSFSW-T9G-AB-122-3	NOTCH-SKIN/SINGLE-PASS	1.9	2.05	420	1200	2	• Macrograph
SSFSW-T9G-AB-122-4	NOTCH-SKIN/SINGLE-PASS	1.9	2.05	600	1200	2	• Defects in the AS
SSFSW-T9G-AB-123-1	NOTCH-SKIN/SINGLE-PASS	1.9	2.05	300	1000	2	• Macrograph
SSFSW-T9G-AB-123-2	NOTCH-SKIN/SINGLE-PASS	1.9	2.05	420	1000	2	• Macrograph
SSFSW-T9G-AB-123-3	NOTCH-SKIN/SINGLE-PASS	1.9	2.05	600	1000	2	• Defects in the AS (same as 122-4)
SSFSW-T9G-AB-124-1	NOTCH-SKIN/SINGLE-PASS	1.9	2.05	300	1500	2	• Defects in the AS (reduced contact shoulder) • Macrograph
SSFSW-T9G-AB-124-2	NOTCH-SKIN/SINGLE-PASS	1.9	2.05	420	1500	2	• Defects in the AS (reduced contact shoulder)
SSFSW-T9G-AB-125-1	NOTCH-SKIN/SINGLE-PASS	1.9	2.05	300	800	2	• Macrograph
SSFSW-T9G-AB-125-2	NOTCH-SKIN/SINGLE-PASS	1.9	2.05	420	800	2	• Macrograph
SSFSW-T9G-AB-125-3	NOTCH-SKIN/SINGLE-PASS	1.9	2.05	600	800	2	• Defects in the AS
SSFSW-T9G-AB-126	NOTCH-SKIN/DOUBLE-PASS	1.9	2.05	420	1000	2	• Small defect in the AS at the first pass • Wrong distance between the two passes (0.8 instead of 1.6mm) • Macrograph
SSFSW-T9G-AB-127-1	NOTCH-SKIN/SINGLE-PASS	1.9	2.05	420	1000	2	• Macrograph
SSFSW-T9G-AB-127-2	NOTCH-SKIN/SINGLE-PASS	1.9	2.1	420	1000	2	• Macrograph

SSFSW-T9G-AB-127-3	NOTCH-SKIN/SINGLE-PASS	1.9	2.1	600	1000	2	• Defect in the AS • Reduce defect size with the higher penetration
SSFSW-T9G-AB-152	NOTCH-SKIN/SINGLE-PASS	1.9	2.05	420	1000	2	• Welded in order to center the probe • **Corr(y)=0.25 mm** • Macrograph
SSFSW-T9G-AB-153	NOTCH-SKIN/DOUBLE-PASS	1.9	2.05	420	1000	2	• Welded in order to establish distances from the center • **Corr(y)=0.15 mm** • Distance from the center +0.95 mm, -0.65 mm • Macrograph
WELDS FOR THE PARAMETER STUDY IN CASE OF NOTCH-SKIN/SINGLE-PASS							**Each weld is 500 mm long**
SSFSW-T9G-AB-154	NOTCH-SKIN/SINGLE-PASS	1.9	2.05	300	800	2	• Samples for testing
SSFSW-T9G-AB-155	NOTCH-SKIN/SINGLE-PASS	1.9	2.1	420	800	2	• Samples for testing • Necessary to go 0.05 mm deeper to increase shoulder touch and avoid defects
SSFSW-T9G-AB-156	NOTCH-SKIN/SINGLE-PASS	1.9	2.05	300	1000	2	• Samples for testing
SSFSW-T9G-AB-157	NOTCH-SKIN/SINGLE-PASS	1.9	2.05	420	1000	2	• Samples for testing
SSFSW-T9G-AB-158	NOTCH-SKIN/SINGLE-PASS	1.9	2.05	300	1200	2	• Samples for testing
SSFSW-T9G-AB-159	NOTCH-SKIN/SINGLE-PASS	1.9	2.15	420	1200	3	• Samples for testing • Same as -155, necessary to go 0.1 mm deeper and increase the TA of 1 degree • First 13 mm WS=600 mm/min
SSFSW-T9G-AB-160	NOTCH-SKIN/SINGLE-PASS	1.9	2.05	180	1200	2	• Samples for testing • Best parameters of Msc Thesis
WELDS FOR THE PARAMETER STUDY IN CASE OF NOTCH-SKIN/DOUBLE-PASS							**Each weld is 500 mm long**
SSFSW-T9G-AB-161	NOTCH-SKIN/DOUBLE-PASS	1.9	2.05	300	800	2	• Samples for testing
SSFSW-T9G-AB-162	NOTCH-SKIN/DOUBLE-PASS	1.9	2.05	420	800	2	• Samples for testing • Rolling and welding directions are perpendicular

SSFSW-T9G-AB-163	NOTCH-SKIN/DOUBLE-PASS	1.9	2.05	300	1000	2	• Samples for testing
SSFSW-T9G-AB-164	NOTCH-SKIN/DOUBLE-PASS	1.9	2.05	420	1000	2	• Samples for testing
SSFSW-T9G-AB-165	NOTCH-SKIN/DOUBLE-PASS	1.9	2.05	300	1200	2	• Samples for testing
SSFSW-T9G-AB-166	NOTCH-SKIN/DOUBLE-PASS	1.9	2.15	420	1200	3	• Samples for testing • Same as -159
SSFSW-T9G-AB-167	NOTCH-SKIN/DOUBLE-PASS	1.9	2.05	180	1200	2	• Samples for testing • Best parameters of Msc Thesis
WELDS FOR THE PARAMETER STUDY IN CASE OF 3-PARTS/SINGLE-PASS							**Each weld is 500 mm long**
SSFSW-T9G-AB-169-1	3-PARTS/SINGLE-PASS	1.9	2.05	180	1200	2	• Definition of correct PD • Necessity to clamp the two plates laterally • Macrograph
SSFSW-T9G-AB-169-2	3-PARTS/SINGLE-PASS	1.9	2.05	420	1200	2	• Definition of correct PD • Necessity to clamp the two plates laterally • Macrograph
SSFSW-T9G-AB-170	3-PARTS/SINGLE-PASS	1.9	2.1	180	1200	2	• Samples for testing
SSFSW-T9G-AB-171	3-PARTS/SINGLE-PASS	1.9	2.1	420	1000	2	• Samples for testing
SSFSW-T9G-AB-172	3-PARTS/SINGLE-PASS	1.9	2.1	300	800	2	• Samples for testing
SSFSW-T9G-AB-173	3-PARTS/SINGLE-PASS	1.9	2.1	420	1200	2	• Samples for testing

ANNEX B: Cutting plan

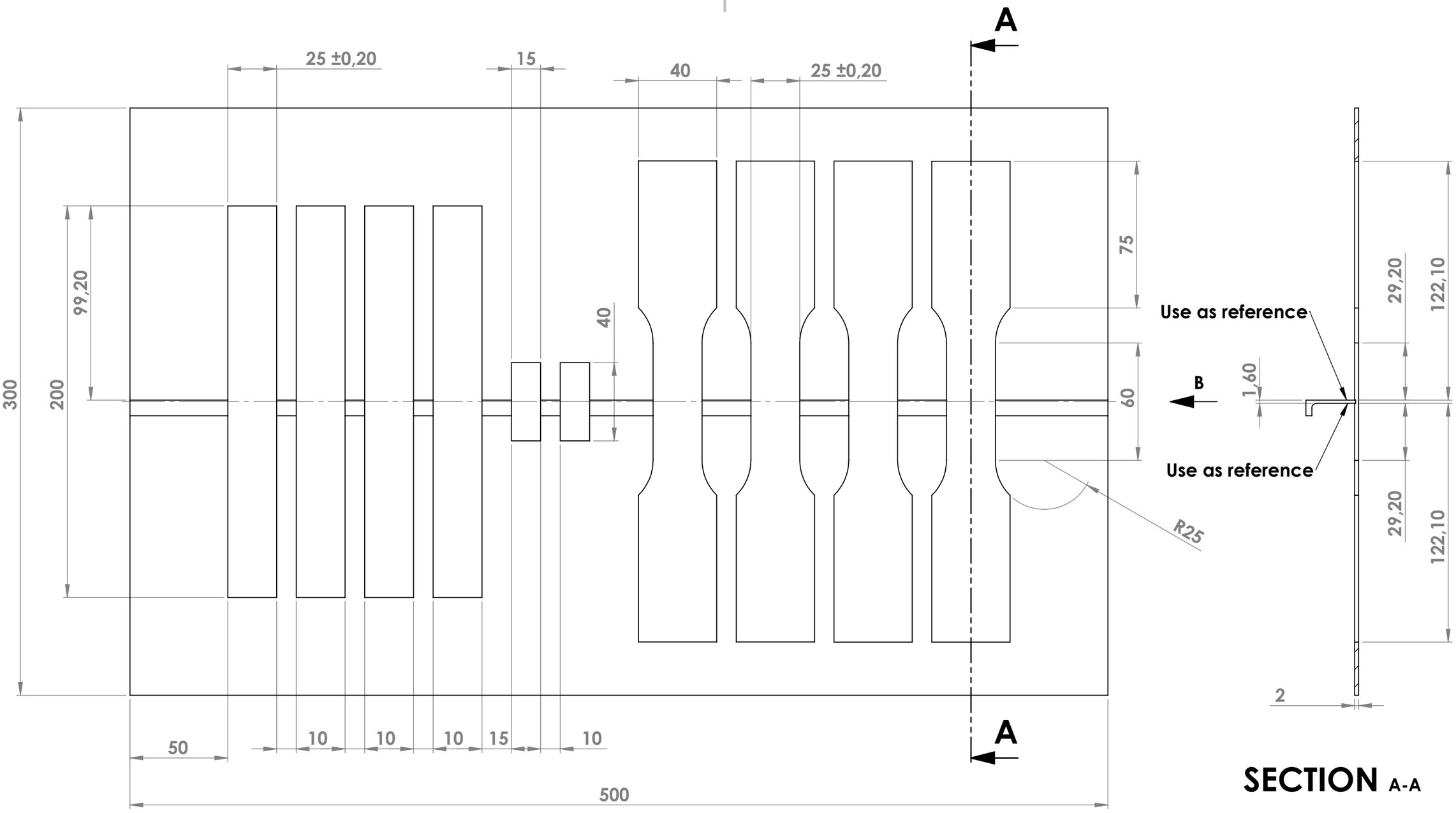

SECTION A-A

Proben erodiert

UNLESS OTHERWISE SPECIFIED: DIMENSIONS ARE IN MILLIMETERS SURFACE FINISH: TOLERANCES: LINEAR: ANGULAR:	FINISH:		DEBURR AND BREAK SHARP EDGES			DO NOT SCALE DRAWING	REVISION
	NAME	SIGNATURE	DATE			TITLE:	
DRAWN						Z-SSFSW-AB-HS-PO-2	
CHK'D							
APPV'D							
MFG							
Q.A				MATERIAL: AA 2024		DWG NO.	A3
				WEIGHT:		SCALE:1:2	SHEET 1 OF 1